(12) INTERNATIONAL APPLICATION PUBLISHED UNDER THE PATENT COOPERATION TREATY (PCT)

(19) World Intellectual Property Organization
International Bureau

(43) International Publication Date
27 November 2008 (27.11.2008)

PCT

(10) International Publication Number
WO 2008/144449 A2

(51) International Patent Classification:
A61B 8/13 (2006.01)

(21) International Application Number:
PCT/US2008/063799

(22) International Filing Date: 15 May 2008 (15.05.2008)

(25) Filing Language: English

(26) Publication Language: English

(30) Priority Data:

60/938,446	16 May 2007 (16.05.2007)	US
60/938,359	16 May 2007 (16.05.2007)	US
60/938,371	16 May 2007 (16.05.2007)	US

(71) Applicant *(for all designated States except US)*: **VERATHON INC.** [US/US]; 20001 North Creek Parkway, Bothell, WA 98021 (US).

(72) Inventors; and

(75) Inventors/Applicants *(for US only)*: **YANG, Fuxing** [CN/CN]; 17910 142nd NE #A-11, Woodinville, WA 98072 (US). **MCMORROW, Gerald** [US/US]; 6319 240th Way NE, Redmond, WA 98053 (US).

(74) Agent: **BYRNE, Mark, D.**; BLACK LOWE & GRAHAM PLLC, 701 Fifth Avenue, Suite 4800, Seattle, WA 98104 (US).

(81) Designated States *(unless otherwise indicated, for every kind of national protection available)*: AE, AG, AL, AM, AO, AT, AU, AZ, BA, BB, BG, BH, BR, BW, BY, BZ, CA, CH, CN, CO, CR, CU, CZ, DE, DK, DM, DO, DZ, EC, EE, EG, ES, FI, GB, GD, GE, GH, GM, GT, HN, HR, HU, ID, IL, IN, IS, JP, KE, KG, KM, KN, KP, KR, KZ, LA, LC, LK, LR, LS, LT, LU, LY, MA, MD, ME, MG, MK, MN, MW, MX, MY, MZ, NA, NG, NI, NO, NZ, OM, PG, PH, PL, PT, RO, RS, RU, SC, SD, SE, SG, SK, SL, SM, SV, SY, TJ, TM, TN, TR, TT, TZ, UA, UG, US, UZ, VC, VN, ZA, ZM, ZW.

(84) Designated States *(unless otherwise indicated, for every kind of regional protection available)*: ARIPO (BW, GH, GM, KE, LS, MW, MZ, NA, SD, SL, SZ, TZ, UG, ZM, ZW), Eurasian (AM, AZ, BY, KG, KZ, MD, RU, TJ, TM), European (AT, BE, BG, CH, CY, CZ, DE, DK, EE, ES, FI, FR, GB, GR, HR, HU, IE, IS, IT, LT, LU, LV, MC, MT, NL, NO, PL, PT, RO, SE, SI, SK, TR), OAPI (BF, BJ, CF, CG, CI, CM, GA, GN, GQ, GW, ML, MR, NE, SN, TD, TG).

Published:

— *without international search report and to be republished upon receipt of that report*

(54) **Title:** SYSTEM AND METHOD FOR BLADDER DETECTION USING ULTRASONIC HARMONIC IMAGING

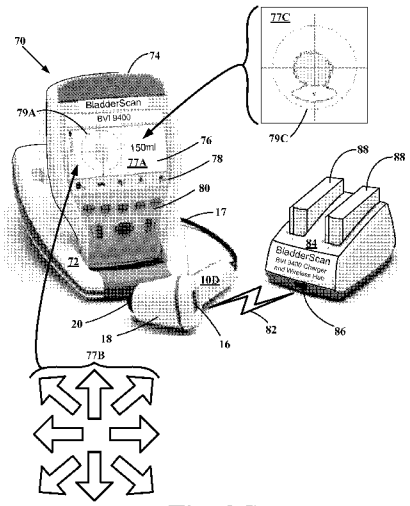

Fig. 2C

(57) **Abstract:** Systems, methods, and ultrasound transceivers equipped and configured to execute harmonic analysis and extract harmonic information related to a targeted organ of a subject are described. The methods utilize neural network algorithms to establish improved segmentation accuracy of the targeted organ or structures within a region-of- interest. The neural network algorithms, refined for detection of the bladder and to ascertain the presence or absence of a uterus, is optimally applied to better segment and thus confer the capability to optimize measurement of bladder geometry, area, and volumes.

WO 2008/144449 A2

SYSTEM AND METHOD FOR BLADDER DETECTION USING HARMONIC IMAGING

INVENTORS
Fuxing Yang
Gerald McMorrow

COPYRIGHT NOTICE

CROSS REFERENCE TO RELATED APPLICATIONS

[0001] This application is a continuation-in-part of, claims priority to, and incorporates by reference in its entirety to U.S. patent application serial number 11/968,027 filed December 31, 2007.

[0002] This application is a continuation-in-part of, claims priority to, and incorporates by reference in its entirety to U.S. patent application serial number 11/926,522 filed October 27, 2007.

[0003] This application is a continuation-in-part of, claims priority to, and incorporates by reference in its entirety to U.S. patent application serial number 11/925,887 filed October 27, 2007.

[0004] This application is a continuation-in-part of, claims priority to, and incorporates by reference in its entirety to U.S. patent application serial number 11/925,896 filed October 27, 2007.

[0005] This application is a continuation-in-part of, claims priority to, and incorporates by reference in its entirety to U.S. patent application serial number 11/925,900 filed October 27, 2007.

[0006] This application is a continuation-in-part of, claims priority to, and incorporates by reference in its entirety to U.S. patent application serial number 11/925,850 filed October 27, 2007.

[0007] This application is a continuation-in-part of, claims priority to, and incorporates by reference in its entirety to U.S. patent application serial number 11/925,843 filed October 27, 2007.

[0008] This application is a continuation-in-part of, claims priority to, and incorporates by reference in its entirety to U.S. patent application serial number 11/925,654 filed October 26, 2007.

[0009] This application incorporates by reference in their entirety and claims priority to U.S. Provisional Patent Application Nos. 60/938,359 filed May 16, 2007; 60/938,371 filed May 16, 2007; and 60/938,446 filed May 16, 2007.

[0010] All applications incorporated by reference in their entirety.

FIELD OF THE INVENTION

[0011] Embodiments of the invention pertain to organ imaging using ultrasonic harmonics.

BACKGROUND OF THE INVENTION

[0012] It has been shown that ultrasonic waves traveling through different mediums undergo harmonic distortion. The various attributes of these mediums determine what type of harmonic distortion is dominant when an ultrasonic wave passes through the medium. Ultrasound imaging depending on Fast Fourier Transforms (FFT) and other algorithms may lack the needed spectral information to generate diagnostically useful images. The deficiency inherent in these algorithms can be overcome by using other approaches.

SUMMARY OF THE PARTICULAR EMBODIMENTS

[0013] Systems, methods, and ultrasound transceivers equipped to probe structures and cavity filed organs with fundamental and/or harmonic ultrasound energies under A-mode, B-mode, and C-mode configurations. Systems and methods provide for

implementing and executing harmonic analysis of ultrasound frequencies and extract harmonic information related to a targeted organ of a subject are described. The methods utilize neural network algorithms to establish improved segmentation accuracy of the targeted organ or structures within a region-of-interest. The neural network algorithms refined for detection of the bladder and to ascertain the presence or absence of a uterus, is optimally applied to better segment and thus confer the capability to optimize measurement of bladder geometry, area, and volumes.

BRIEF DESCRIPTION OF THE DRAWINGS

[0014] The file of this patent contains at least one drawing executed in color in the detailed description of the particular embodiments. Copies of this patent with color drawing(s) will be provided by the Patent and Trademark Office upon request and payment of the necessary fee. Embodiments for the system and method to develop, present, and use clarity-enhanced ultrasound images are described below.

[0015] FIGURES 1A-D depicts a partial schematic and a partial isometric view of a transceiver, a scan cone comprising a rotational array of scan planes, and a scan plane of the array of an ultrasound harmonic imaging system;

[0016] FIGURE 2A depicts a partial schematic and partial isometric and side view of a transceiver, and a scan cone array comprised of 3D-distributed scan lines in alternate embodiment of an ultrasound harmonic imaging system;

[0017] FIGURE 2B illustrates a side and partial isometric that schematically depicts an harmonic ultrasound scanner employing C-mode and B-mode ultrasound modalities;

[0018] FIGURE 2C illustrates a partial isometric and schematic view of an ultrasound harmonic bladder scanner system;

[0019] FIGURE 3 is a schematic illustration of a server-accessed local area network in communication with a plurality of ultrasound harmonic imaging systems;

[0020] FIGURE 4 is a schematic illustration of the Internet in communication with a plurality of ultrasound harmonic imaging systems;

[0021] FIGURE 5 depicts a flowchart of a bladder detection algorithm employing fundamental ultrasound energies;

[0022] FIGURE 6 depicts a flowchart of the Find Initial Walls sub-algorithm of FIGURE 5;

[0023] FIGURE 7 depicts a flowchart of the Fix Initial Walls sub-algorithm of FIGURE 5;

[0024] FIGURE 8 depicts a flowchart of the Bladder or Uterus decision diamond of FIGURE 5;

[0025] FIGURES 9A-F schematically illustrates algorithm flow charts of a BVI9400 bladder detection algorithm in the BVI9400 transceiver substantially similar to transceiver 10C of FIGURE 2B;

[0026] FIGURE 10 schematically illustrates sound wave distortion with increasing harmonics;

[0027] FIGURE 11 illustrates frequency spectra of 6 RF lines from a human subjects, from which, the difference between the 2^{nd} harmonic and the fundamental can be found;

[0028] FIGURE 12 illustrates a frequency spectra example on how a quantification of harmonic information is made via harmonic ratio;

[0029] FIGURE 13 illustrates a second harmonic ratio distribution;

[0030] FIGURES 14A illustrates clinical cases of bladder overestimation arising from the use of non-harmonic information;

[0031] FIGURE 14B illustrates scan line grading to correct for over-estimation of segmented bladder cavity interfaces;

[0032] FIGURE 15A illustrates clinical cases of under-estimation of segmented bladder cavity interfaces;

[0033] FIGURE 15B illustrates scan line grading to correct for under-estimation of segmented bladder cavity interfaces;

[0034] FIGURE 16 illustrates a depiction of the anatomical locations of uterus and bladder and other anatomical structures;

[0035] FIGURE 17 presents a 4-panel scan image set of ultrasound scanned female patients, where the uterus is adjacent to the bladder region and it has very similar pattern in B-mode image;

[0036] FIGURE 18 illustrates one example on how to distinguish the bladder region from the uterus along scan line; If the scan is on a female patient, there must be a boundary between uterus and bladder region and the uterus is always under the bladder if both regions appear on a scan line. In the B-mode image, for each scan line passing through both regions, a small ridge exists. If the ridge can be found, we can tell them apart. So, by using gender information, the algorithm is able to refine the segmentation by separate the bladder region from uterus region.;

[0037] FIGURE 19 illustrates another example on how to distinguish the bladder region from the uterus along scan line;

[0038] FIGURES 20 and 21 presents a series of bladder scan segmentations resulting without using the gender information;

[0039] FIGURES 22 and 23 presents a series of bladder scan segmentations resulting using the gender information;

[0040] FIGURE 24 presents segmentations presented in polar coordinate form of planes 1-12 and 13-24, with a diagrammatic presentation of the interpolated shapes presented in an all the cuts of a C-mode acquired view;

[0041] FIGURE 25 presents a 3-D plot of an inconsistency case (upper plot) and a consistency case (lower plot) as a means to check the consistency of the segmentation results;

[0042] FIGURE 26 illustrates interpolated shapes before smoothing (top diagram) and after smoothing based on the mass center (bottom diagram);

[0043] FIGURE 27 illustrates the output of interpolated shapes between smoothed cuts before smoothing without interpolation;

[0044] FIGURE 28 illustrates a representation of two walls for the interpolated shape;

[0045] FIGURE 29 showing the different arrow feedback modes of the aiming indicator 22 of transceivers 10A-B-C;

[0046] FIGURE 30 illustrates a decision tree for the arrow feed back from the indicator 22;

[0047] FIGURE 31 illustrates shadow and segmentation regions of the pubic bone;

[0048] FIGURE 32 illustrates examples of grading results derived from Neural Harmonics Algorithms;

[0049] FIGURE 33 illustrates a series of intermediate C-mode shapes generated as a screenshot interface or virtual painting board based on the grading results from Figure 32;

[0050] FIGURE 34 illustrates segmentation results before and after using reverberation control method;

[0051] FIGURE 35 illustrates models for volume computation;

[0052] FIGURE 36 illustrates a regression analysis result between pre void bladder volume measurement and the sum of the post void bladder volume measurement and urine volume without harmonic analysis;

[0053] FIGURE 37 illustrates a regression analysis result between prevoid bladder volume measurement and the sum of the post void bladder volume measurement and urine volume with harmonic analysis and using the neural network algorithm;

[0054] FIGURE 38 illustrates a regression analysis result between prevoid bladder volume measurement and the sum of the post void bladder volume measurement and urine volume by the BVI3000 system which is not capable to execute harmonic analysis;

[0055] FIGURE 39 presents a comparison of the bladder line classification results between the method using harmonic ration as a feature and the method without

using harmonic ratio as a feature. The comparisons are made multiple times using different classifiers, including RBF (Radial Basis Function), SMO, BayesNet and Backpropogation Neural Network ;

[0056] FIGURE 40 is an illustration of a KI threshold algorithm;

[0057] FIGURES 41A and 41B illustrated B-mode 1058 plane after thresholding at 29 and 28; and

[0058] FIGURES 42-44 are regression plot analyses results of the clinical experiment on May 11-14, 2007, which are based on three different bladder scan system, 9400, 3000 and 6400.

DETAILED DESCRIPTION OF THE PARTICULAR EMBODIMENTS

[0059] Systems and methods described that encompass ultrasound detection and measurement of cavity containing organs that are amendable to detection and measurement employing fundamental ultrasound and harmonics of ultrasound frequencies analysis. Ultrasound transceivers equipped with deliver and receive fundamental ultrasound energies utilize different signal processing algorithms than ultrasound transceivers equipped to probe cavity-containing organs with ultrasound harmonic energies. Algorithms described below are developed to optimally extract organ information from fundamental and/or harmonic ultrasound echoes delivered under A-mode, B-mode, and/or C-mode methodologies. Alternate embodiments of the algorithms may be adapted to detect bladders in males, females that have not undergone hysterectomy procedures, females that have undergone hysterectomy procedures, and small male and female children.

[0060] Ultrasound transceivers equipped for utilizing ultrasound harmonic frequencies employ a neural network algorithm. The neural network algorithm is defined in computer executable instructions and employs artificial intelligence to echogenic signals delivered from ultrasound transceivers equipped with ultrasound harmonic functionality. The neural network algorithm uses returning first and second echo wavelength harmonics that arise from differential and non-linear wavelength distortion

and attenuation experienced by transiting ultrasound energy returning from a targeted region-of-interest (ROI). Using the harmonic ratios with the sub-aperture algorithm provides diagnostically useful information of the media though which ultrasound passes. The 9400 transducer described below has been redesigned to allow extraction of useful ultrasound information that distinguishes different mediums through which the ultrasound energy traverses. The sub-aperture algorithms are substantially fast enough to be implemented in real time within the time constraints enforced by ultrasound scanning protocols to acquire organ size information besides the original ultrasound B-mode image. The harmonic information is collected using a long interrogating pulse with a single fundamental frequency. The received signal is collected, analyzed for its spectrum information about the first and second harmonics. The ratio of these two harmonics provides the quantitative information on how much harmonics have been generated and attenuated along its propagation. The neural network sub-aperture algorithm is executed in non-parametric mode to minimize data modeling errors.

[0061] Disclosure below includes systems and method to detect and measure an organ cavity involving transmitting ultrasound energy having at least one of a fundamental and harmonic frequency to the organ cavity, collecting ultrasound echoes returning from the organ cavity and generating signals from the ultrasound echoes, and identifying within the ultrasound signals those attributable to fundamental ultrasound frequencies or those attributable to harmonic ultrasound frequencies. Thereafter, the fundamental frequency derived signals and the harmonic frequency derived signals undergo signal processing via computer executable program instructions to present an image of the organ on a display and/or its organ cavity, and calculating the volume of the organ and/or its organ cavity. The signal processing applied to the transceiver echoic fundamental and harmonic ultrasound signals include a neural network algorithm having computer readable instructions for ascertaining the certainty that a given scan line traverses a given organ's cavity region, a non-cavity region, or both a cavity and a non-cavity region using a grading algorithm for predicting the scan line's cavity or non-cavity

classification. The organs include, for example, the internal void of a bladder, the void of a uterus, or the ventricular and atrial chambers of a heart. The grading algorithm includes weighting the contributions of at least one of an ultrasound harmonic ration, an organ's tissue difference or delta that is proportional to the attenuation that a given ultrasound fundamental and/or harmonic frequency experiences transiting through the tissue, a minRsum value, a cavity front wall location, and a cavity back wall location.

[0062] Using harmonic information to distinguish different scan lines are based on the harmonic model we built. The model is set up based on a series of water tank experiments by using simulated body fluids, simulated body tissue, and combination simulated body fluids and body tissues for transducers having the characteristics of a 13 mm, 2.949 MHz transducer in an ultrasound transceiver developed by Verathon®, Inc. These tests prove that it is feasible to distinguish different kinds of scan lines. In general the larger the harmonic ratio, the larger the possibility that the scan line is passing through water region; the harmonic ratio is increasing linearly based upon the water region size.

[0063] The ultrasound transceivers or DCD devices developed by Verathon®, Inc are capable of collecting *in vivo* three-dimensional (3-D) cone-shaped ultrasound images of a patient. Based on these 3-D ultrasound images, various applications have been developed such as bladder volume and mass estimation. The clarity of images from the DCD ultrasound transceivers depends significantly upon the functionality, precision, and performance accuracy of the transducers used in the DCD ultrasound transceivers.

[0064] During the data collection process initiated by DCD, a pulsed ultrasound field is transmitted into the body, and the back-scattered "echoes" are detected as a one-dimensional (1-D) voltage trace, which is also referred to as a RF line. After envelope detection, a set of 1-D data samples is interpolated to form a two-dimensional (2-D) or 3-D ultrasound image.

[0065] FIGURES 1A-D depicts a partial schematic and a partial isometric view of a transceiver, a scan cone comprising a rotational array of scan planes, and a scan plane

of the array of various ultrasound systems 60A-D capable of collecting RF line and employing harmonic analysis.

[0066] FIGURE 1A is a side elevation view of an ultrasound transceiver 10A that includes an inertial reference unit, according to an embodiment of the invention. The transceiver 10A includes a transceiver housing 18 having an outwardly extending handle 12 suitably configured to allow a user to manipulate the transceiver 10A relative to a patient. Ultrasound transducers operating within the transceiver 10A may be equipped to collect and ready signals for ultrasound fundamental and/or harmonic frequency analysis.

[0067] The handle 12 includes a trigger 14 that allows the user to initiate an ultrasound scan of a selected anatomical portion, and a cavity selector (not shown). The transceiver 10A also includes a transceiver dome 20 that contacts a surface portion of the patient when the selected anatomical portion is scanned. The dome 20 generally provides an appropriate acoustical impedance match to the anatomical portion and/or permits ultrasound energy to be properly focused as it is projected into the anatomical portion. The transceiver 10A further includes one, or preferably an array of separately excitable ultrasound transducer elements (not shown in FIGURE 1A) positioned within or otherwise adjacent with the housing 18. The transducer elements may be suitably positioned within the housing 18 or otherwise to project ultrasound energy outwardly from the dome 20, and to permit reception of acoustic reflections generated by internal structures within the anatomical portion. The one or more array of ultrasound elements may include a one-dimensional, or a two-dimensional array of piezoelectric elements that may be moved within the housing 18 by a motor. Alternately, the array may be stationary with respect to the housing 18 so that the selected anatomical region may be scanned by selectively energizing the elements in the array.

[0068] A directional indicator panel or aiming guide panel 22 includes a plurality of arrows that may be illuminated for initial targeting and guiding a user to access the targeting of an organ or structure within an ROI. In the 9400 system described in FIGURE 2C below, the directional indicator panel 22 has a virtual equivalent in the form

of a targeting icon screenshot 77B, both indicator panel 22 and targeting icon 77B functioning to guide a transceiver user to place the transceiver to obtain a centered bladder or other cavity-containing organ. In particular embodiments if the organ or structure is centered from placement of the transceiver 10A acoustically placed against the dermal surface at a first location of the subject, the directional arrows may be not illuminated. If the organ is off-center, an arrow or set of arrows may be illuminated to direct the user to reposition the transceiver 10A acoustically at a second or subsequent dermal location of the subject. The acrostic coupling may be achieved by liquid sonic gel applied to the skin of the patient or by sonic gel pads to which the transceiver dome 20 is placed against. The directional indicator panel 22 may be presented on the display 54 of computer 52 in harmonic imaging subsystems described in FIGURES 3 and 4 below, or alternatively, presented on the transceiver display 16.

[0069] Transceiver 10A may include an inertial reference unit that includes an accelerometer 22 and/or gyroscope 23 positioned preferably within or adjacent to housing 18. The accelerometer 22 may be operable to sense an acceleration of the transceiver 10A, preferably relative to a coordinate system, while the gyroscope 23 may be operable to sense an angular velocity of the transceiver 10A relative to the same or another coordinate system. Accordingly, the gyroscope 23 may be of conventional configuration that employs dynamic elements, or it may be an optoelectronic device, such as the known optical ring gyroscope. In one embodiment, the accelerometer 22 and the gyroscope 23 may include a commonly packaged and/or solid-state device. One suitable commonly packaged device may be the MT6 miniature inertial measurement unit, available from Omni Instruments, Incorporated, although other suitable alternatives exist. In other embodiments, the accelerometer 22 and/or the gyroscope 23 may include commonly packaged micro-electromechanical system (MEMS) devices, which are commercially available from MEMSense, Incorporated. As described in greater detail below, the accelerometer 22 and the gyroscope 23 cooperatively permit the determination of positional and/or angular changes relative to a known position that is proximate to an

anatomical region of interest in the patient. Other configurations related to the accelerometer 22 and gyroscope 23 concerning transceivers 10A,B equipped with inertial reference units and the operations thereto may be obtained from copending U.S. Patent Application Serial No. 11/222,360 filed September 8, 2005, herein incorporated by reference.

[0070] The transceiver 10A includes (or if capable at being in signal communication with) a display 16 operable to view processed results from an ultrasound scan, and/or to allow an operational interaction between the user and the transceiver 10A. For example, the display 24 may be configured to display alphanumeric data that indicates a proper and/or an optimal position of the transceiver 10A relative to the selected anatomical portion. Display 16 may be used to view two- or three-dimensional images of the selected anatomical region. Accordingly, the display 16 may be a liquid crystal display (LCD), a light emitting diode (LED) display, a cathode ray tube (CRT) display, or other suitable display devices operable to present alphanumeric data and/or graphical images to a user.

[0071] Still referring to FIGURE 1A, the cavity selector (not shown) includes a pressable button similar to the trigger 14 may be operable to adjustably adapt the transmission and reception of ultrasound signals to the anatomy of a selected patient. In particular, the cavity selector adapts the transceiver 10A to accommodate various anatomical details of male and female patients. For example, when the cavity selector is adjusted to accommodate a male patient, the transceiver 10A may be suitably configured to locate a single cavity, such as a urinary bladder in the male patient. In contrast, when the cavity selector is adjusted to accommodate a female patient, the transceiver 10A may be configured to image an anatomical portion having multiple cavities, such as a bodily region that includes a bladder and a uterus. Alternate embodiments of the transceiver 10A may include a cavity selector configured to select a single cavity scanning mode, or a multiple cavity-scanning mode that may be used with male and/or female patients. The

cavity selector may thus permit a single cavity region to be imaged, or a multiple cavity region, such as a region that includes a lung and a heart to be imaged.

[0072] To scan a selected anatomical portion of a patient, the transceiver dome 20 of the transceiver 10A may be positioned against a surface portion of a patient that is proximate to the anatomical portion to be scanned. The user actuates the transceiver 10A by depressing the trigger 14. In response, the transceiver 10 transmits ultrasound signals into the body, and receives corresponding return echo signals that may be at least partially processed by the transceiver 10A to generate an ultrasound image of the selected anatomical portion. In a particular embodiment, the transceiver 10A transmits ultrasound signals in a range that extends from approximately about two megahertz (MHz) to approximately about ten MHz. Ultrasound energies beyond 10 MHz may be utilized.

[0073] In one embodiment, the transceiver 10A may be operably coupled to an ultrasound system that may be configured to generate ultrasound energy at a predetermined frequency and/or pulse repetition rate and to transfer the ultrasound energy to the transceiver 10A. The system also includes a processor that may be configured to process reflected ultrasound energy that is received by the transceiver 10A to produce an image of the scanned anatomical region. Accordingly, the system generally includes a viewing device, such as a cathode ray tube (CRT), a liquid crystal display (LCD), a plasma display device, or other similar display devices, that may be used to view the generated image. The system may also include one or more peripheral devices that cooperatively assist the processor to control the operation of the transceiver 10A, such a keyboard, a pointing device, or other similar devices. In still another particular embodiment, the transceiver 10A may be a self-contained device that includes a microprocessor positioned within the housing 18 and software associated with the microprocessor to operably control the transceiver 10A, and to process the reflected ultrasound energy to generate the ultrasound image. Accordingly, the display 16 may be used to display the generated image and/or to view other information associated with the operation of the transceiver 10A. For example, the information may include

alphanumeric data that indicates a preferred position of the transceiver 10A prior to performing a series of scans. In yet another particular embodiment, the transceiver 10A may be operably coupled to a general-purpose computer, such as a laptop or a desktop computer that includes software that at least partially controls the operation of the transceiver 10A, and also includes software to process information transferred from the transceiver 10A, so that an image of the scanned anatomical region may be generated. The transceiver 10A may also be optionally equipped with electrical contacts to make communication with receiving cradles 50 as illustrated in FIGURES 3 and 4 below. Although transceiver 10A of FIGURE 1A may be used in any of the foregoing embodiments, other transceivers may also be used. For example, the transceiver may lack one or more features of the transceiver 10A. For example, a suitable transceiver need not be a manually portable device, and/or need not have a top-mounted display, and/or may selectively lack other features or exhibit further differences.

[0074] FIGURE 1B is a graphical representation of a plurality of scan planes that form a three-dimensional (3D) array having a substantially conical shape. An ultrasound scan cone 40 formed by a rotational array of two-dimensional scan planes 42 projects outwardly from the dome 20 of the transceivers 10A. Other transceiver embodiments of transceiver 10A may also be configured to develop a scan cone 40 formed by a rotational array of two-dimensional scan planes 42. The pluralities of scan planes 40 may be oriented about an axis 11 extending through the transceivers 10A-B. One or more, or preferably each of the scan planes 42 may be positioned about the axis 11, preferably, but not necessarily at a predetermined angular position θ. The scan planes 42 may be mutually spaced apart by angles θ_1 and θ_2. Correspondingly, the scan lines within each of the scan planes 42 may be spaced apart by angles ϕ_1 and ϕ_2. Although the angles θ_1 and θ_2 are depicted as approximately equal, it is understood that the angles θ_1 and θ_2 may have different values. Similarly, although the angles ϕ_1 and ϕ_2 are shown as approximately equal, the angles ϕ_1 and ϕ_2 may also have different angles. Other scan

cone configurations are possible. For example, a wedge-shaped scan cone, or other similar shapes may be generated by the transceiver 10A.

[0075] FIGURE 1C is a graphical representation of a scan plane 42. The scan plane 42 includes the peripheral scan lines 44 and 46, and an internal scan line 48 having a length r that extends outwardly from the transceivers 10A. Thus, a selected point along the peripheral scan lines 44 and 46 and the internal scan line 48 may be defined with reference to the distance r and angular coordinate values ϕ and θ. The length r preferably extends to approximately 18 to 20 centimeters (cm), although any length is possible. Particular embodiments include approximately seventy-seven scan lines 48 that extend outwardly from the dome 20, although any number of scan lines is possible.

[0076] As described above, the angular movement of the transducer may be mechanically effected and/or it may be electronically or otherwise generated. In either case, the number of lines 48 and the length of the lines may vary, so that the tilt angle ϕ sweeps through angles approximately between -60° and +60° for a total arc of approximately 120°. In one particular embodiment, the transceiver 10 may be configured to generate approximately about seventy-seven scan lines between the first limiting scan line 44 and a second limiting scan line 46. In another particular embodiment, each of the scan lines has a length of approximately about 18 to 20 centimeters (cm). The angular separation between adjacent scan lines 48 (FIGURE 1B) may be uniform or non-uniform. For example, and in another particular embodiment, the angular separation ϕ_1 and ϕ_2 (as shown in FIGURE 1C) may be about 1.5°. Alternately, and in another particular embodiment, the angular separation ϕ_1 and ϕ_2 may be a sequence wherein adjacent angles may be ordered to include angles of 1.5°, 6.8°, 15.5°, 7.2°, and so on, where a 1.5° separation is between a first scan line and a second scan line, a 6.8° separation is between the second scan line and a third scan line, a 15.5° separation is between the third scan line and a fourth scan line, a 7.2° separation is between the fourth scan line and a fifth scan line, and so on. The angular separation between adjacent scan lines may also be a combination of uniform and non-uniform angular spacings, for example, a sequence of

angles may be ordered to include 1.5°, 1.5°, 1.5°, 7.2°, 14.3°, 20.2°, 8.0°, 8.0°, 8.0°, 4.3°, 7.8°, and so on.

[0077] FIGURE 1D a graphical representation of a plurality of scan lines emanating from a hand-held ultrasound transceiver forming a single scan plane 42 extending through a cross-section of an internal bodily organ. The number and location of the internal scan lines emanating from the transceivers 10A within a given scan plane 42 may thus be distributed at different positional coordinates about the axis line 11 as may be required to sufficiently visualize structures or images within the scan plane 42. As shown, four portions of an off-centered region-of-interest (ROI) are exhibited as irregular regions 49. Three portions may be viewable within the scan plane 42 in totality, and one may be truncated by the peripheral scan line 44.

[0078] FIGURE 2A depicts a partial schematic and partial isometric and side view of a transceiver, and a scan cone array comprised of 3D-distributed scan lines in alternate embodiment of an ultrasound system. A plurality of three-dimensional (3D) distributed scan lines emanating from a transceiver that cooperatively forms a scan cone 30. Each of the scan lines have a length *r* that projects outwardly from the transceivers 10A-10E of FIGURES 1A-1E. As illustrated the transceiver 10A emits 3D-distributed scan lines within the scan cone 30 that may be one-dimensional ultrasound A-lines. The other transceiver embodiments 10B-10E may also be configured to emit 3D-distributed scan lines. Taken as an aggregate, these 3D-distributed A-lines define the conical shape of the scan cone 30. The ultrasound scan cone 30 extends outwardly from the dome 20 of the transceiver 10A, 10B and 10C centered about an axis line 11. The 3D-distributed scan lines of the scan cone 30 include a plurality of internal and peripheral scan lines that may be distributed within a volume defined by a perimeter of the scan cone 30. Accordingly, the peripheral scan lines 31A-31F define an outer surface of the scan cone 30, while the internal scan lines 34A-34C may be distributed between the respective peripheral scan lines 31A-31F. Scan line 34B may be generally collinear with the axis 11, and the scan cone 30 may be generally and coaxially centered on the axis line 11.

[0079] The locations of the internal and peripheral scan lines may be further defined by an angular spacing from the center scan line 34B and between internal and peripheral scan lines. The angular spacing between scan line 34B and peripheral or internal scan lines may be designated by angle Φ and angular spacings between internal or peripheral scan lines may be designated by angle Ø. The angles Φ_1, Φ_2, and Φ_3 respectively define the angular spacings from scan line 34B to scan lines 34A, 34C, and 31D. Similarly, angles $Ø_1$, $Ø_2$, and $Ø_3$ respectively define the angular spacings between scan line 31B and 31C, 31C and 34A, and 31D and 31E.

[0080] With continued reference to FIGURE 2A, the plurality of peripheral scan lines 31A-E and the plurality of internal scan lines 34A-D may be three dimensionally distributed A-lines (scan lines) that are not necessarily confined within a scan plane, but instead may sweep throughout the internal regions and along the periphery of the scan cone 30. Thus, a given point within the scan cone 30 may be identified by the coordinates r, Φ, and Ø whose values generally vary. The number and location of the internal scan lines emanating from the transceivers 10A-10E may thus be distributed within the scan cone 30 at different positional coordinates as required to sufficiently visualize structures or images within a region of interest (ROI) in a patient. The angular movement of the ultrasound transducer within the transceiver 10A-10E may be mechanically effected, and/or it may be electronically generated. In any case, the number of lines and the length of the lines may be uniform or otherwise vary, so that angle Φ sweeps through angles approximately between -60° between scan line 34B and 31A, and +60° between scan line 34B and 31B. Thus angle Φ in this example presents a total arc of approximately 120°. In one embodiment, the transceiver 10A, 10B and 10C may be configured to generate a plurality of 3D-distributed scan lines within the scan cone 30 having a length r of approximately 18 to 20 centimeters (cm). Alternate embodiments of the transceivers 10A-10E may employ gender charger button and related circuitry to serve as a means for informing software algorithms discussed below that ultrasound energy scans arise from either a female or a male patient that is undergoing ultrasound probing.

The gender button provided definitional information that may employs modification to the algorithms to optimize detection and measurement of bladders in males, females that have not undergone hysterectomy procedures, females that have undergone hysterectomy procedures, and small male and female children.

[0081] FIGURE 2B illustrates a transceiver 10C configured with a transducer designed to provide a fan-like conic scan cone 41 utilizing C-mode and B-mode ultrasound modalities. The transceiver 10C projects a series of B-mode scan planes 43A and 43B that oscillate like a pendulum between extremes within the scan cone 41. The B-mode scan planes 43 are derived from a plurality of scan lines similar to scan lines 44, 46, and 48 of FIGURES 1C and D. The pendulum oscillating scan planes 43A and 43B may be arranged substantially at right angles to each other as depicted at axis crossing 47. The oscillating scan planes 43A and/or 43B may define a series of C-scan planes 45 that vary in depth location from the transceiver dome 20. The C-scan planes 45 move from the transducer vanishing point, and the B-scan planes angularly radiate from the transducer vanishing point. For transceiver 10C users, a portion of the bladder taken as a C-mode shape is displayed on the transceiver display 16. The C-scan geometry showed as scan planes 45 present a substantially square-like ultrasound area within the scan cone 41. The C-Scan image information contained within scan planes 45 presents a cross-section view of the ultrasound at a particular depth probed by the transceiver 10C. The C-mode is more representative of a portion of the bladder than the actual whole of the bladder. In this depiction, the C-Scan illustrates a cross-section view of the ultrasound at a particular depth to obtain a targeting image of the bladder. The targeting image is more of a binary image showing the lines and spaces that are inside the bladder versus those that are outside of the bladder. The definition of C-mode image basically is a plane parallel to the face of the transducer to obtain a projection image of the bladder region. The C-mode acquired projection image yields bladder information not confined to simply one a single plane parallel to the transducer surface, but multiple planes denoted as C-scans. In the transceivers 10A/B/C substantially similar to the BVI9400 transceiver product, the C-

mode acquired projection image is binary, and includes a non-bladder region and a bladder region. The bladder region is presented as an interpolated shape that is generated from one side to the opposite side, for example the left most and the right most sides of a valid segmentation, or cut, the bladder region on all planes. A method of acquiring a C-mode final image is described in FIGURE 9D below.

[0082] FIGURE 2C illustrates a partial isometric and schematic view of an ultrasound harmonic bladder scanner system 70 utilizing a transceiver probe 10D and console 74 combination 74. The harmonic bladder scanner system 70 is battery powered and portable and may also be referred to as the BVI9400 BladderScan system. Other embodiments may include line power. The ultrasound transceiver 10D is configured to send out and receive ultrasound RF signals. The received RF is transmitted to console 74. The DSP in console processed the RF information to extract the harmonic ratio as an important feature of each line. Then an artificial neural network is used to classify each line as bladder line or tissue line. The result gradings are integrated with the image processing module for accurate segmentation and volume measurement.

[0083] The transceiver 10D presents a similar transceiver display 16, housing 18 and dome 20 design as transceivers 10A, 10B and 10C, and is in signal communication to console 74 via signal cable 17. The console 74 may be pivoted from console base 72. The console 74 includes a display 76, detection and operation function panel 78, and select panel 80. The detection and operation function provide for targeting the bladder, allow user voice annotation recording, retrieval and playback of previously recorded voice annotation files, and current and previously stored 3D and 2D scans. In the display 76 is screenshot 76 having a targeting icon 79A with cross hairs centered in a cross sectional depiction of a bladder region. Other screen shots may appear in the display 76 depending on which function key is pressed in the function panel 78. A targeting icon screenshot 77B with a plurality of directional arrows may appear and flash to guide the user to move the transceiver 10C to center the bladder. The targeting icon screenshot 77B may also appear on the display 16 of the transceiver 10D. The targeting icon screenshot

77B similarly guides the user to place the transceiver 10D to center the bladder or other organ of interest as the directional indicator panel 22 depicted in FIGURE 1A above. An initial bladder view screenshot 77C may appear in which target icon 79A shows a central bladder region appearing within the cross hairs above the oval shaped pubic bone. In wireless communication via wireless signal 82, the output from the transceiver 10D may be outputted to a wireless hub 84 via wireless signal port 86. The wireless hub 84 also serves to charge batteries 88 for loading into the battery compartment (not shown) of console 74. All the calculations may be performed in the imaging console 74. The 9400-embodiment system 70 does not require a computer or network to complete the harmonic analysis and imaging processing. In other embodiments, the system 70 may utilize the wireless hub 84 as a gateway to transmit transceiver 10D acquired harmonic imaging information in local and Internet systems similar to those described in FIGURES 3 and 4 below.

[0084] FIGURE 3 is a schematic illustration of a server-accessed local area network in communication with a plurality of ultrasound harmonic imaging systems. An ultrasound system 100 includes one or more personal computer devices 52 that may be coupled to a server 56 by a communications system 55. The devices 52 may be, in turn, coupled to one or more ultrasound transceivers 10A and/or 10B and/or 10C, for examples the ultrasound sub-systems 60A-60D. Ultrasound based images of organs or other regions of interest derived from either the signals of echoes from fundamental frequency ultrasound and/or harmonics thereof, may be shown within scan cone 30 or 40 presented on display 54. The server 56 may be operable to provide additional processing of ultrasound information, or it may be coupled to still other servers (not shown in FIGURE 3) and devices. Transceivers 10A/B/C may be in wireless communication with computer 52 in sub-system 60A, in wired signal communication in sub-system 10B, in wireless communication with computer 52 via receiving cradle 50 in sub-system 10C, or in wired communication with computer 52 via receiving cradle 50 in sub-system 10D. The ultrasound system 100 may be adapted for harmonic analysis by employing the console

74 algorithmic functions depicted in the harmonic bladder scanner system 70 of FIGURE 2C into the personal computer devices 52.

[0085] FIGURE 4 is a schematic illustration of the Internet in communication with a plurality of ultrasound systems. An Internet system 110 may be coupled or otherwise in communication with the ultrasound harmonic sub-systems 60A-60D. The ultrasound system 110 may be adapted for harmonic analysis by employing the console 74 algorithmic functions depicted in the harmonic bladder scanner system 70 of FIGURE 2C into the personal computer devices 52.

[0086] FIGURE 5 depicts a flowchart of a bladder detection algorithm 70 employing fundamental ultrasound energies. The 3000 and 6000 transceivers utilize the bladder detection algorithm 70 to obtain bladder volume measurement via a bladder detection module employing B-mode image information for segmentation and subsequent 3D volume computations based on the B-mode segmentation. However, female uterus and/or B-mode image noise may obscure bladder detection accuracy in the 3000 and 6100 series transceivers.

[0087] The fundamental frequency based bladder detection algorithm 70 utilizes a particular embodiment of the transducers 10A-B designated as transducer device model BVI6100. The algorithm 70 describes the segmentation processes defined by computer executable instructions employed in concert with the BVI6100 device. The BVI6100 imaging characteristics are different from another particular embodiment of the transducer 10A-B designated as a BVI3000 device that employs a different computer executable algorithm for bladder detection.

[0088] The fundamental bladder detection algorithm 70 used in the BVI 3000 and 6100 devices begins with process block Find Initial Wall process block 100 using A-mode ultrasound data that incorporates data-smoothing. Find Initial Wall 100 looks for the front and back walls of the bladder illustrated and described in FIGURE 6 below. After the front and back walls are found, a line passing through the center of the bladder is determined in the following process block Find Centroid 142. This center bladder line

is used as a seed from which process block Fix Initial Walls 150 utilizes as illustrated and described in FIGURE 7 below. Fix Initial Walls 150 refines the initial wall points, removes any outliers, and fills gaps in the detected wall location regions. Thereafter, an answer is sought to the query "Bladder or Uterus?" in decision diamond block 160 more fully described and illustrated in FIGURE 8 below. Briefly, "Bladder or Uterus" decision 160 determines whether the detected region is a bladder or a uterus when the gender button on the transceivers 10A-D devices indicate that the scan is for a female. If affirmative for bladder detection, its volume is computed and displayed on the output. This is achieved in algorithm 70 at process block Clear Walls 170, followed by process block Display Volume 188 wherein the volume is displayed on the BVI6100 or its transducer 10A-B equivalents.

[0089] If negative for bladder detection, in other words that a uterus was detected, algorithm 70 continues the calculated volume is cleared and a zero volume is displayed. For a non-uterus region, if the volume is very small, then checks are made on the size of and signal characteristics inside the detected region to ensure that it is bladder and not another tissue. This is achieved in algorithm 70 by securing an answer to the query "Is volume less than 40 ml?" at decision diamond 180. If negative for a volume < 40 ml, algorithm 70 continues to process block Display Volume 188 wherein the volume is displayed on the BVI6100 or transducers similar to transducers 10A-B. If affirmative for a volume < 40 ml, algorithm 70 continues to answer the query "Is it a bladder region?" at decision diamond 184. If negative, algorithm 70 proceeds to Clear Walls 70, and if affirmative, proceeds to Display Volume 188. After Display Volume 188, the Fundamental Bladder Detection algorithm 70 is completed.

[0090] FIGURE 6 depicts a flowchart of the Find Initial Walls sub-algorithm of FIGURE 5. Find Initial Walls 72 process is executed on every A-mode scan line and is subjected to averaging and low-pass filtering using a 15 or 16 sample set beginning with process block 74. Next, a local gradient 76 at process block 76 is computed for each

sample point using a central difference formulation taken for seven samples. The central difference formulation is defined by equations 1-6 (Eq. 1-6) below:

[0091] The standard central difference formula is given in Equation 1:

[0092] Eq. 1 $dx_i = x_{i+1/2} - x_{i-1/2}$

[0093] This formula assumes that the function is defined at the half-index, which is usually not the case. The solution is to widen the step between the samples to 2 and arrive at the equation in Eq. 2.

[0094] Eq. 2 $dx_i = \frac{1}{2}(\bar{x}_{i+1} - \bar{x}_{i-1})$

[0095] The normalization factor is simply the distance between the two points. In

[0096] , the distance separating the two means in the calculation was 1, and in Eq. 2, the step between the two means is 2. The normalization of the gradient by the step size, while mathematically correct, incurs a cost in terms of operation. This operation is neglected in the gradient calculation for the bladder wall detection algorithm with minimal effect: since the same calculation is performed for every data sample, every data sample can have the same error and thus the relative gradient values between different samples remain unchanged.

[0097] To further amplify wall locations, the gradient calculation is expanded to three neighboring points to each side of the sample in question. This calculation is shown in

[0098] Eq. 3. This calculation is simply the sum of three gradient approximations and thus the end result can be 12 times its normal value. This deviation from the true mathematical value has minimal effect since the calculation is the same at each point and thus all the gradient values can be 12 times their usual value. The advantage to using the three neighboring points is that more information about the edge is included in the calculation, which can amplify the strong edges of the bladder and weaken the false-edges caused by the noise process in the image.

[0099] Eq. 3 $dx_i = \bar{x}_{i+3} + \bar{x}_{i+2} + \bar{x}_{i+1} - \bar{x}_{i-1} - \bar{x}_{i-2} - \bar{x}_{i-3}$

[00100] The full calculation is written in

[00101] Eq.4. The first line shows the summation calculation to obtain the means, and the difference operations to obtain the gradient. The entire sum is normalized by 15, the number of points included in each local mean. The second line of the operation shows the result when the summations are simplified, and represents the maximal implementation of the calculation. This calculation incurs a cost of 23 additions or subtractions, 2 floating-point multiplications, 1 floating point division, and at least 1 temporary variable. This operation cost is incurred for 91% of the data samples.

[00102] Eq.4

$$dx_i = \frac{\sum_{j=i+3-7}^{j=i+3+7} x_j - \sum_{j=i-3-7}^{j=i-3+7} x_j + \sum_{j=i+2-7}^{j=i+2+7} x_j - \sum_{j=i-2-7}^{j=i-2+7} x_j + \sum_{j=i+1-7}^{j=i+1+7} x_j - \sum_{j=i-1-7}^{j=i-1+7} x_j}{15}$$

$$= \frac{x_{i+10} - x_{i-10} + x_{i+5} - x_{i-5} + 2\left(x_{i+9} - x_{i-9} + x_{i+6} - x_{i-6}\right) + 3\left(x_{i+8} - x_{i-8} + x_{i+7} - x_{i-7}\right)}{15}$$

[00103] The cost of the calculation can be reduced by not simplifying the summations and using a running sum operation. In that manner, only one mean needs to be calculated for each point, but that mean needs to be for the i+3 point. The running sum calculation uses the previous sum, and then corrects the sum by subtracting the old "left hand" end point and adding the new "right hand" end point. The operation is shown in

[00104] Eq. 5. This running sum operation incurs a cost of 5 additions and subtractions.

[00105] Eq. 5 $\bar{x}_{i+3} = \sum_{j=i+3-7}^{j=i+3+7} x_j = \bar{x}_{i+3-1} - x_{i+3-8} + x_{i+3+7} = \bar{x}_{i+2} - x_{i-5} + x_{i+10}$

Since the running sum was calculated for the i+3 point, all average values are available for the gradient calculation. This calculation is shown in Equation 6:

[00106] Eq. 6 $dx_i = \frac{-\bar{x}_{i-3} - \bar{x}_{i-2} - \bar{x}_{i-1} + \bar{x}_{i+1} + \bar{x}_{i+2} + \bar{x}_{i+3}}{16}$

[00107] This equation has the same form as the one in

[00108] Eq. 3 except for the normalization factor of 16. This normalization factor is not a result of the gradient operation, but rather it is the normalization factor mean calculation. The factor of 16 is used instead of the standard value of 15 that one

would expect in a 15-point average for this simple reason: using a factor of 16 eliminates floating-point division. If the means are normalized by 16, then the division operation can be replaced by a "right"-shift by 4 at a significantly lower cost to the embedded system. Therefore the gradient operation has eleven additions and subtractions and one shift by 4.

[00109] Adding the operational cost of the running sum calculation gives an overall cost of 16 additions and subtractions and the shift. The clear victory in this simplification is the elimination of multiplication and division from the operation.

[00110] Returning to FIGURE 6, the results from local gradient 76 is the subjected to loop limit processing between blocks 80 and 94 to obtain the best front wall and back wall pair for each scan line denoted as a tissue gradient or tissue delta. The best front wall and back wall pair on each line is defined as the front wall and back wall pair for which the pixel intensity difference in the back wall gradient and front wall gradient is the maximum and the smallest local average between front wall and back wall pair is the minimum.

[00111] The loop limit processing begins with loop limit block 80 that receives pixel values for each sample in the detection region and subjects the pixel intensity values to determine whether the gradient is minimum at decision diamond 84. If affirmative, then the pixel values are ascertained whether it s the best front wall-back wall (FW/BW) candidate combination at decision diamond 86. If affirmative, the FW/BW candidate pair is saved and loop limit processing returns to limit block 80. If negative, at process block 88, the Front Wall pixel value is saved and another back wall candidate is sought with a subsequent return to loop limit block 88.

[00112] Returning to decision diamond 84, if the answer is negative for "Is gradient Minimum?, sub-algorithm 72 continues to decision diamond 92 to determine whether the back wall and the gradient is maximum. If affirmative, at process block 90, a candidate BW/FW pair is established and sub-algorithm re-routes to loop limit block 80.

If negative, the end of analysis for a particular FW/BW candidate occurs at loop limit block 94 either routes back to the limit loop block 80 or exits to find centroid 100.

[00113] Formulations relating to Find Centroid 100 are based on coordinate geometries described in equations 7 and 8 utilizing coordinate conversions. The coordinate conversions are shown in

[00114] Eq. 7 where 38 is the index of the broadside beam (the ultrasound ray when ϕ=0), ϕ is the index of the line, θ is the angle of the plane. The plane angle is shifted by π to ensure that the sign of the x and y coordinates match the true location in space.

[00115] Eq. 7
$$\begin{aligned} x &= (38-\phi)\cos(\pi-\theta) \\ y &= (38-\phi)\sin(\pi-\theta) \end{aligned}$$

[00116] The trigonometric functions can be calculated for a table of θ values such that the cosine and sine calculations need not be performed for each of the points under consideration. The closest plane can be found by finding the shortest vector from each plane to the centroid. The shortest vector from a plane to a point can be the perpendicular to the projection of the centroid on the plane. The projection of the centroid on the plane is defined as the dot product of the centroid vector, **c**, with the plane definition vector, **a**, divided by the length of the plane definition vector. If the plane definition vector is a unit vector, then the division operation is unnecessary. To find the perpendicular to the projection, it is sufficient to subtract the projection vector from the centroid vector as shown in Eq. 8:

[00117] Eq. 8
$$\left\|\mathbf{c}-proj_{\mathbf{c}}\mathbf{a}\right\|^2 = \left\|\mathbf{c}-\frac{\mathbf{c}\bullet\mathbf{a}}{\left\|\mathbf{a}\right\|^2}\right\|^2$$

[00118] The length of these projections can be found by calculating the Euclidean norm for each line. The Euclidean norm is more commonly known as the length or magnitude of the vector. To find the plane closest to the centroid, calculate the

lengths for the perpendicular to the projection of the centroid on each plane, and take the plane with the shortest of these lengths.

[00119] FIGURE 7 depicts a flowchart of the Fix Initial Walls sub-algorithm 104 of FIGURE 5. Fix Initial Walls 104 is responsible for refining the initial wall points, removing any outliers, and filling any gaps in the wall locations. The FixInitialWalls 104 operates on a plane-by-plane basis with the first plane to be processed being the one that is closest to the centroid of the initial walls and then the planes are processed moving in either direction of that plane. The FixInitialWalls 104 step starts with processing block 106 for correcting the "center line" in terms of where the "center line" is defined as the line on that plane with the maximum gradient difference between front wall and back wall. The correction of the front wall and back wall location at any line is carried out by a matched filtering-like step where the best location within a search limit is defined as the one for which the difference between points immediately outside the bladder and points immediately inside the bladder is maximum. Next, at process block 108, for 5 central lines, the back wall intensity is computed and if this intensity is less than expected noise at that depth, the lines are cleared and the algorithm proceeds to the next plane. At decision diamond 110, an answer to the query "Is BW level less than noise?" is sought. If affirmative, Wall data is cleared at process block 112, and fix initial walls 104 exits to decision diamond 160, "Bladder or Uterus"? If negative, then at process block 114, 3 central lines are fixed. This is followed by block 116 to continuously correct two lines on either side of the central lines using a line-fitting algorithm to set the line index to center –2. A missing line of data may be filled by the algorithm and any outliers are removed. Thereafter the results from continuous correction block 116 is then subjected to loop limit processing between blocks 118 and 140 to obtain the best front wall and back wall pair for each scan line denoted as a tissue gradient or tissue delta. The best front wall and back wall pair on each line is defined as the front wall and back wall pair for which the pixel intensity difference in the back wall gradient and front wall gradient is the maximum and the smallest local average between front wall and back wall pair is the minimum.

[00120] The loop limit processing begins with loop limit block 118 that receives pixel values for each sample in the detection region and subjects the pixel intensity values to prepare a wall location adjustment at subsidiary loop limit 120. The wall is adjusted at block 122 and forwarded subsidiary loop limit 124. The value obtained at loop limit 124 is compared with the line index while valid loop limit 118 by checking wall growth at block 126 and consistency at block 128. Thereafter, at decision diamond 130, an answer is sought to the query If the FW and BW pair provides a "Working Left Half Plane (LHP)" of a given scan plane undergoing analysis. If affirmative, at process block 132 a decrement line index is done, followed by a query "If line index is invalid" at decision diamond 134. If invalid, then at block 136, the line is reset 2 spaces from center, results forwarded to end loop limit 140, and fix initial walls 104 is completed and exits to decision diamond 160, "Bladder or Uterus". If valid, results are forwarded to end loop limit 140 for exiting to decision diamond 160. Returning to decision diamond 130, if the answer is negative for a working LHP, the line is incremented and forwarded to end loop limit 140, and fix initial walls 104 is completed and exits to decision diamond 160, "Bladder or Uterus".

[00121] FIGURE 8 depicts a flowchart of the Bladder or Uterus decision diamond of FIGURE 5. In the "Bladder or Uterus?" decision diamond 160 of FIGURE 5, entering from either Clear Wall Data process block 112 or End while valid line process block 140, the pixel values are ascertained whether the Enhancement is less than the MaxE at decision diamond 162. If negative for enhancement > MaxE, the cavity being detected is a bladder and decision diamond 160 is completed and exits to processing block Clear Walls 170. If affirmative that Enhancement < MaxE, then an answer is sought to the query "Is volume less than MaxV1?", a maximum first volume, at decision diamond 164. If affirmative, then cavity being measured is a uterus and decision diamond 160 is completed and exits to "Is volume < 40 ml?" decision diamond 180. If, at decision diamond 164, it is negative to the statement "volume < MaxV1", then an answer is sought to the query "Is volume less than MaxV2?", a maximum second volume, at

decision diamond 166. If negative, the cavity being detected is a bladder. If affirmative, then an answer is sought to the query "Is volume less than MaxV1?", a maximum first volume, at decision diamond 164

[00122] FIGURES 9A-F schematically illustrate algorithm flow charts of a BVI9400 bladder detection algorithm in the BVI9400 transceiver substantially similar to transceiver 10C of FIGURE 2B. Other particular embodiments of the BVI9400 transceiver may be configured to be substantially equivalent to transceivers 10A and 10B respectively depicted in FIGURES 1A-D and FIGURE 2B. The BVI9400 utilizes a 9400 series transducer that is more powerful and can achieve a duo format task of acquiring C-mode and B-mode based images with RF information collection and processing as described for FIGURES 9A-D. The B-mode image also renders higher resolution than the images produced by the 3000 and 6400 transceivers.

[00123] FIGURE 9A depicts a flowchart of a harmonic bladder detection algorithm 200 employing harmonic ultrasound energies. The harmonic bladder detection algorithm 200 begins by targeting block 202 in which the bladder is initially and approximately detected by C-mode ultrasound. A diagrammatic example of C-mode targeting is shown in FIGURE 2B above in which a substantially square-like imaging plane is depicted. Transceivers 10A-B-C are placed against the patients lower abdominal area above the symphysis pubis (see FIGURE 16 below), the cartilaginous joint located between the two pubic bones. The transceiver dome 20 is immersed into a sonic gel previously applied to the dermis of the patient above the symphysis pubis. A view sufficient to visualize and/or analyze the bladder is obtained. The view is guided by the directional arrows 22 depicted in FIGURE 1A to center the bladder in the display 16 of the transceivers 10A-B-C or other display or monitor similar to monitor 54 in signal communication with the transceivers 10A-B-C. Bladder image views devoid of the pubic bone may be acquired as described below. Once a sufficient view of the bladder is obtained by transceivers 10A-B-C, harmonic algorithm 200 continues to acquire block 208 in which an intermediate shape of the targeted bladder is acquired using harmonic

frequency analysis and scan line classification via a Neural Network Grading Algorithm to establish final bladder shape. Scan planes similar to 44, 43A, 43B, and 45 depicted in FIGURES 1B-D, and 2B are acquired by the transceivers 10A-B-C using A-mode scan lines similar to those depicted in FIGURES 1D. Echoes returning from the bladder region are captured by the transceivers 10A-B-C and echoic signals there from are conveyed to computers 52 configured to signal process the echoic signals by harmonic processes. Thereafter, once the final C-scan targeted bladder image is obtained, the bladder measurements are calculated and reported from the final bladder shape at process block 290 to complete the harmonic bladder detection algorithm 200.

[00124] FIGURE 9B depicts an expanded flow chart of the acquire intermediate bladder shape sub-algorithm 208 of FIGURE 9A. In algorithm 208, intermediate shapes of organ cavities, i.e. the bladder is obtained. The algorithm draws the C-scan (or C-Mode) view of the bladder. The C-scan geometry is shown in Figure 2B above and presents a substantially square ultrasound plane substantially perpendicular to the longitudinal projection the scan cone 41. The C-Scan presents a cross-section view of the ultrasound at a particular depth. In the case of the C-mode it is more representative for the bladder than an accurate depiction of the bladder. It is more of a binary image showing the lines and spaces that are inside the bladder versus those that are outside of the bladder. The output of figure 9B is the bladder segmentation and serves as the input to FIGURE 9D below. The intermediate bladder shape sub-algorithm 208 includes harmonic find walls block 210, establish final shape of targeted bladder block 280, and confirm location of targeted bladder process block 284.

[00125] FIGURE 9C depicts an expanded flow chart of the Harmonic Find Walls process block 210 of FIGURE 9B. Entering from C-mode Targeting block 204, Harmonic Find Walls 210 begins with Radio Frequency B-mode Ultrasound acquisition block 70 described in FIGURE 70 above, and includes variations of theta and phi rotation angle information from blocks 212 and 214. Thereafter, initial bladder walls block 216 is utilized to obtain front and back wall candidates similar to process 72 of FIGURE 6. This

is followed by Frequency analysis block 220 in which ultrasound RF signals are analyzed for their fundamental and harmonic frequency content. Then, at process block 224, the harmonic signals of the scan lines are analyzed for their likelihood of being classified as a cavity residing or non-cavity residing scan lines using a Neural Network Grading algorithm. Thereafter, the classified cavity residing or bladder residing scan lines are judged to constitute a validly segmented cavity or bladder region in a Grading to Cuts block 236. Using the valid segmentations or cuts, an intermediate cavity or bladder shape is obtained at process block Intermediate Shape 240. Thereafter, at decision diamond 250, answers to the query "Last Plane?" is sought. If negative, different theta and Phi rotation values are selected respectively from process blocks 212 and 214 for another cycle through process blocks 70-240. If affirmative, then harmonic find walls algorithm 210 routes to fix bladder Walls block 104 to undergo the processing described in FIGURE 7. Thereafter, a median filter 260 is applied to the intermediate shaped image to which a use gender information algorithm is applied at process block 262. Thereafter, the volume of the bladder or cavity is calculated at block 274 and the Harmonic Find Walls sub-algorithm is completed and exits to process block 280, establish final shape of targeted bladder of FIGURE 9B.

[00126] FIGURE 9D depicts an expansion of the Neural Network Grading sub-algorithm used for intermediate C-mode shape generation of process block 224 of FIGURE 9C. The output of this Neural Network classifier not only helps determine the C-mode shape, but also helps segmentation of the bladder region in each plane and finally it will sharpen the bladder volume measurement. The final C-mode shape generation algorithm 216 is used to draw the C-scan (or C-Mode) view of the bladder. The C-scan geometry is shown in Figure 2B as scan planes 45 having a substantially square-like ultrasound area within the scan cone 41. The C-Scan image information contained within scan planes 45 presents a cross-section view of the ultrasound at a particular depth probed by the transceiver 10C. In the case of the C-mode is more representative of a portion of the bladder than the actual whole of the bladder. It is more of a binary image showing the

lines and spaces that are inside the bladder versus those that are outside of the bladder. FIGURES 23-26 represent various stages of C-mode shape generation algorithm 216. The Neural Network algorithm 224 (NNA 224) is parametric and is used to determine the statistical likelihood that a give scan line passing through a bladder or cavity appearing region does pass through a bladder or cavity. Its weights are all the parameters which are calculated by pre-training. This training is to describe how a classifier learns to make correct classification using preclassified results and corresponding features, which include harmonic ratio at one important feature. Then, a statistical likelihood expressed or termed as line grading represents the output of the NNA 224. The neural network algorithm 224 employs the harmonic analysis kernel described in the appendix and provides a better estimation of scan line grading, prediction, or likelihood that a given scan line is a bladder scan line. The NNA 224 is representative of the workings of cranial neurons where one neuron accepts inputs from millions of other neurons at one layer, then sends an output signal to millions of other neurons and eventually after enough layers of neurons work together to develop a meaningful pattern. The NNA 224 examines parameters that affect its accuracy to perform scan line classification via its predictive functioning. The factors are examined within a Neural Network classifier that predicts how variation in separate factors, or the collective effects of several or all factors that are examined, affect the ability to accurately predict scan line classification, either as a bladder scan line, a non-bladder scan line, and/or a combination bladder and non-bladder scan line.

[00127] The NNA 224 represents a summation of the signals (represented by lines) entering a plurality of neural circles from Frequency Analysis process block 220 depicted in FIGURE 9C. The neural circles in the first column denote respectively the informational content concerning of harmonic ratios, tissue delta (gradient at front wall and back wall locations), minRsum, front wall location (FW location), and back wall location (BW location). The neural circles on the second column are the hidden units, the number of which can be adjusted. We choose 5 hidden units for this case. Each connection between neural circle is assigned a weight, which is, as mentioned before,

based on pre training. The grading or likelihood estimation may be a linear combination of the inputs from process block frequency analysis 220. The relative contributions of the inputs can be varied enough to provide more fidelity in developing a grading system that can be used to make a decision. Spectral estimation algorithms used to provide improved spectral estimation results include parametric and nonparametric. Parametric approaches are more sensitive to data modeling errors and so are incorporated in the NNA 224 to foster accurate organ delineation or organ cavity delineation, for example the bladder, and is based on a sub-aperture processing strategy employing a deconvolution process.

[00128] The Neural Network Algorithm 224 combines harmonic features with B-mode image properties. The method is basically a pre-trained 5 by 5 by 1 Neural Network with different features as inputs and a single grading [0 - 1] as output. For each scan line, after initial walls are estimated based on gradient information, the corresponding features can be computed and the grading value from this network can show how likely the current line is a bladder line. If the grading is low, that means the current line is very likely a tissue line. The initial walls may be wrong or there should be no walls at all. If the grading is high, that means the current line is very likely a bladder line. The initial walls may be correct. The Neural Network algorithm advantageously uses exponential calculation in a logistic function [logistic (x) = 1.0/(1+exp(-x))]. In the digital signal processing (DSP), a lookup table is used to give a fast implementation. For more details about the Neural Network training, please refer to the Appendix.

[00129] In order to get the exact values for all the weights in the network, a training protocol is incorporated into the system to give correct grading based on different inputs. The training procedure for the NNA 224 includes collecting clinical data on human subjects acquired under B-mode ultrasound procedures. From the collected clinical data, a bladder line known to pass through the bladder region is manually selected, and a non-bladder line known to pass through a non-bladder region is selected. The manually picked bladder line is given a grading or probability of 1, and the manually picked non-bladder line is given a grading or probability of 0. From these known

extremes, the NNA 224 generates grading or probability values that a given scan line from the clinical data is a bladder scan line. Then the graded values of all the lines are other features pertaining to the features to train the network using NNA-based Perceptron Learning Rules. Perceptron Learning Rules encompass protocols that allow neural networks to solve classification problems involving weighted sums of a signal matrix so as to ascertain or learn via modification of the weights and biases of a network. In so doing the Perceptron Leaning Rules function as a training algorithm to solve pattern recognition of cavity residing scan lines (i.e., bladder) from the pattern recognition of non-cavity residing scan lines (i.e., non-bladder). The learning algorithms may comprise supervised learning by inputting a set of scan line signal in a training set of output examples, reinforced learning of outputs generated from a set of input scan line signals, or unsupervised learning in which clustering operations are applied to inputted scan line signals. After the training procedure converges, the weights are decided.

[00130] Applying the NNA 224 to the harmonic information improves the volume measurement accuracy and help user locate bladder regions faster by optimizing segmentation accuracy of the bladder region. With the harmonic information, the validity of the segmentation or detection of bladder walls on each scan line is determined. The scan line grading from the Neural Network Algorithm 224 provides a more robust and accurate approach to obtain bladder volume calculations.

[00131] FIGURE 9E depicts an expansion of the Interpolate shape sub-algorithm 240 of FIGURE 9C. Entering from Grading to Cuts block 236, Interpolate shape 240 begins with seeking answers to the query "Is segmentation empty?" in decision diamond 242. If affirmative, the interpolated shapes are outputted at block 256 and algorithm 250 is completed and returns to Last Plane decision diamond 258 of Figure 9C. If negative, algorithm 250 routes to process block Re-compute corresponding radius and angle of valid cuts 250, followed by smooth computed radiuses at block 252, then linearly interpolate the smooth wall cuts at block 254, then finally output interpolated shape at

block 256 for exiting Interpolate Shape algorithm 240 to return to Last Plane decision diamond 258 of Figure 9C.

[00132] FIGURE 9F depicts an expansion of the Gender Information sub-algorithm 262 of FIGURE 9C. Entering from Medium filter block 260, Gender information 262 begins with seeking answers to the query "Is gender female?" in decision diamond 264. If negative, algorithm 262 is completed and returns Calculate Bladder Volume 276 of Figure 9C. If affirmative, algorithm 262 routes to process block Determine Searching Range for Ridge based on Front Wall and Back Wall (FW/BW) intensities at process block 266. Once the ridge is found, at process block 266, the intensities of the ridge are subjected to a computation to determine the maximum running sum for the ridge range. Thereafter, answers are sought to the query "Does FW/BW location correspond to maximum running sum of a valid ridge?" in decision diamond 268. If negative, gender information 262 is completed and exits to calculate bladder volume 276. If affirmative, gender information 262 routes to adjust the front wall and/or the back wall locations at process block 272 to complete gender information 262 and exiting to calculate bladder volume block 276 of Figure 9C.

[00133] Transceivers not having harmonic functionality utilize a BVI3000 algorithm. In the BVI3000 algorithm, the FindWalls() step, which also includes a smoothing step, is run on the A-mode data and leads to candidate front wall and back wall pairs. The MassageWalls() and Plane2planeCorrelation() steps refine the candidate walls, and finally the tissue discrimination step distinguishes between a bladder and a uterus.

[00134] The FindWalls() process starts with a low pass filter of the data to smooth the data and remove the noise. Next, on each A-mode line the minimum filtered value is determined. After finding the minimum point, the back wall location is then determined using the decision criteria shown in the box and then the front wall location is determined. As a final step, to accept the front wall and the back wall candidate the total energy between front wall and the back wall should be less than a threshold value.

[00135] In the tissue discrimination step checks are made to ensure that the uterus is not detected in the scans and that the tissue detected is indeed the bladder. The most significant features that are actually being used for bladder verses uterus determination in this algorithm are the valley mean and detected area on a single plane.

[00136] Next, using these initial front walls and back walls, a line passing through the center of the bladder is determined. This center bladder line is used as a seed from which the FixInitialWalls() stage of the algorithm starts. This stage of the algorithm is responsible for refining the initial wall points, removing any outliers, and filling any gaps in the wall locations. The next step in the algorithm tries to answer the question of whether the detected region is a bladder or a uterus – this step is executed only when the gender button on the device indicates that the scan is for a female. If the region is indeed found to be a uterus, it is cleared and a zero volume is displayed. For a non-uterus region, if the volume is very small, then checks are made on the size of and signal characteristics inside the detected region to ensure that it is bladder and not another tissue. If a region is indeed a bladder, its volume is computed and displayed on the output.

[00137] The BVI6100 algorithm uses several parameters or constant values that are plugged into the algorithm formulas to detect and measurement organ structures and organ cavities. The values of these parameters for the DCD372 and the DCD372A platform are summarized in Table 1:

[00138] The parameters used for uterus detection depend on software versions utilized to signal process scan data received from transceivers 10A-B, encompassing its variants that define particular embodiments of the 3000, 6000, and 9000 series, including BVI models 3100, 6400, and 9400. The parameters 372 Value and the 372A Value (in Table 1 below), and the 9400 Value (in Table 2 below) relate to the definition of a plane in geometry is $Ax + By + Cz + D = 0$. Particular values of A, B, C, and D can define a particular plane detected by a given transceiver 10A-B design. The values of the parameters allow tuning the functioning of a given transceiver 10A-B design in acquiring harmonic frequency based imaging data, scan line grading, and the ability to improve

segmentation accuracy based on harmonic imaging and to improve uterus detection and exclusion to minimize it masquerading as a bladder.

Table 1: Parameters for transceivers series 3100 and 6400:

Parameter Name	Description	372A Value	372 Value
MAXGRAD	Minimum gradient for back wall – Used in Find Initial Walls	16	8
MINGRAD	Maximum gradient for front wall – Used in Find Initial Walls	-10	-8
WINDOWLENGTH	The length of the smoothing window – Used in Find Initial Walls	16	15
NORMALFACTOR	The normalization factor to shift gradient values – Used in Find Initial Walls	4	4
EDGELINESTOCLEAR	Number of lines at the edges to clear – Used in CleanWalls function.	0	2
MINGRAYLEVEL	Unused.	NA	NA
MINDYNAMICRANGE	Unused.	NA	NA
DOMEREVERBDEPTHMM	Unused.	NA	NA
OVERLAPTHRESHOLD	Unused.	NA	NA
WALLDETECTIONLIMIT	Number of samples at start and end of scanline in which bladder cannot exist.	40	20
GRADIENTWINDOWLENGTH	The width of the gradient central difference gradient window. Used in Find Initial Walls.	3	Unused
MINGRADIENTDELTA	Used towards the end of the algorithm to reject abdominal muscle	100	80

Parameter Name	Description	372A Value	372 Value
	in small bladders.		
MINBWWIDTH	Minimum backwall thickness in samples – used in Fix Walls – FindBackWall function.	3	3
MINBWINTENSITY	Minimum backwall intensity - used in Fix Walls – FindBackWall function.	30	16
MINBLADDERWIDTH	Minimum width between fw and bw in samples – used at the end to reject small bladders.	15	8
MAXMINIMUMRUNSUM	The maximum value for the minimum running sum for a FW/BW candidate pair. Used in Find Initial Walls.	254	190
MAX_VOLUME1_UTERUS	The lower limit test for volume to call uterus	96	70
MAX_VOLUME2_UTERUS	The upper limit test for volume to call uterus	200	130
MAX_ENHANCEMENT_UTERUS	The maximum enhancement at the back wall for a uterus.	44	27
MIN_VALLEYMEAN_UTERUS	The minimum valley mean inside the uterus	17	11

[00139] The algorithms operating within the 9400 transceivers 10A-B utilize harmonic based imaging data and neural network processing illustrated for the NNA 224 in detecting bladders. The BVI9400 describes the segmentation algorithm used in the BVI9400 ultrasound transceiver device equipped with ultrasound harmonic functionality.

The BVI9400 is equipped with harmonic analysis functionality to improve segmentation accuracy base on the neural harmonics described below.

[00140] In general, BVI3000 and BVI6100 algorithmic methods extract gradient information from fundamental frequency ultrasound echoes returning along scan lines transiting through the bladder region. However, artifacts like reverberations, shadows and etc degrade ultrasound images. Therefore, the corresponding gradient information in B-mode images, in some cases, may be incomplete and lead to inaccurate bladder detection and subsequent measurement. Improving and making more accurate bladder diction and volume measurements by completing incomplete gradient information is achieved by the algorithmic signal processing applied to harmonic frequency ultrasound echoes returning along scan lines transiting though the bladder region. Harmonic analysis provided in the BVI9400 algorithm and device provides a solution. The method is very similar as the FindInitialWalls() phase of the BVI6100 algorithm but uses different parameter constant values described in Table 2:

[00141] Table 2. BVI9400 Parameters. The parameters used for uterus detection depend on software versions utilized to signal process scan data received from transceivers 10A-B.

		Value		
Parameter Name	**Description**	**372A**	**372**	**9400**
MAXGRAD	Minimum gradient for back wall – Used in Find Initial Walls	16	8	10
MINGRAD	Maximum gradient for front wall – Used in Find Initial Walls	-10	-8	-8
WINDOWLENGTH	The length of the smoothing window – Used in Find Initial Walls	16	15	16
NORMALFACTOR	The normalization	4	4	4

		Value		
Parameter Name	**Description**	**372A**	**372**	**9400**
	factor to shift gradient values – Used in Find Initial Walls			
EDGELINESTOCLEAR	Number of lines at the edges to clear – Used in CleanWalls function.	0	2	0
MINGRAYLEVEL	Unused.	NA	NA	NA
MINDYNAMICRANGE	Unused.	NA	NA	NA
DOMEREVERBDEPTHMM	Unused.	NA	NA	NA
OVERLAPTHRESHOLD	Unused.	NA	NA	NA
WALLDETECTIONLIMIT	Number of samples at start and end of scanline in which bladder cannot exist.	40	20	40
GRADIENTWINDOWLENGTH	The width of the gradient central difference gradient window. Used in Find Initial Walls.	3	Unused	3
MINGRADIENTDELTA	Used towards the end of the algorithm to reject abdominal muscle in small bladders.	100	80	100
MINBWWIDTH	Minimum backwall thickness in samples – used in Fix Walls – FindBackWall function.	3	3	3
MINBWINTENSITY	Minimum backwall	30	16	10

		Value		
Parameter Name	**Description**	**372A**	**372**	**9400**
	intensity - used in Fix Walls – FindBackWall function.			
MINBLADDERWIDTH	Minimum width between fw and bw in samples – used at the end to reject small bladders.	15	8	15
MAXMINIMUMRUNSUM	The maximum value for the minimum running sum for a FW/BW candidate pair. Used in Find Initial Walls.	254	190	175
MAX_VOLUME1_UTERUS	The lower limit test for volume to call uterus	96	70	NA
MAX_VOLUME2_UTERUS	The upper limit test for volume to call uterus	200	130	NA
MAX_ENHANCEMENT_UTERUS	The maximum enhancement at the back wall for a uterus.	44	27	NA
MIN_VALLEYMEAN_UTERUS	The minimum valley mean inside the uterus	17	11	NA

[00142] Echo signals received from structures in the body carry not only the frequencies of the original transmit pulse, but also include multiples, or harmonics of

these frequencies. Echoes from tissue have predominantly linear components, i.e. e. the echo frequencies are the same as the transmit frequencies. These linear components are used in conventional, fundamental B-mode imaging. Harmonic echo frequencies are caused by non-linear effects during the propagation of ultrasound in tissue.

[00143] FIGURE 10 schematically illustrates sound wave distortion with increasing harmonics. The traditional THI (tissue harmonic imaging) is based on the effect that ultrasound signals are distorted while propagating through tissue with varying acoustic properties. In conventional frequency-based 2nd Harmonic Imaging, the received frequencies are selected to be twice the transmit frequencies. In contrast, the disclosure applicable to the harmonic transceiver embodiments utilizes substantially different methods to obtain harmonic information. The harmonic methods quantify the harmonic change along each RF line as harmonic ratio and we use this ratio to distinguish the media the RF line passes through. This process is made in the frequency domain.

[00144] Harmonic information provides improved image depth information that otherwise would remain hidden in the fundamental frequency domain. The harmonic information provides an effective indicator for harmonic build-up on each scan line at different depth, based on which, bladder lines and tissue lines can be separated. However, inside bladder region, there is not enough reflection. Deep behind the bladder wall, harmonic can be attenuated fast. Then, harmonic information can be most abundant behind the back wall of the bladder. So, the harmonic information around the back wall location, instead using the RF data at a fixed range, is discussed in greater detail.

[00145] Quantification of the harmonic information

[00146] FIGURE 11 illustrates a frequency analysis of an RF2 harmonic that presents a challenge to effectively quantify in tissues more distant from the transceivers 10A-B-C. As illustrated, there are 6 different scan lines. The frequency response is at different levels basically and it is hard to be compared to each other. The different levels are because the different scan lines are through different path with different materials.

[The dot lines in red are the windows defined by back location for harmonic analysis. Red circles are the initial wall locations.]

[00147] FIGURE 12 illustrates a frequency spectra example on how a quantification of harmonic information is made via harmonic ratio. One way to use the harmonic information is to see relative change of the harmonic information around the 2nd harmonic frequency compared with response at fundamental frequency. The ratio of the peak value around the 2^{nd} harmonic and the peak value around the fundamental frequency is a suitable indicator for such change.

[00148] FIGURE 13 illustrates second harmonic ratio distributions corresponding to two types of scan lines, bladder lines and tissue lines. The distributions are based on real clinical data sets. We manually graded all the scan lines in data sets collected from 01-05-2007, including 12males and 1 female. The data sets include pre-void and post-void cases. Totally, there are 20736 scan lines. (8250 for bladder lines, 12486 for tissue lines). We use the manual grading as the ground truth for two different groups of scan lines, bladder lines and tissue lines. We computed the probability density functions (PDF) corresponding to these two different groups of scan lines

[00149] Examples of how scan lines are graded as to likelihood of residing within or separate from a cavity is described by returning to a more explanation of the neural network algorithm 224 (NNA 224) for scan line grading depicted in FIGURE 9D. The neural network algorithm employs a harmonic analysis kernel described in the appendix and provides a better estimation of scan line grading, prediction, or likelihood that a given scan line is a bladder scan line.

[00150] Applying the NNA 224 to the harmonic information improves the volume measurement accuracy and help user locate bladder regions faster by optimizing segmentation accuracy of the bladder region. With the harmonic information, the validity of the segmentation or detection of bladder walls on each scan line is determined. The grading from the Neural Network Algorithm 224 provides more robust information to fix the initial bladder walls.

[00151] How the validity of the segmentation that a given scan line is validly declared a bladder scan line is determined by categorizing the width of scan lines into G and W groups and performing a G & W analysis. Each G or W group defines a width of G and W can be up to the number of lines of ultrasounds in a plane. G represents lines where the neural network grading (including harmonic analysis) indicated the presence of a bladder. W represents the set of lines identified as passing through the bladder based on the original algorithm that's been in use in several generations of devices. The two sets G and W are combined in a way to result in the final set of lines for which the bladder is likely to exist. The final set must include all lines in G if G overlaps W and no lines in W that do not overlap with G.

[00152] An example of the G and W analysis procedure utilizing the harmonic derived grading value includes arranging the G and W lines to make it easier to remove the wrong segmentation line and make it more difficult to add new lines by averaging the non-zero initial wall on current line and the non-zero fixed wall from its neighboring line. This is achieved by adding to the new bladder walls with the large grading values to the nearest valid initial bladder wall pair. Thereafter a region G is defined in which all lines having a grading value higher than the threshold value. To remove the bladder walls having a too small grading value, a region W is defined which is based on the cuts, or the validly segmented regions, obtained from the fixed walls algorithm. Thus for region G and region W, there can be five different cases to consider:

[00153] Case 1. G and W are not overlapped (including empty G or empty W):

remove both

G |----------|

W |----------|

Case 2. G inside W: remove the walls in W, while not in G

G |----------|

W |----------|

Case 3. W inside G: add the walls outside W, while in G

G |----------|

W |----------|

Case 4. G and W are partly overlapped: remove and add

G |----------|

W |----------|

Case 5. G and W are exactly the same: do nothing

G |----------|

W |----------|

[00154] FIGURES 14A-14B illustrate differences in bladder wall segmentations as computed and outlined in light peripheral boundary lines.

[00155] FIGURES 14A illustrates clinical cases of bladder overestimation arising from the use of non-harmonic information. Bladder volume accuracy using non-harmonic information is less as using harmonic method as described for FIGURE 9C. In FIGURE 14A, a panel of twelve sonograms having different inter-scan plane θ values in 15 degree increments between 0 and 165 degrees show examples of bladder overestimation due to non-optimal placement of boundary lines along the bladder cavity and tissue interface. The overestimation is the result using original wall fixing method, without utilizing the harmonic information and neural network grading. The computed result from this segmentation is approximately 145 ml pre-void from a bladder previously measured to have a post-void volume of 15 ml. Thus the expected value less the post-void volume is approximately 130 ml. The urine flow measured was 85 ml, or an overestimation of 45 ml.

[00156] FIGURE 14B illustrates scan line grading to correct for over-estimation of segmented bladder cavity interfaces. The result is based using harmonic ratio and neural network grading for fixing. In this set the computed total bladder volume is approximately 90 ml pre-void, from the bladder determined to have a 3 ml post-void volume. Thus the computed urine volume is approximately 87 ml, for a 2 ml

overestimation. With utilization of the harmonic information and neural network grading, there was a 43 ml (> 90%) reduction in the overestimated computed value.

[00157] FIGURE 15A illustrates scan line grading to correct for under-estimation of segmented bladder cavity interfaces. A panel of twelve sonograms having different inter-scan plane θ values in 15 degree increments between 0 and 165 degrees show examples of bladder overestimation due to non-optimal placement of boundary lines along the bladder cavity and tissue interface. The overestimation is the result using original wall fixing method, without utilizing the harmonic information and neural network grading.. The computed result from this segmentation is approximately 472 ml pre-void from a bladder previously measured to have a post-void volume of 163 ml. Thus the expected value less the post-void volume is approximately 309 ml. The urine flow measured was 520 ml, or an overestimation of 211 ml.

[00158] FIGURE 15B illustrates scan line grading to correct for under-estimation of segmented bladder cavity interfaces. The result is based using harmonic ratio and neural network grading for fixing. Here the computed total bladder volume is approximately 658 ml pre-void, from the bladder determined to have a 159 ml post-void volume. Thus the computed urine volume is approximately 499 ml, for a 21 ml overestimation. With utilization of the harmonic information and neural network grading, there was a 190 ml (~ 90%) reduction in the overestimated computed value.

[00159] FIGURE 16 illustrates a depiction of the anatomical locations of uterus and bladder and other anatomical structures. Other non-bladder structures include the Symphysis Pubis, the ovary, and ovarian tube.

[00160] FIGURE 17 presents a 4-panel scan image set of ultrasound scanned female patients. Bladder detection task is more challenging for female patient due to the presence of uterus. In general, the uterus is adjacent to the bladder region and it has very similar pattern in B-mode image. It is optionally advantageous to exclude the uterus region from the final segmentation. Therefore, the computed volume is the actual urine inside the bladder. Previously, a uterus detection method is proposed in FIGURE 8 for the

6x00 ultrasound transceiver product series. This method is dealing with the whole segmentation after wall detection using volume. In another words, the segmentation is bladder or uterus. However, some times, it is not so simple to refine the result, because the segmentation includes both bladder and uterus. The more reasonable and accurate way to solve the problem is to tell which part in the segmentation belongs to bladder and which part in the segmentation is uterus. The difficulty in determining which part of the segmentation belongs to a bladder or uterus is compounded when the bladder is a small size.

[00161] The uterus can be located side by side with the bladder and it can also be located under the bladder. For the first case, the method we proposed in previous section can be used to classify the scan lines passing through uterus only from the scan lines passing through bladder. However, the method could not solve the second problem. When a scan line is propagating through both bladder region and uterus region, further processing has to be made to find which part on the line belongs to bladder. In the following, we design a new method for excluding uterus from the final segmentation based on gender information.

[00162] FIGURE 18 illustrates one example on how to distinguish the bladder region from the uterus along scan line. If the scan is on a female patient (gender information provided by user), a boundary between uterus and bladder region is observable and the uterus presents itself under the bladder if both regions appear on a scan line. In the B-mode image, for each scan line passing through both regions, a small ridge exists. If the ridge can be found, then both regions can be discerned. The uterus is under the bladder if both regions appear on a scan line. In this B-mode image, each scan line 302 passes through both regions having a small ridge. If the ridge can be found, discernment of it allows delineation of the bladder from the uterus. As shown in FIGURE 18, an observable ridge in the echo histogram 302A derived from scan line 302 is seen between the bladder and uterus of the female patient. This ridge finding procedure can be executed on initial walls or the final walls.

[00163] FIGURE 19 illustrates another example on how to distinguish the bladder region from the uterus along scan line. In this B-mode image, each scan line 306 passes through both regions, having a small ridge between the two regions. If the ridge can be found, discernment of it allows delineation of the bladder from the uterus. As shown in FIGURE 19, an observable ridge in the echo histogram 306A derived from scan line 306 is seen between the bladder and uterus of the female patient.

[00164] FIGURES 20 and 21 presents a series of bladder scan segmentations resulting without using the gender information.

[00165] FIGURES 22 and 23 presents a series of bladder scan segmentations resulting using the gender information. After using the gender information, the incorrectly segmentation can be modified.

[00166] FIGURE 24 presents segmentations presented in polar coordinate form of planes 1-12 and 13-24, with a diagrammatic presentation of the interpolated shapes presented in an all the cuts of a C-mode acquired view. The left most and right most cuts are extracted for the cuts based on segmentation on all planes. The diagrammatic presentation, in color codes, illustrates the interpolated shape, the cuts from after smoothing, and the cuts from the original segmentation. Here the volume of the bladder was estimated to be 256 ml.

[00167] FIGURE 25 presents a 3-D plot of an inconsistency case (upper plot) and a consistency case (lower plot) as a means to check the consistency of the segmentation results. The inconsistency case arises from an abnormal case for bladder segmentation where more than one connected regions are based on the segmentation on all planes. The consistency case reflects a normal case for bladder segmentation, where only one connected region is based on the segmentation on all planes. Theoretically, bladder in the Bladder scan is a single connected 3D volume. Due to different reasons (One optionally advantageous reason is the segmentation algorithm searches for bladder wall blindly plane by plane.), there may be more than one 3D regions and the corresponding bladder walls are also stored in the segmentation results. This step can make a topological

consistency checking to guarantee that there is only one connected region in the C-mode view/

[00168] FIGURE 26 illustrates interpolated shapes before smoothing (top diagram) and after smoothing based on the mass center (bottom diagram). Compute the mass center of all the valid cuts. Re-compute the corresponding radius and angle of every valid cut. Then smooth the radius.

[00169] The Cartesian coordinates are computed for each valid cut and get the mass center. Based on this mass center, compute the corresponding radius and angle of very valid cut. Sort the new angles in ascending order. At the same time align the corresponding radius. In order to smooth the final interpolated shape, we average the radiuses from above result in a pre-defined neighborhood

[00170] FIGURE 27 illustrates the output of interpolated shapes between smoothed cuts before smoothing (top diagram) without interpolation and after linear interpolation (bottom diagram). Output the walls of the interpolated shape.

[00171] FIGURE 28 illustrates a representation of two walls for the interpolated shape. The final output which is used to represent the interpolated shape is stored in two arrays, the size of which is 250. The dimension of the final display is on a 2D matrix, 250 by 250. The two arrays store the upper wall and lower wall location in each column respectively.

[00172] FIGURE 29 showing the different arrow feedback modes of the aiming indicator 22 of transceivers 10A-B-C. The aiming indicator 22 depicted in FIGURE 1A functions equivalently as the targeting icon screenshot 77B depicted in FIGURE 2C in aiding or guiding a transceiver user to position the transceivers 10A-B-C to obtain a centered image of the bladder or other cavity-containing organ. The C-mode view of the interpolated shape. An optionally advantageous application is to provide guidance for the users find the best scanning location and angle. This task is called aiming. Basically, the aiming is based on the segmentation results and it is similar as the C-mode shape functionality. There are two kinds of aiming information, arrow on the probe and the

intermediate shapes: Arrow feedback--Use extra displaying panel on the scanner, 9400 also provides arrow feedback after a full scan. The error feedback is totally based on the C-mode view shape. There are totally 4 different arrow feedback modes. Eight arrows may be used. Which arrow should be used is determined by the location of the mass center of the interpolated shape in C-mode view. Based on the vector between ultrasound cone center and the mass center, the corresponding angle can be computed in a range from -180 degree to +180 degree. The [-180 180] range is divide into 8 parts and each part is corresponding to each arrow.

[00173] FIGURE 30 illustrates a decision tree for the arrow feed back from the indicator 22. This tree describes how the program determines to show flashing arrow or solid arrow on the indicator panel. Here are the descriptions of all parameters we defined in this tree:

inner cone = 0.78radians (~80 degree□)

outer cone = 1.01radians (~116 degree□)

percentCentered = (#lines inside inner cone) / (#lines inside ultrasonic cone)

singleViolation = if any line is outside outer cone

dualViolation = if any plane has lines outside outer cone on both positive & negative phi.

The procedure to determine the arrow displaying can be described as following:

Compute the mass center of the C-mode shape

Calculate the direction based on the mass center location

Check if there is singleViolation (any line is outside outer cone), dualViolation (if any plane has lines outside outer cone on both positive & negative phi) or no singleViolation(all lines are inside outer cone)

Calculate percentCentered and compare it with the 70%threshold to finally determine arrow type if there is no singleViolation or singleViolation.

[00174] As relating to pubic bone detection, arrow feedback provides accurate aiming feedback information, the shadow caused by pubic bone should also be

considered. In the ultrasound image, the only feature associated with the pubic bone is the big and deep shadow. If the shadow is far from the bladder region we are interested in for volume calculation, there is no need to use this information. However, if the shadow is too close to the bladder region, or the bladder is partly inside the shadow caused by pubic bone, the corresponding volume can be greatly influenced. If the bladder walls are incomplete due to the shadow, we can underestimate the bladder volume.

[00175] Therefore, if the user is provided with the pubic bone information, a better scanning location can be chosen and a more accurate bladder volume measurement can be made. We proposed the following method to make pubic bone detection based on the special shadow behind it.

[00176] On each plane, extract the left most and right most location with valid bladder wall, WL and WR. If there is no bladder walls on current plane or the wall width is too small, exit; else go on.

[00177] Compute the average frontwall depth ave_FW.

[00178] Determine the KI_threshold based on the whole image

[00179] From WL ->0 searching for the shadow which is higher than ave_FW +searching_range, if there are more than N shadow lines in a row, record the shadow location WL_S.

[00180] From WR ->nScanlines searching for the shadow which is higher than ave_FW + searching_range, if there are more than N shadow lines in a row, record the shadow location WR_S

[00181] On one plane, it is only possible to have the pubic bone on one side of the bladder region. The starting location of the shadow is used to choose the most probable location for public bone.

[00182] Combine all valid shadow information and generate the location for pubic bone displaying

[00183] In the above procedure, the most optionally advantageous factor is to determine the KI_threshold based on the B-mode images. We utilized an automated

thresholding technique in image processing, Kittler & Illingworth thresholding method. Additional details may be found in the appendix.

[00184] FIGURE 31 illustrates shadow and segmentation regions of the pubic bone. Two examples with pubic bones close to the bladder region are illustrated. For the first one, the shadow is not affecting the volume measurement since the pubic bone is far from the bladder region; for the second case, the shadow is strong since the pubic bone blocks the bladder region partly. Using the pubic icon on the feedback screen, operators are trained to recognize when a new scanning location should be chosen and when not. Also, the symbol ">" may be used when the bladder region is blocked by the pubic bone.

[00185] Intermediate shape. Basically, this step is still to show the C-mode shape. The difference between this step and the final C-mode shape is that this step is only using the grading information from the previous planes and gives instant response to the operator of current scanning status during a full scan. The first step is to use the grading values to find the cuts on current plane: For each plane, there are N scan lines gradings for all lines from previous step; Find the peak value and the corresponding line index; Special smoothing: Find the cuts on each plane: the left and right most line indices with grading values larger than a pre-specified threshold. [default threshold is 0.5]

[00186] FIGURE 32 illustrates examples of grading results derived from Neural Harmonics Algorithms. The grading for all lines in data set 1028 are displayed for scan planes ranging from zero to 165 degrees in 15 degree increments.

[00187] FIGURE 33 illustrates a series of intermediate C-mode shapes generated as a screenshot interface or virtual painting board. The cuts are found on each plane from the grading results shown in Figure 32: the left and right most line indices with grading values larger than a pre-specified threshold. A default threshold of 0.5 may be used. The virtual painting board provides a vehicle to draw lines between the cuts or validly segmented regions of the organ cavity (i.e., bladder cavity) on current planes and cuts from previous planes. Shown are a series of intermediate C-mode shapes on data set 1028.

[00188] FIGURE 34 illustrates segmentation results before and after using reverberation control method. Before we calculate the bladder volume based on the detected front and back walls, another extra step should be made to remove the wrong segmentation due to strong reverberation noise. The disclosed bladder wall detection method has the advantage over previous detection methods in that the grading information can help find the bladder lines as complete as possible. In previous transceiver versions (3000 and 6x00), the bladder wall detection can stop early when strong reverberation noise presents. However, under some circumstances the disclosed bladder wall detection method may not be able to fix the inaccurate segmentation on some lines due to reverberation noises. Some regions in front of and behind the reverberation noise may be lost. After application of the reverberation control method, these regions were recovered as bladder region. Basically, the reverberation method is an interpolation approach using adjacent bladder wall shape in cases when the bladder shape is indeed with large convex part on the front or back wall by defining two parameters (valid_FW_change and valid_BW_change). The reverberation method below provides the capability to remove the small wedges on the bladder walls using the shape information:

[00189] If there is front wall on current line, search for the nearest front wall on the left, which has a front wall valid_FRONT WALL_change shallower than current front wall; search for the nearest front wall on the right, which also has a front wall valid_FRONT WALL_change shallower than current front wall. If the searching is successful on both sides, we use the found front wall pair to generate a new front wall at current location.

[00190] If there is bw on current line, search for the nearest front wall on the left, which has a bw valid_BW_change shallower than current bw; search for the nearest bw on the right, which also has a bw valid_BW_change shallower than current back wall. If the searching is successful on both sides, the found back wall pair is utilized to generate a new back wall at the current location.

[00191] FIGURE 35 illustrates models for volume computation. In order to compute the bladder volume, the following information is optionally advantageous: Spherical coordinate phi and theta, the axial front wall and back wall locations, and the axial resolution. For every scan line except the broadside scan line (phi=0), a spherical wedge shape defined, with the physical scan line passed through the center of the wedge. The spherical wedge is bounded on top by the front wall and on the bottom by the back wall, on the sides by the average of the current scan line spherical angles and the next closest spherical angles (the left image of FIGURE 36). For broadside scan line, a truncated cone is used (the right image of FIGURE 36).

[00192] Clinical results. A large clinical experiment was made to evaluate the performance of the new bladder detection method designed for 9400. Twenty-two data sets were selected from a clinical trail and 38 data sets from another clinical trail, which include both pre-void and post-void cases. Based on the parameters we defined in Table 2 above, the following results are obtained as shown in Table 3:

Table 1: result without using harmonic information

tient	Visit No	Gender	Weight	Uroflow	Pre-Void	Post-Void	Post-Void + Uroflow	error
1002	1/5/2007	Male	175	450	470	28	478	0.017778
1004	1/5/2007	Male	170	230	284	14	244	0.173913
1012	1/5/2007	Male	166	270	262	9	279	0.1
1015	1/5/2007	Male	200	100	51	10	110	0.59
1016	1/5/2007	Male	140	250	345	43	293	0.208
1017	1/5/2007	Male	175	280	361	24	304	0.203571
	1/24/2007	Male	203	85	146	15	100	0.629412
	1/25/2007	Male	205	359	474	12	371	0.266908
	1/25/2007	Male	170	181	125	23	204	0.426464
	1/23/2007	Female	115	443	553	52	496	0.130926
	1/24/2007	Female	140	217	262	44	261	0.004609
	1/25/2007	Female	150	172	238	9	181	0.331395
1049	1/5/2007	Male	190	200	358	19	219	0.695
1051	1/5/2007	Male	162	480	540	39	519	0.04375
1052	1/5/2007	Male	170	310	347	18	328	0.06129
	1/25/2007	Female	180	62	65	18	80	0.241935
	1/23/2007	Female	160	326	337	73	399	0.190184
	1/24/2007	Female	150	167	218	37	204	0.083832
	1/25/2007	Female	130	227	296	36	263	0.145374
	1/24/2007	Female	143	271	160	2	273	0.416974
1068	1/5/2007	Male	185	520	472	163	683	0.405769
	1/23/2007	Male	180	188	114	47	235	0.643617
	1/24/2007	Male	260	249	253	13	262	0.036145
	1/24/2007	Female	189	114	150	28	142	0.070175
	1/24/2007	Female	118	322	468	15	337	0.406832
	1/24/2007	Male	180	345	351	10	356	0.011594
	1/24/2007	Male	150	190	282	24	214	0.357895
	1/25/2007	Female	118	315	355	35	350	0.015873
	1/25/2007	Female	112	226	266	74	300	0.150442

mean error	0.241023
mean error 1	0.249907
mean error 2	0.236347

[00193] FIGURE 36 illustrates a regression analysis result between prevoid bladder volume measurement and the sum of the post void bladder volume measurement and urine volume without harmonic analysis. An R^2 value of 0.7151 is obtained.

[00194] Table 4 is a tabulation of results after using harmonic information processed by the neural network algorithm:

Table 1: result after using harmonic information in Neural Network

Patient ID	Visit No	Gender	Weight	Uroflow	Pre-Void	Post-Void	Post-Void + Uroflow	error
1002	1/5/2007	Male	175	460	429	29	479	0.111111
1004	1/5/2007	Male	170	230	290	4	234	0.243478
1012	1/5/2007	Male	166	270	289	3	273	0.059259
1015	1/5/2007	Male	200	100	54	2	102	0.48
1016	1/5/2007	Male	140	250	286	15	265	0.084
1017	1/5/2007	Male	175	280	352	7	287	0.232143
	1/24/2007	Male	203	85	98	3	88	0.117647
	1/25/2007	Male	205	359	606	12	371	0.376045
	1/25/2007	Male	170	191	195	2	193	0.255193
	1/23/2007	Female	115	443	819	53	496	0.275395
	1/24/2007	Female	140	217	301	18	235	0.317972
	1/25/2007	Female	150	172	233	6	178	0.319767
1049	1/5/2007	Male	190	200	196	19	219	0.115
1051	1/5/2007	Male	162	480	559	56	536	0.047917
1052	1/5/2007	Male	170	310	320	5	315	0.016129
	1/25/2007	Female	180	82	55	7	89	0.225806
	1/23/2007	Female	160	326	339	9	335	0.01227
	1/24/2007	Female	150	167	201	8	175	0.155689
	1/25/2007	Female	130	227	278	13	240	0.167401
	1/24/2007	Female	143	271	242	8	279	0.136531
1068	1/5/2007	Male	185	620	643	176	696	0.101923
	1/23/2007	Male	180	188	173	25	214	0.219095
	1/24/2007	Male	260	249	271	13	262	0.039145
	1/24/2007	Female	189	114	119	11	125	0.052632
	1/24/2007	Female	118	322	406	32	354	0.161491
	1/24/2007	Male	180	345	377	15	360	0.049275
	1/24/2007	Male	150	190	203	13	203	0
	1/25/2007	Female	118	315	308	5	320	0.038095
	1/25/2007	Female	112	236	253	44	270	0.075221

	mean error	0.15488345
For Jan 5 data	mean error 1	0.149096
For Jan 23-25 data	mean error 2	0.15792947

[00195] FIGURE 37 illustrates a regression analysis result between prevoid bladder volume measurement and the sum of the post void bladder volume measurement and urine volume with harmonic analysis and using the neural network algorithm. An R^2 value of 0.9226 is obtained employing harmonic analysis—a much improved correlation than using the fundamental ultrasound frequencies shown in FIGURE 36.

[00196] Table 5 is a tabulation of volume using the BVI3000 device on the same patient just before using the harmonic capable BVI9400 ultrasound transceiver.

Table 1: Jan 23-25 results using BVI3000

Patient ID	Visit No	Gender	Weight	Uroflow	Pre-Void BVI 3000	Post-Void BVI 3000	Post-Void BVI 3000 + Uroflow	3000 error
	1/24/2007	Male	203	85	104	0	85	0.223529
	1/25/2007	Male	205	359	410	0	359	0.142061
	1/25/2007	Male	170	181	141	0	181	0.220994
	1/23/2007	Female	115	443	452	23	466	0.031603
	1/24/2007	Female	140	217	239	0	217	0.101382
	1/25/2007	Female	150	172	154	56	228	0.430233
	1/25/2007	Female	180	62	108	91	153	0.725806
	1/23/2007	Female	160	326	376	30	356	0.058282
	1/24/2007	Female	150	167	166	0	167	0.005988
	1/25/2007	Female	130	227	277	28	255	0.096916
	1/24/2007	Female	143	271	168	0	271	0.306273
	1/23/2007	Male	180	188	187	0	188	0.005319
	1/24/2007	Male	260	249	311	0	249	0.248996
	1/24/2007	Female	189	114	222	0	114	0.947368
	1/24/2007	Female	118	322	304	0	322	0.055901
	1/24/2007	Male	180	345	314	0	345	0.089855
	1/24/2007	Male	150	190	321	0	190	0.689474
	1/25/2007	Female	118	315	339	0	315	0.07619
	1/25/2007	Female	112	226	280	27	253	0.119469
							mean error	0.240823

[00197] FIGURE 38 illustrates a regression analysis result between prevoid bladder volume measurement and the sum of the post void bladder volume measurement and urine volume by the BVI3000 system which is not capable to execute harmonic analysis. An R^2 value of 0.7166 is obtained—a much lowered correlation than to FIGURE 37 above that derives from the harmonic capable BVI9400 transceiver.

[00198] A simple comparison can be made that:

[00199] Using harmonic information in Neural Network decreases the error by 8.61%.(Table 3), 24.10%(Table 4), and 15.49%(Table 5).

[00200] Correlation coefficient after using harmonic in Neural Network is increased by 0.12. (Table 3), [$\sqrt{0.9226}$ (Table 4), and $\sqrt{0.7151}$ (Table 5).

[00201] BVI9400 is more accurate than BVI3000 and the error is decreased by 8.29% (Table 3), 24.08% (Table 4), and 15.79% (Table 5).

[00202] FIGURE 39 presents a comparison of the bladder line classification results between the method using harmonic ratio as a feature and the method without using harmonic ratio as a feature. The comparisons are made multiple times using different classifiers, including RBF (Radial Basis Function), SMO, BayesNet and Backpropogation Neural Network. For each classification problem, the selection of

features is directly related to the system performance. In the bladder line classification problem, the performance by choosing different feature combinations are compared and different classifiers for the evaluation are examined using a 10-fold cross validation method, using 9 folds for training and one for testing.

[00203] Three different feature combinations are tested:

[00204] Without harmonic ratio: tissueDelta, minRsum, FRONT WALL and BW, 4 features only.

[00205] With traditional harmonic ratio: tissueDelta, old harmonic ratio, minRsum, FRONT WALL and BW, 5 features.

[00206] With harmonic ratio computed using harmonic analysis kernel: tissueDelta, new harmonic ratio, minRsum, FRONT WALL and BW, 5 features. Four different classifiers include, RBF network, Support Vector Machine and BayesNet, Back Propagation Network

[00207] FIGURE 40 is an illustration of a KI threshold algorithm. Consult appendix for further explanations of thresholding procedures.

[00208] FIGURES 41A and 41B illustrated B-mode 1058 plane after thresholding at 29 and 28.

[00209] FIGURES 42-44 are regression plot analyses of clinical data described below,

[00210] The performance of the BVI9400 compared with the BVI3000 and BVI6400 transceivers 10A-B is described in a study undertaken using two ultrasound scans of patient's bladders using 2 different BladderScan® 9400 and BVI 3000 devices and BVI6400 on 1 occasion. Subjects were not required to drink more water before scanning. There can be total of 8 scans (2 pre-void and 2 post-void) during the visit. After successful scan, the participants can be asked to void into the Uroflow device and wait for the resulting printout. The participant shall give the investigator the printed record from the Uroflow so that it may be stored with the other trial records. The participant shall then return for post-void scan using the same collection protocol as for the pre-void.

[00211] A clinical sample derived from 42 healthy and consenting individuals underwent bladder volume measurements using the BVI model 3000, 6000, and 9400 series transceivers having configurations similar to transceivers 10A-B. The 3000 and 6000 transceivers are different from the 9400 series by the transducer design and algorithms employed. The 9400 transducer is more powerful and can achieve a duo format task of acquiring B-mode based images and harmonic information collection. The 9400 B-mode image renders higher resolution than the images produced by the 3000 and 6400 transceivers.

[00212] The algorithms operating within the 9400 transceivers 10A-B utilize harmonic based imaging data and neural network processing illustrated for the NNA 224in detecting bladders. In contrast the algorithms employed in the 3000 and 6400 transceivers obtain bladder volume measurement is made via a bladder detection module employing B-mode image information for segmentation and subsequent 3D volume computations based on the B-mode segmentation. However, female uterus and/or B-mode image noise may obscure bladder detection accuracy in the 3000 and 6400 series transceivers.

[00213] A total of 42 subjects (21 males and 21 females) participated in this study utilizing three BVI9400 devices. Regression analysis is made between the prevoid volume and postvoid volume + uroflow. The charts are given in the following. The dashed lines give the ±15% ±15ml range. Data sets are summarized in the below:

[00214] 1097 female: no uroflow

[00215] 1005 female: no uroflow

[00216] 1035 female: no measurement using the second 9400 1096 female: no measurement using the second 9400 1071 female: no measurement using the second 9400

[00217] The new segmentation method uses the extra information associated with the 2^{nd} harmonic ratio to provide a more robust and accurate bladder volume measurement. The harmonic based algorithms may be applied to other organs having cavity structures, for example the heart. The extra information is combined with the

features from B-mode images. Then instead of using many simple hard-threshold based criterions for segmentation, a more powerful Neural Network is constructed. Each scan line is classified as tissue line or bladder line. The classifier is pre-trained upon a large data sets and the accuracy is high, which guaranteed the detection of the bladder region in current scan. In general, the new design has the advantage over previous designs in the following aspects: The detection of the bladder region can be more robust since more information, including harmonic ratio, is integrated instead of using B-mode intensity (gradient information) only. The female uterus or B-mode image noise can be recognized by the pre-trained classifier and the segmentation cannot give large over or underestimation of the bladder volume.

The slope and square of the correlation coefficient (R^2) is used for accuracy evaluation and cross-instrument comparison.

	9400	3000	6400
R^2	0.9599	0.8513	0.82
Slope	1.0125	0.9525	0.944

From the above testing result, we are confident that our 9400 product is able to achieve more robust bladder measurement and higher accuracy than previous versions.

[00218] The detection method is described for the BVI9400 transceiver and its alternate embodiments illustrated for transceivers 10A-B-C. Compared with previous products, including 3000 and 6100 series, 9400 is equipped with harmonic analysis function, which is utilizing the information embedded in frequency for more accurate bladder volume measurement. In addition to that, fast aiming functionality is added, which provide the operator to locate the best scanning direction and angle. The new bladder detection method is the foundation for all these new DSP applications and new functionalities.

APPENDIX A. DSP IMPLEMENTATION OF LOGARITHM

DSP implementation of logarithm computation (source code in matlab) method 1.

```
function [result] = Goldberg_log(M,fdigits,base)
%%%%%%%%%%%%%%%%%%%%%%%%%%%%%%%%%%%%%%%%%%%%%%%%
%%%%%%%%%%%%%%%%%%%%%%
%The function is to implement the method proposed in Goldberg, M.:
%Computing Logarithms Digit by Digit. BRICS Research Series, Aarhus;
%(RS?04?17): 6, 2004. The method is an algorithm for computing logarithms
%of positive real numbers, that bares structural resemblance to the
%elementary school algorithm of long division. Using this algorithm,
%we can compute successive digits of a logarithm using a 4-operation
%pocket calculator. The algorithm makes no use of Taylor series or
%calculus, but rather exploits properties of the radix-d representation
%of a logarithm in base d. As such, the algorithm is accessible to
%anyone familiar with the elementary properties of exponents and logarithms."
%
%   M  :  input positive real value
%   fdigits:  the fractional digitis, which determines the accuracy
%   base :  the base of the logarithms
%
%   result: the result of the Logarithms operation
%
%   Fuxing Yang 2006-03-01 Initial created

%%%%%%%%%%%%%%%%%%%%%%%%%%%%%%%%%%%%%%%%%%%%%%%%%%%%%
%%%%%%%%%%%%%%%%%%%%%%%%%

if (M<=0)
   fprintf('Invalid input: M has to be a negative real value.\n');
   return;
elseif (M>1)
   [result] = Goldberg_log_lg(M,fdigits,base);
elseif (M<1)
   r = 0;
   temp_M = M;
   while (temp_M<1)
      r = r + 1;
      temp_M = temp_M*base;
   end
   [result] = Goldberg_log_lg(temp_M,fdigits,base);
   result = result - r;
else
   result = 0;
end

%comparison for debugging
%%%%%%%%%%%%%%%%%%%%%%%%%%%%%%%%%%%%%%%%%%%%%%%%%%%%%%
%%%%%%%%%%%%%%%%%%%%%%
% r_result = log2(M);
% fprintf('Result from Goldberg method = %4.10f\n',result);
% fprintf('Result from matlab logarithm operation = %4.10f\n',r_result);

function [lg_result] = Goldberg_log_lg(M,fdigits,base)
r = 0;
temp_M = 1;
while (temp_M<=M)
   if (temp_M==M)
      lg_result = r;
      return;
   end
   r = r + 1;
   temp_M = temp_M*base;
end
first_digit = r-1;
last_M = M;
```

```
last_a = first_digit;
for f = 1:fdigits
   r = 0;
   temp_M = 1;
   M_f = 1;
   for x =1:last_a
      M_f = M_f * base;
   end
   M_e = last_M/M_f;
   M_c = 1;
   for x =1:base
      M_c = M_c * M_e;
   end
   while (temp_M<M_c)
      r = r + 1;
      temp_M = temp_M*base;
   end
   f_digit(f) = r-1;
   last_M = M_c;
   last_a = r-1;
end

lg_result = first_digit;
for f = 1:fdigits
   f_base = 1;
   for x =1:f
      f_base = base*f_base;
   end
   lg_result = lg_result+f_digit(f)/f_base;
end
```

DSP implementation of logarithm computation (source code in matlab) method 2.

This method is based the IEEE Standard for Binary Floating-Point Arithmetic (IEEE 754).

Single-precision 32 bit (adopted from Wikipedia at http://en.wikipedia.org/wiki/IEEE_754)

A single-precision binary floating-point number is stored in a 32-bit word:

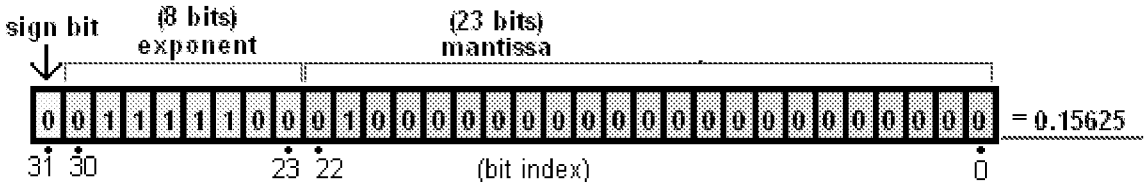

The exponent is biased by $2^{8-1} - 1 = 127$ in this case, so that exponents in the range −126 to +127 are representable. An exponent of −127 would be biased to the value 0 but this is reserved to encode that the value is a denormalized number or zero. An exponent of 128 would be biased to the value 255 but this is reserved to encode an infinity or not a number (NaN). See the chart above.

For normalised numbers, the most common, Exp is the biased exponent and Fraction is the fractional part of the significand. The number has value v:

$$v = s \times 2^e \times m = \text{sign} \times 2^{\text{exponent}} \times \text{mantissa}$$

Where

s = +1 (positive numbers) when the sign bit is 0

s = −1 (negative numbers) when the sign bit is 1

e = Exp − 127 (in other words the exponent is stored with 127 added to it, also called "biased with 127")

m = 1.Fraction in binary (that is, the significand is the binary number 1 followed by the radix point followed by the binary bits of Fraction). Therefore, $1 \leq m < 2$.

In the example shown above, the sign is zero, the exponent is −3, and the significand is 1.01 (in binary, which is 1.25 in decimal). The represented number is therefore $+1.25 \times 2^{-3}$, which is +0.15625.

Based on IEEE754, a fast log2 (log10 and ln) algorithm can be designed as following c code

```
float log2 (float value)
{
  int * const   ptr = (int *) (&value);
  int     intval = *ptr;

  //In theory, the bias is 127 for floats. But in this method, the polynomial is to map [1 ; 2] onto [1 ; 2] (instead of
[0 ; 1]
  //as it would be required if 127 is used). Thus it could be easily removed for faster (linear) approximation. A
possible optimization
  //could be done by moving the bias in the polynomial.
  int     log_2 = ((x>>23) & 255) - 128;    //exponent
  intval &= ~(255 << 23);                   //mantissa
  intval += 127 << 23;                      //exponent of mantissa
  *ptr = intval;

  //special process on exponent of mantissa
  //The proposed formula is a 3rd degree polynomial keeping first derivate continuity. Higher degree could be
used for
 //more  accuracy. For faster results, one can remove this line, if accuracy is not the matter (it gives some linear
interpolation between
  //powers of 2).
  value = ((-1.0f/3) * value + 2) * value - 2.0f/3;

  //combine the original exponent and exponent of mantissa
  return (value + log_2);
} ;

Log10 (value)= log2(value)/ 3.3219f;
Ln(value) = log2(value)/ 1.4427f;
```

For example: Value = 0.00213 (binary format used by IEEE754) 00111011000010111001011101111000

Note: 0 – sign bit

0 – exponent bit

0 – significand (mantissa) bit

Exponent is -10 (01110110 – 128 = 118 – 128).

Mantissa is 00010111001011101111000.

Exponent of the mantissa is 1.09056.

Special process of the exponent of the mantissa is a 3rd degree polynomial keeping first derivate continuity. Higher degree could be used for more accuracy. For faster results, one can remove this special process, if accuracy is not the matter (it gives some linear interpolation between powers of 2). Then the exponent of the mantissa is changed into 1.15271. Combine the two exponents and the final exponent for input value is -10 + 1.15271 = -8.8473.

APPENDIX B. NEURAL NETWORK TRAINING

Training data sets were collected on Jan 5, 2007. Totally there are 12 patients, including 1002, 1004, 1005, 1008, 1012, 1015, 1016, 1017, 1049, 1051, 1052 and 1068. [post-void and pre-void]. There are 12*72*24 = 20736 scan lines. Based on manual grading, there are 8250 bladder lines and 12486 tissue lines. (It can be regarded as balanced data sets for training.) We implemented a back propagation Neural Network using logistic functions. The structure of the network is 5 by 5 by 1. We used a 10-fold cross validation method and the accuracy of the trained network is 92.26%. The trained network is in the following configuration (please refer to source code defined in NN.h and NN.c.

```
#define n_input_units        5
#define n_hidden_units       5
#define n_output_units       1
#define na_input_units       n_input_units + 1
#define na_hidden_units      n_hidden_units + 1
#define na_output_units      n_output_units + 1
const double BPNN_IH[na_input_units][na_hidden_units] =
{
{0,     0,                          0,                          0,      0,      0},
{0,     13.008636,      -5.242537,      -8.093809,      0.738920,-1.345708},
{0,     2.039624,2.109022,-3.339866,    -3.926513,      -6.129284},
{0,     -4.525894,      -4.832823,      3.689193,-3.612824,         -1.418404},
{0,     -6.834694,      -3.932294,      7.301636,0.151018,-6.567073},
{0,     -0.997530,      -6.582561,      1.040930,-4.179786,         6.771766 }
};
const double BPNN_HO[na_hidden_units][2] =
{
        {0,0},
        {0,2.654482},
        {0,-17.31553},
        {0,-1.429942},
        {0,-11.77292},
        {0,-2.519807}
};
const double maxfeature[na_input_units] =
{0, 238.7272727, 43.49219326, 2048, 294, 536};
```

```
const double minfeature[na_input_units] =
{0, 0,  6.46712798, 1,  0, 0};
```

In order to confirm the performance of the Network, results obtained from a pattern recognition tool kit Weka (available from the University of Waikato, Hamilton, New Zealand), on the same training data sets using different classifiers and we have the following results:

RBFNetwork	Correctly Classified Instances	19056	91.8981 %
	Incorrectly Classified Instances	1680	8.1019 %
SMO	Correctly Classified Instances	19153	92.3659 %
	Incorrectly Classified Instances	1583	7.6341 %

APPENDIX C. CLASSIFICATION AND FEATURES

For classification problem, the selection of features is directly related to the system performance. In our project, for bladder line classification problem, we compared the performance by choosing different feature combinations. Also, we used different classifiers for the evaluation too. The data set for this comparison is based on the clinical data collected on Jan 5th, 2007. The method we used is a 10-fold cross validation method. [Use 9 folds for training and one for testing.] Three different feature combinations are tested:

- without harmonic ratio: tissueDelta, minRsum, FRONT WALL and BW, 4 features
- with traditional harmonic ratio: tissueDelta, old harmonic ratio, minRsum, FRONT WALL and BW, 5 features
- with harmonic ratio computed using harmonic analysis kernel: tissueDelta, new harmonic ratio, minRsum, FRONT WALL and BW, 5 features

Four different classifiers are used:

- RBF network
- Support Vector Machine
- BayesNet
- Back Propagation Network

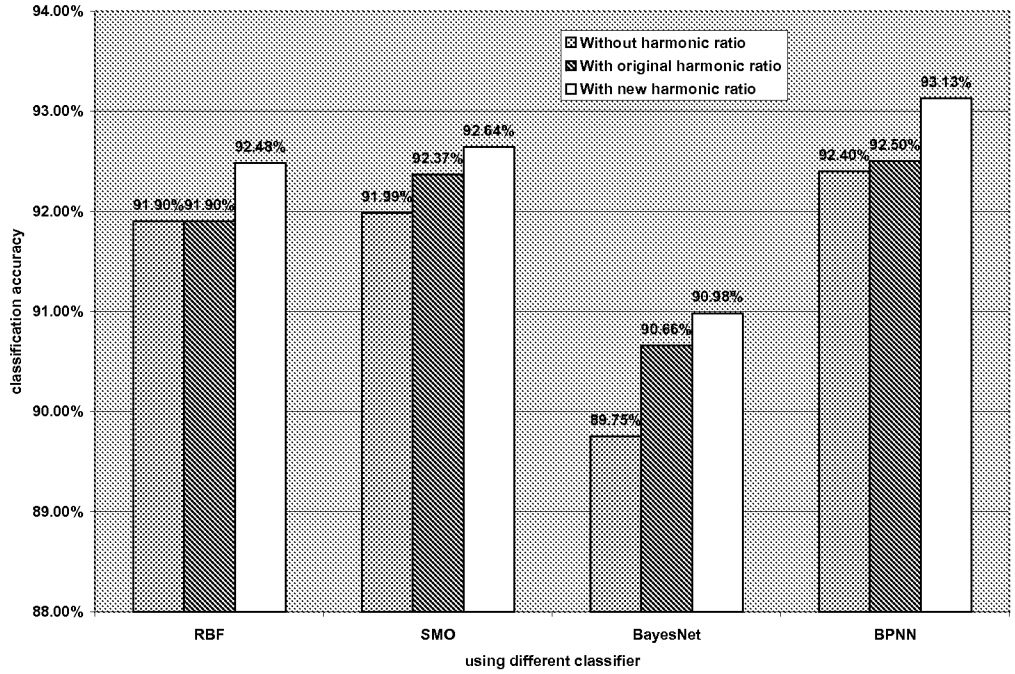

From the results, we are able to make the following conclusions:

- harmonic information can improve the classification accuracy
- the harmonic ratio computed by harmonic analysis kernel yields higher classification accuracy than the original harmonic ratio
- with the consideration of the computational cost and complexity for implementation in DSP, BPNN is used for DSP implementation

APPENDIX D. OPTIMAL THRESHOLDING

Bladder segmentation can be taken as a bi-level analysis from ultrasound image. In another word, inside the image, there are only two kinds of objects, shadows (including real shadow or lumen, like the bladder and etc) and non-shadows. Then, automated threshold in image processing is a potential tool to segment the shadows from no-shadows. There are two widely used automated threshold methods, Otsu and Kittler & Illingworth methods. Threshold techniques can be divided into bi-level and multi-level category, depending on number of image segments. In bi-level threshold, image is segmented into two different regions. The pixels with gray values greater than a certain value T are classified as object pixels, and the others with gray values lesser than T are

classified as background pixels. Otsu's method [1] chooses optimal thresholds by maximizing the between class variance. Sahoo et al. [2] found that in global threshold, Otsu's method is one of the better threshold selection methods for general real world images with regard to uniformity and shape measures. Kittler and Illingworth [3] suggested a minimum error thresholding method.

The KI method gives very good estimation of all the shadow regions in the image, including the lumen of the bladder. The most optionally advantageous is that it gives very good estimation of the shadows behind the pubic only based on this plane itself, as we did using the statistic information from all the collected planes.

Algorithm – KI threshold

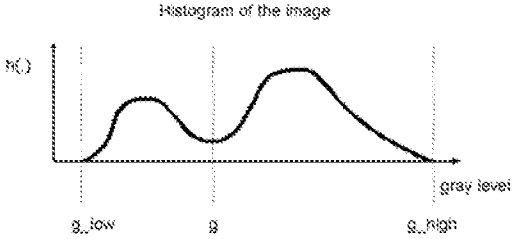

$$s_1 = \sum_{i=g\_low}^{g} h(i) \qquad s_2 = \sum_{i=g}^{g\_high} h(i)$$

$$sg_1 = \sum_{i=g\_low}^{g} (h(i)*i) \qquad sg_2 = \sum_{i=g}^{g\_high} (h(i)*i)$$

$$sgg_1 = \sum_{i=g\_low}^{g} (h(i)*i*i) \qquad sgg_2 = \sum_{i=g}^{g\_high} (h(i)*i*i)$$

$$\mu_1 = sg_1 / s_1 \qquad \mu_2 = sg_2 / s_2$$

$$\sigma_1 = sgg_1 / s_1 - \mu_1 * \mu_1 \qquad \sigma_2 = sgg_2 / s_2 - \mu_2 * \mu_2$$

Find the g which minimize the following energy and the threshold = g

$$E_{kj} = 1 + 2*(s_1 * \log(\sigma_1) + s_2 * \log(\sigma_2)) - 2*(s_1 * \log(s_1) + s_2 * \log(s_2))$$

In the following, we gave examples after using KI thresholding on the Bmode images collected by 9400 system.

[1] Otsu, N., 1979. A Threshold Selection Using Gray Level Histograms. IEEE Trans. Systems Man Cybernet.
9, 62-69

[2] Sahoo, P.K., Soltani, S., Wong, A.K.C., 1988. SURVEY: A survey of thresholding techniques. Comput. Vision Graphics Image Process. 41, 233-260.

[3] Kittler, J., Illingworth, J., 1986, Minimum Error Thresholding, Pattern Recognition, 19, 41-47.

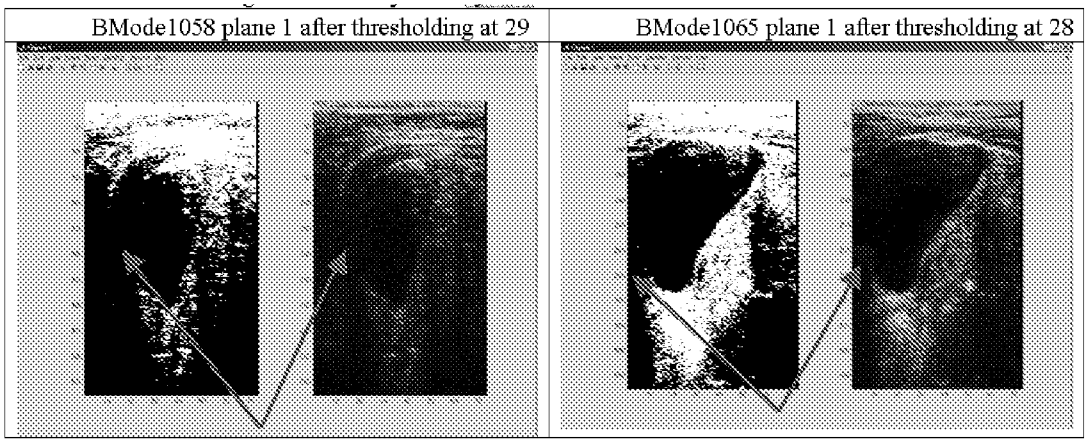

From above examples, we can see that KI threshold method can help us estimate the location of the shadow behind the pubic bone. With appropriate post-processing, the information on all planes can be integrated and the location of the pubic bone can be estimated too.

[00219] While the preferred embodiment of the invention has been illustrated and described, many changes can be made without departing from the spirit and scope of the invention. For example, gelatinous masses may be to develop synthetic tissue and combination fluid models to further define the operational features of the neural network algorithm. Accordingly, the scope of the invention is not limited by the disclosure of the preferred embodiment.

The embodiments of the invention in which an exclusive property or privilege is claimed are defined as follows:

1. A system to detect and measure an organ cavity comprising:

an ultrasound transceiver positioned to deliver ultrasound energy of at least one of a fundamental and a harmonic frequency to the organ cavity and receive echoes of the at least one fundamental and harmonic frequency;

an algorithm configured to signal process the received echoes according to the fundamental and harmonic frequency; and display means for presenting a visual depiction of the organ cavity and a calculated volume of the visual depiction.

2. The system of claim 1, wherein the ultrasound transceiver includes a targeting algorithm to guide positioning of the ultrasound transceiver to center the visual depiction of the organ cavity.

3. The system of claim 1, wherein the algorithm includes at least one of a C-mode component, a B-mode component, and an A-mode component.

4. The system of claim 3, wherein the algorithm includes a neural harmonic process.

5. The system of claim 4, wherein the neural harmonic process includes a grading algorithm to assess the certainty that a given scan line traverses a cavity region.

6. The system of claim 4, wherein the grading algorithm includes weighting the contributions of at least one of an ultrasound harmonic ratio, a tissue delta, a minRsum value, a cavity front wall location, and a cavity back wall location.

7. A method to detect and measure an organ cavity comprising:

transmitting ultrasound energy having at least one of a fundamental and harmonic frequency to the organ cavity;

collecting ultrasound echoes returning from the organ cavity;

generating signals from the ultrasound echoes;

identifying fundamental signals and harmonic signals from the generated signals;

processing at least one of the fundamental and harmonic signals using algorithms designed for fundamental and harmonic signals;

presenting an image of the organ cavity; and

calculating the volume of the organ cavity.

8. The method of claim 7, wherein the transmitting ultrasound energy includes a targeting algorithm to center the presented organ cavity on a display.

9. The method of claim 7, wherein processing at least one of the fundamental and harmonic signals includes a neural network algorithm.

10. The method of claim 9, wherein utilizing a neural network algorithm includes a grading algorithm for ascertaining the certainty that a given scan line traverses a cavity region.

11. The method of claim 10, wherein the grading algorithm includes weighting the contributions of at least one of an ultrasound harmonic ratio, a tissue delta, a minRsum value, a cavity front wall location, and a cavity back wall location.

12. Computer readable media having instructions to execute a method to detect and measure an organ cavity comprising:

transmitting ultrasound energy having at least one of a fundamental and harmonic frequency to the organ cavity;

collecting ultrasound echoes returning from the organ cavity;

generating signals from the ultrasound echoes;

identifying fundamental signals and harmonic signals from the generated signals;

processing at least one of the fundamental and harmonic signals using algorithms designed for fundamental and harmonic signals;

presenting an image of the organ cavity; and

calculating measurements of the organ cavity.

13. The computer readable media of claim 12, wherein the transmitting ultrasound energy includes a targeting algorithm to center the presented organ cavity on a display.

14. The computer readable media of claim 12, wherein processing at least one of the fundamental and harmonic signals includes a neural network algorithm.

15. The computer readable media of claim 14, wherein utilizing a neural network algorithm includes a grading algorithm for ascertaining the certainty that a given scan line traverses a cavity region.

16. The computer readable media of claim 15, wherein the grading algorithm includes weighting the contributions of at least one of an ultrasound harmonic ratio, a tissue delta, a minRsum value, a cavity front wall location, and a cavity back wall location.

17. The computer readable media of claim 16, wherein the executable instructions include presenting a graphic of the cavity in relation to nearby anatomical structures.

18. The computer readable media of claim 17, wherein the executable instructions include visualizing the pubic bone.

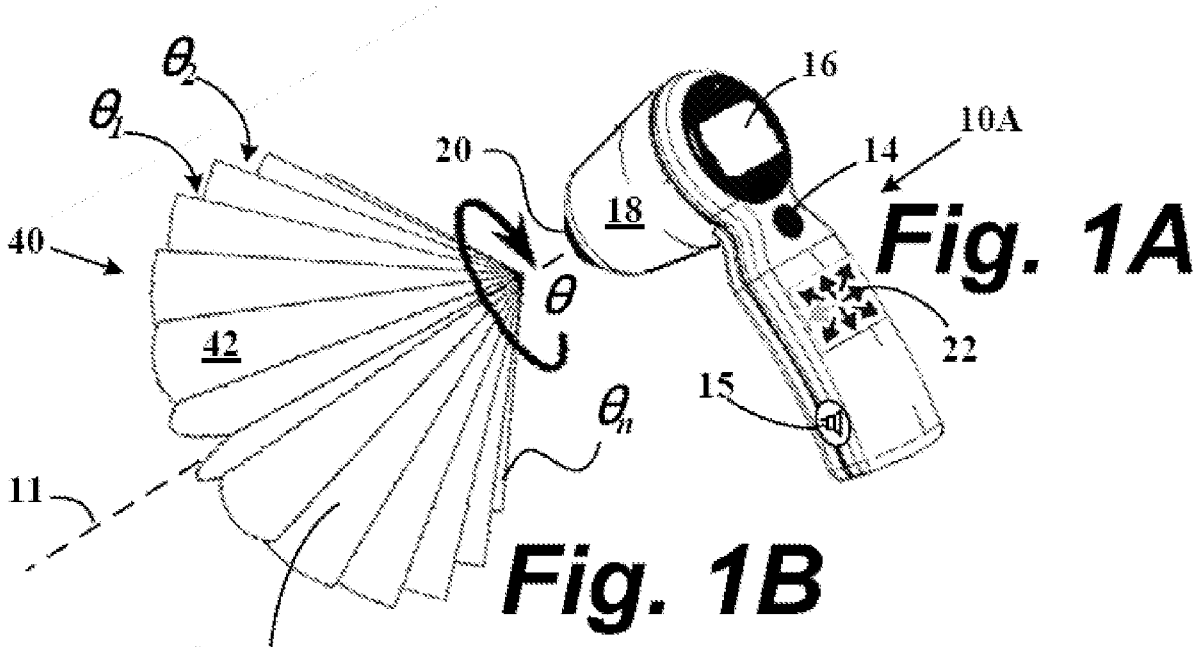

Fig. 1A

Fig. 1B

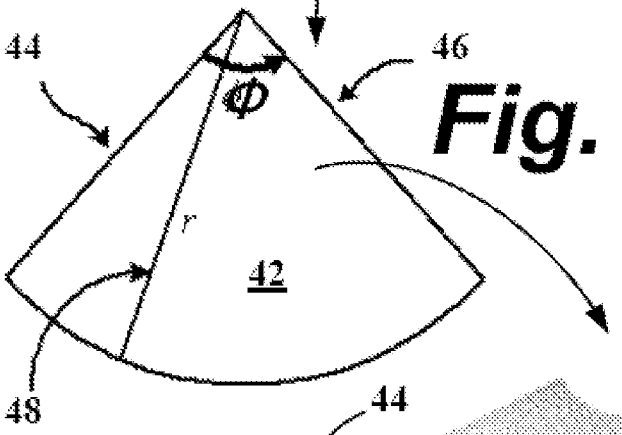

Fig. 1C

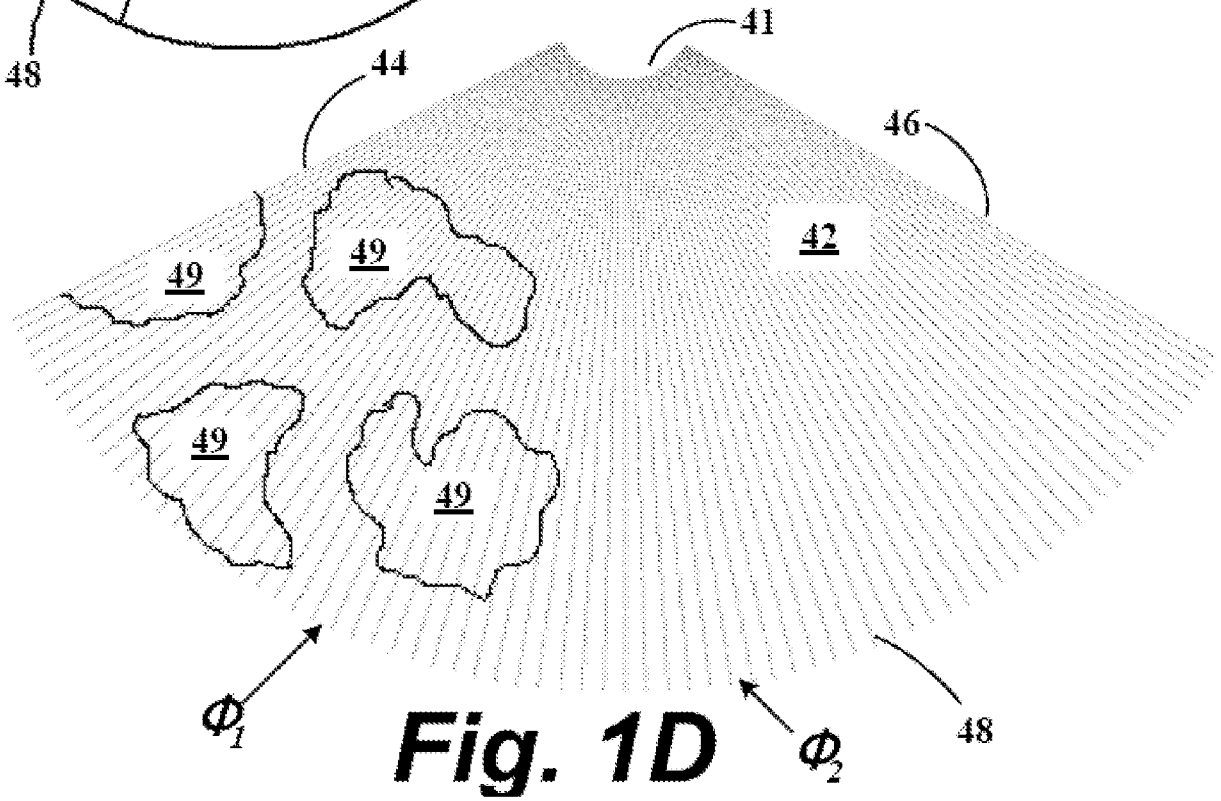

Fig. 1D

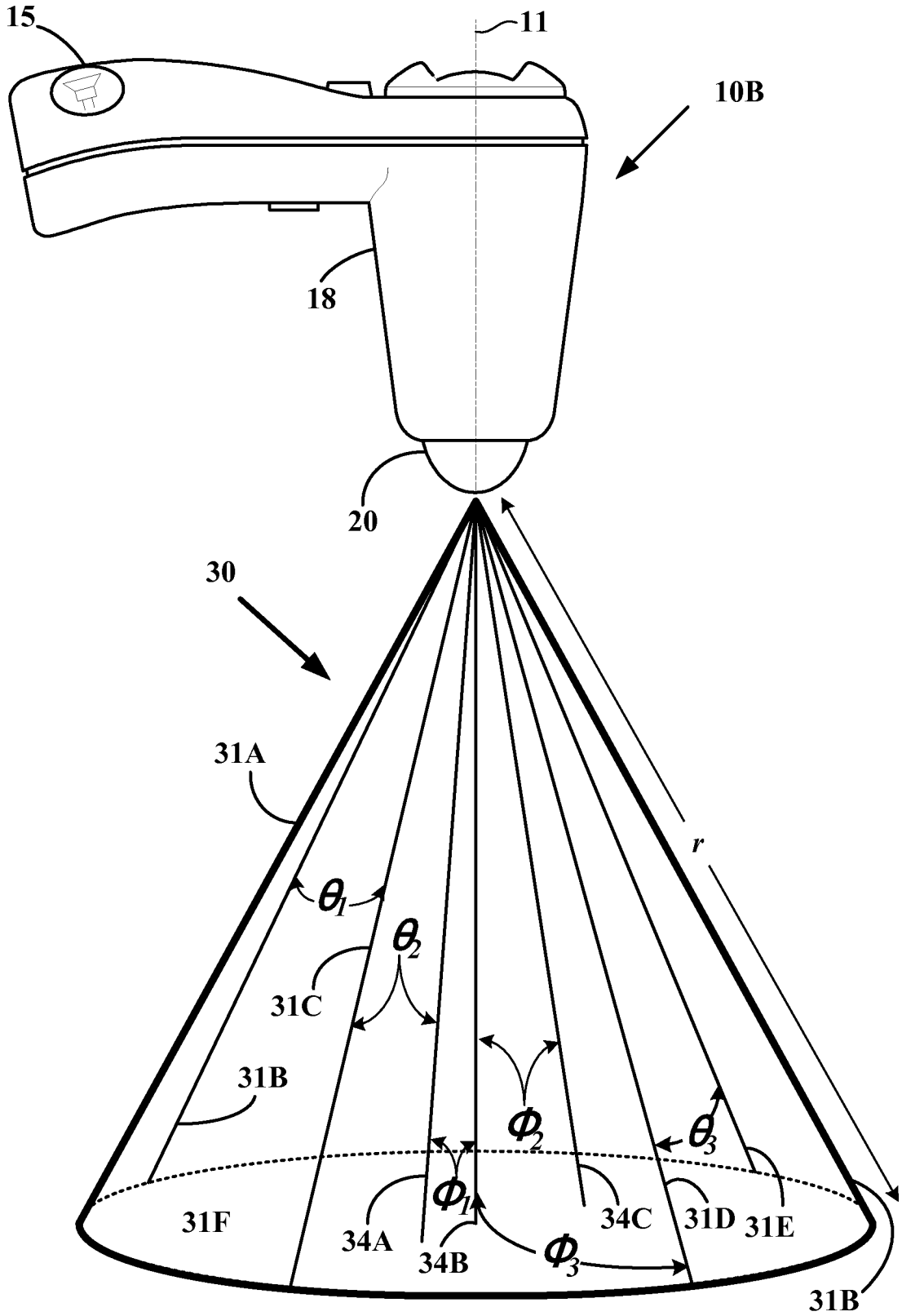
15
11
10B
18
20
30
31A
r
θ1
θ2
31C
31B
Φ2
θ3
Φ1
31F
34A
34B
Φ3
34C
31D
31E
31B

Fig. 2A

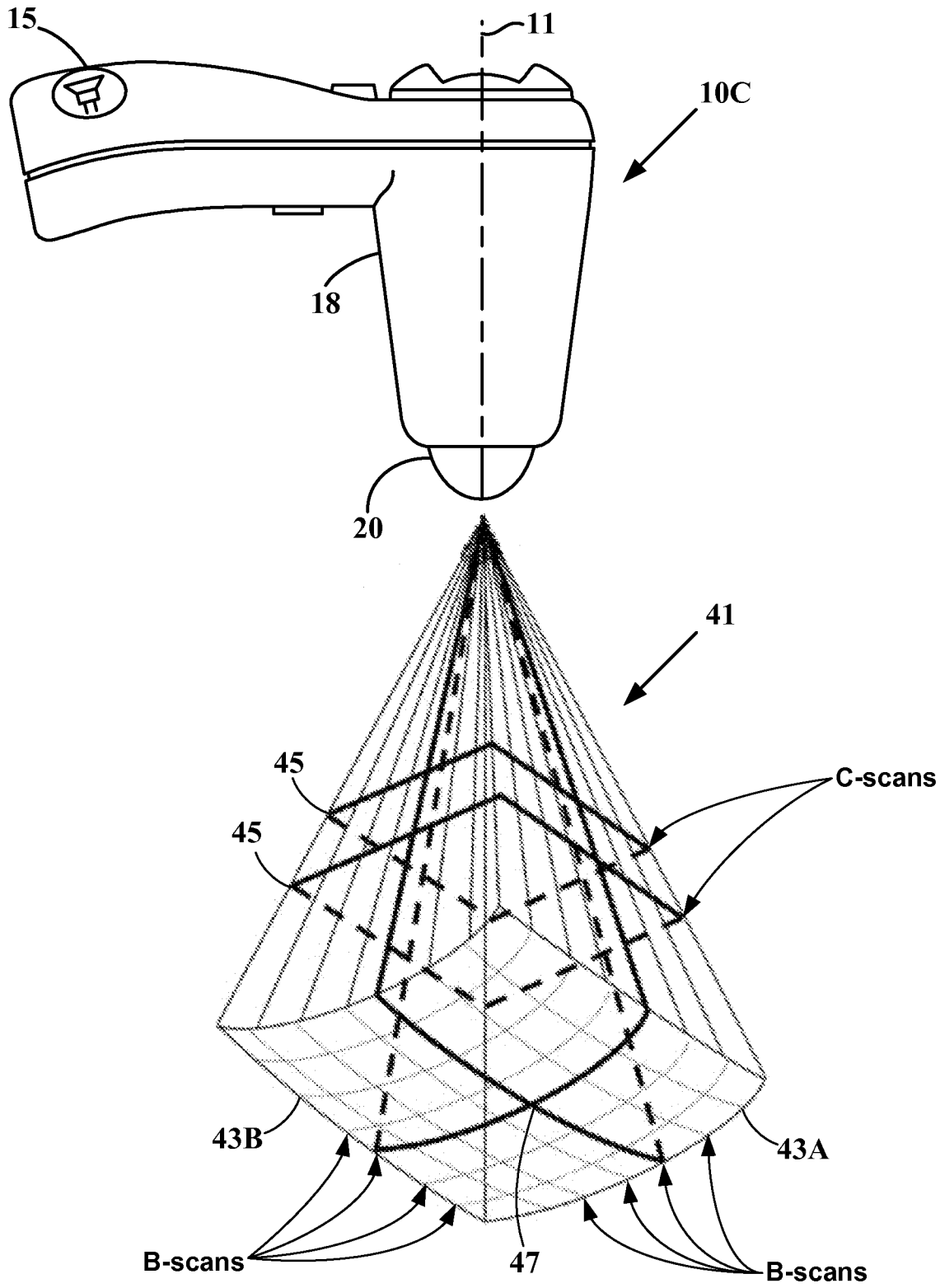

Fig. 2B

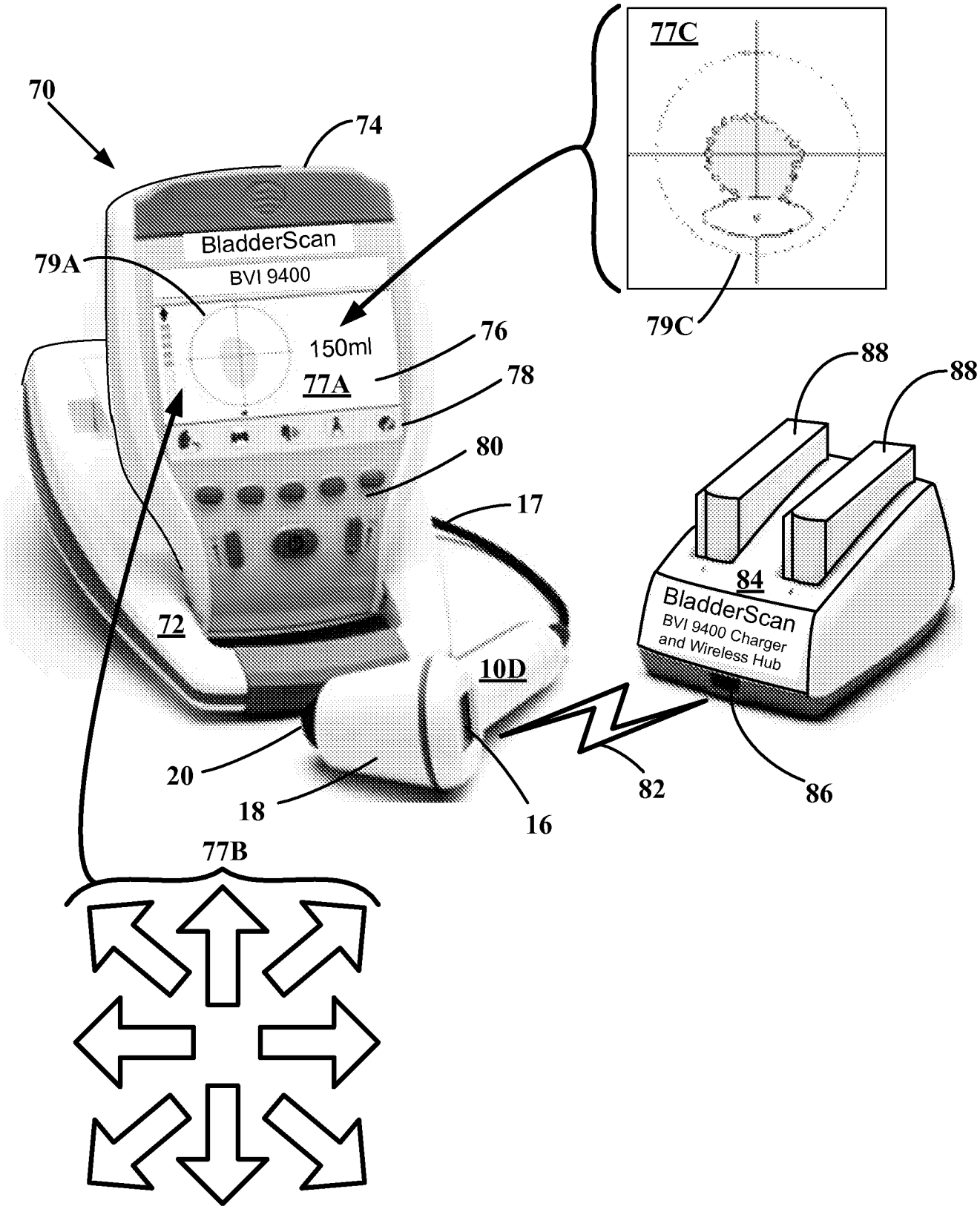
77C
70
74
BladderScan
BVI 9400
79A
150ml
76
77A
78
80
17
88
88
84
BladderScan
BVI 9400 Charger
and Wireless Hub
72
10D
20
18
16
82
86
77B
79C

Fig. 2C

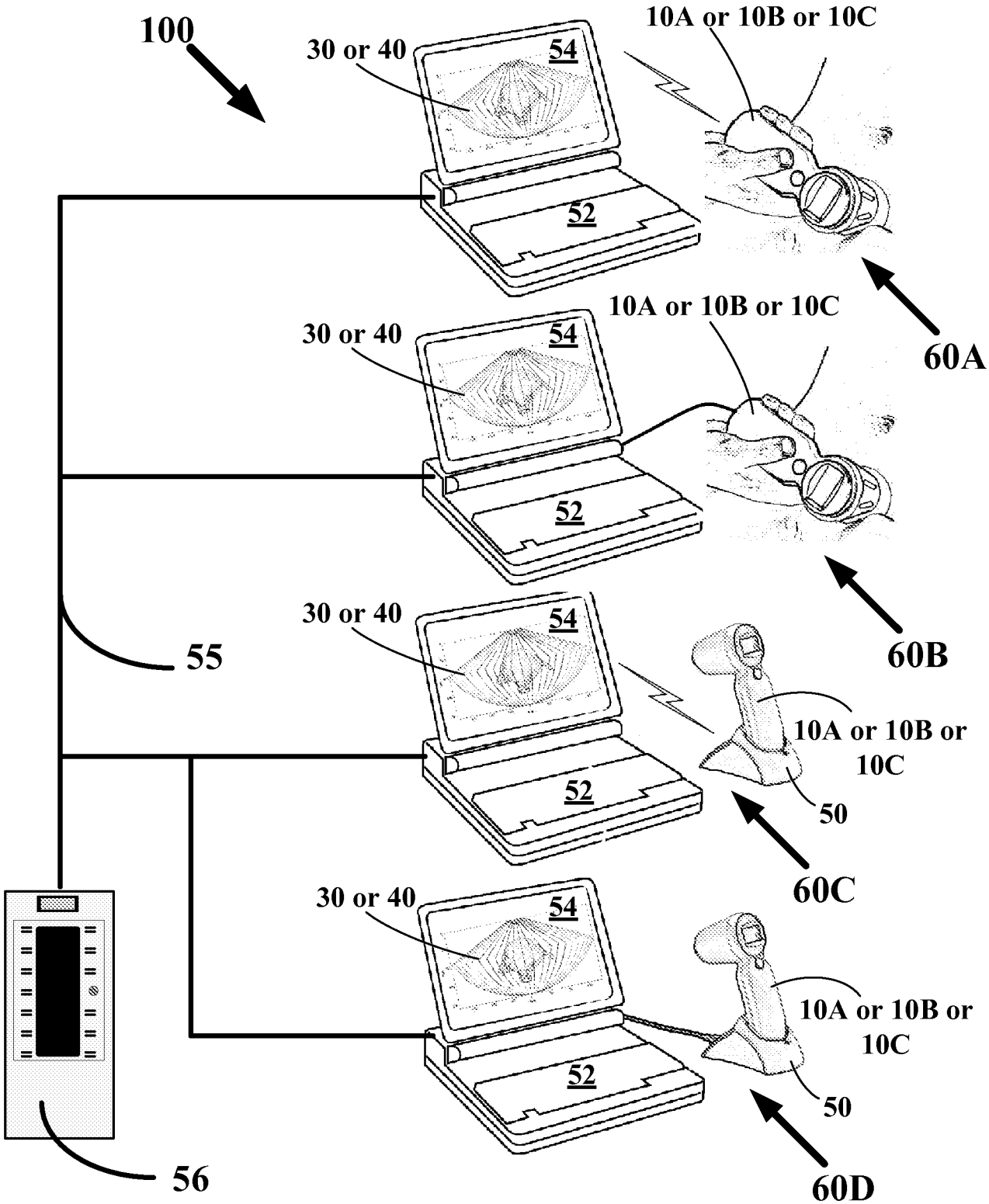
100
30 or 40
54
52
10A or 10B or 10C
60A
30 or 40
54
52
10A or 10B or 10C
60B
55
30 or 40
54
52
10A or 10B or 10C
50
60C
30 or 40
54
52
10A or 10B or 10C
50
60D
56

Fig. 3

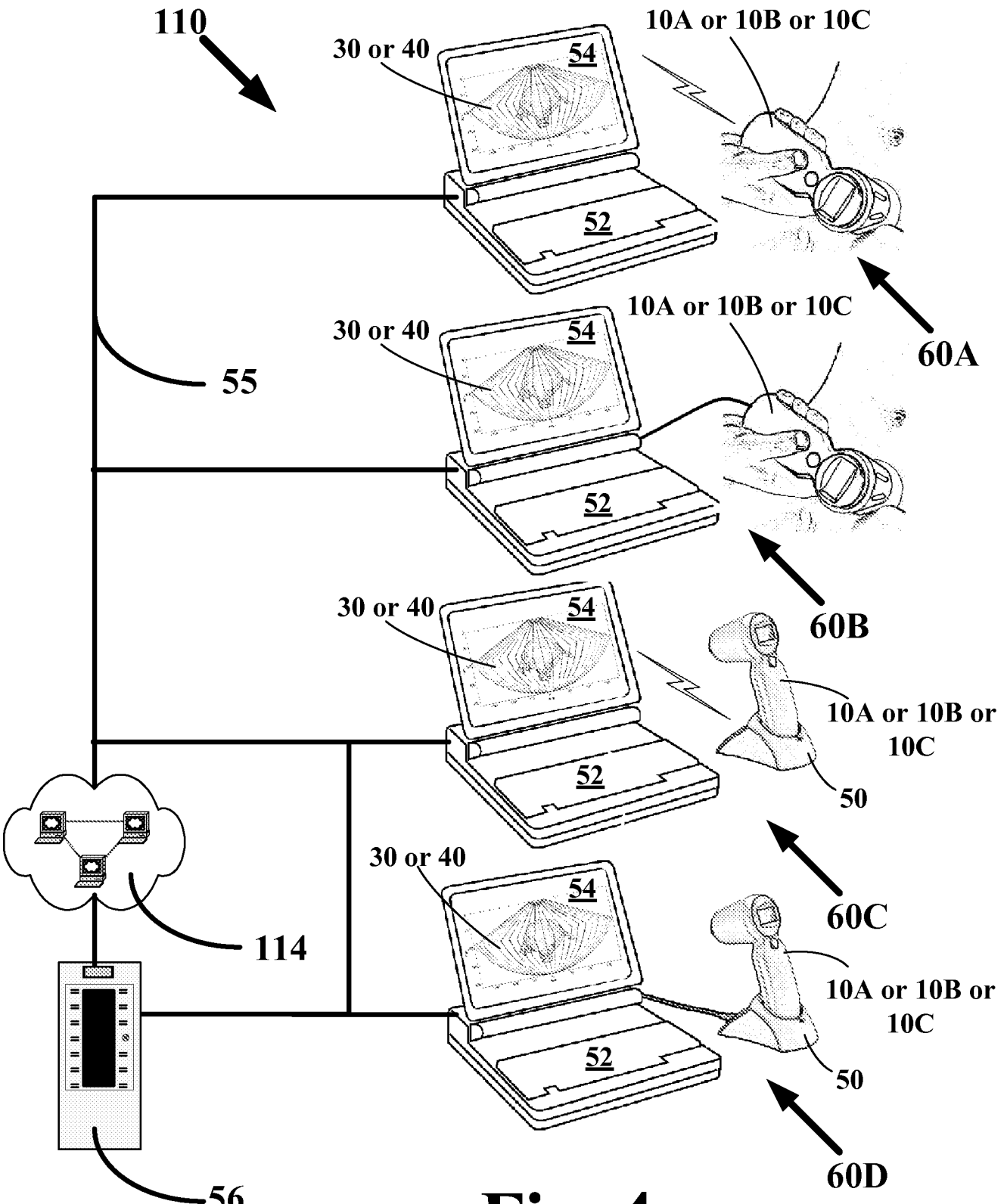

Fig. 4

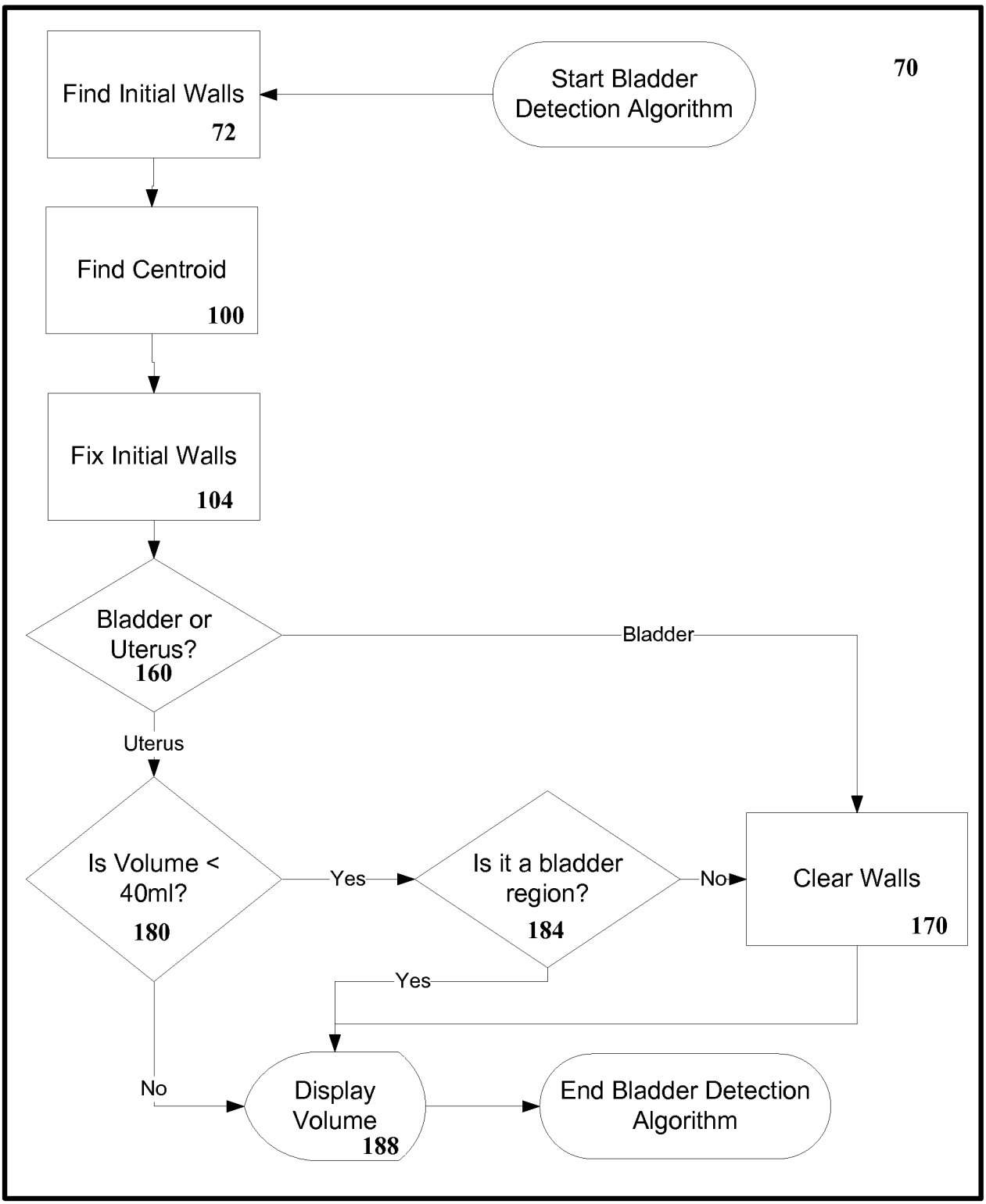
70
Start Bladder Detection Algorithm
Find Initial Walls
72
Find Centroid
100
Fix Initial Walls
104
Bladder or Uterus?
160
Bladder
Uterus
Is Volume < 40ml?
180
Yes
Is it a bladder region?
184
No
Clear Walls
170
Yes
No
Display Volume
188
End Bladder Detection Algorithm

Fig. 5

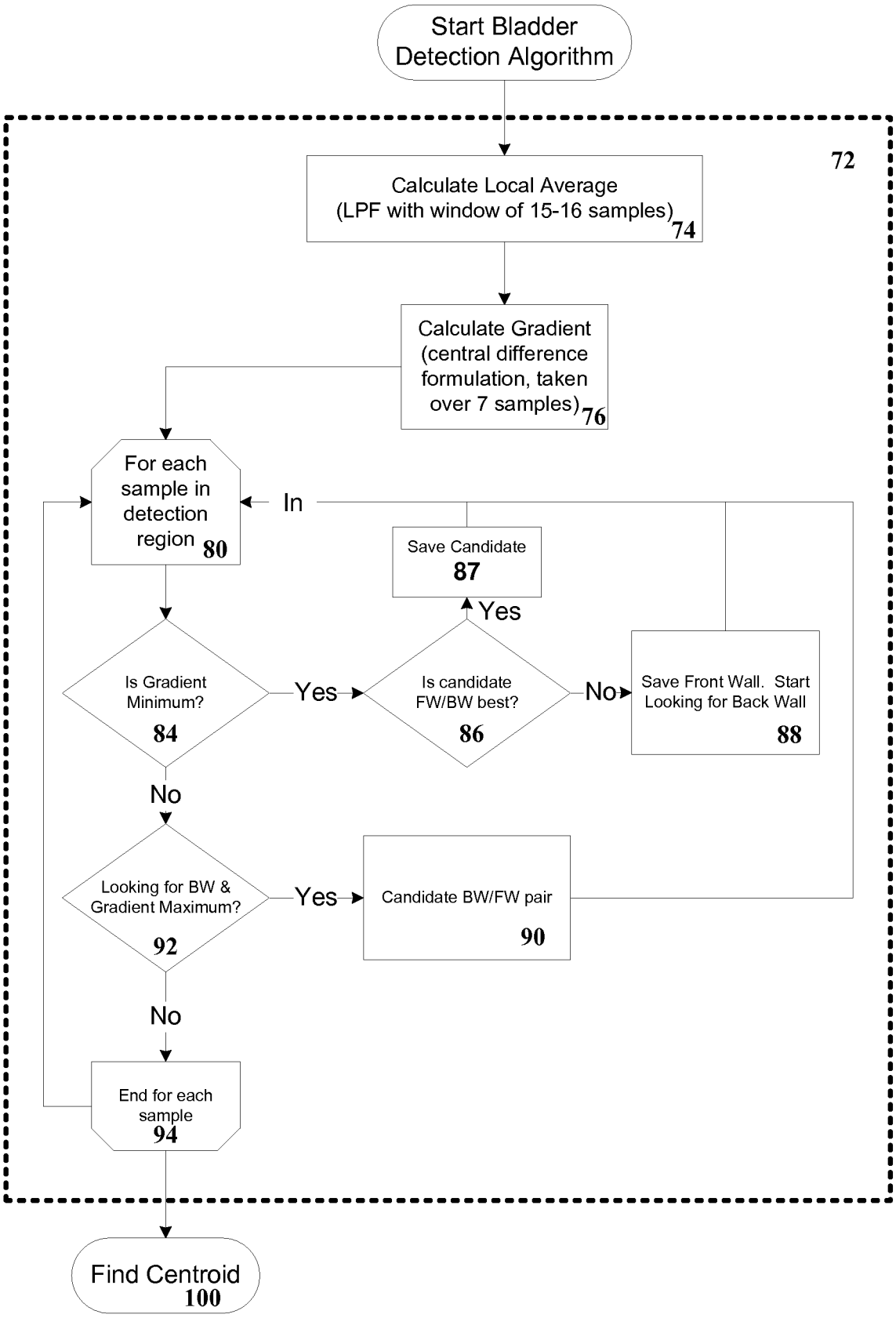
Start Bladder Detection Algorithm
72
Calculate Local Average (LPF with window of 15-16 samples) 74
Calculate Gradient (central difference formulation, taken over 7 samples) 76
For each sample in detection region 80
In
Save Candidate 87
Yes
Is Gradient Minimum? 84
Yes
Is candidate FW/BW best? 86
No
Save Front Wall. Start Looking for Back Wall 88
No
Looking for BW & Gradient Maximum? 92
Yes
Candidate BW/FW pair 90
No
End for each sample 94
Find Centroid 100

Fig. 6

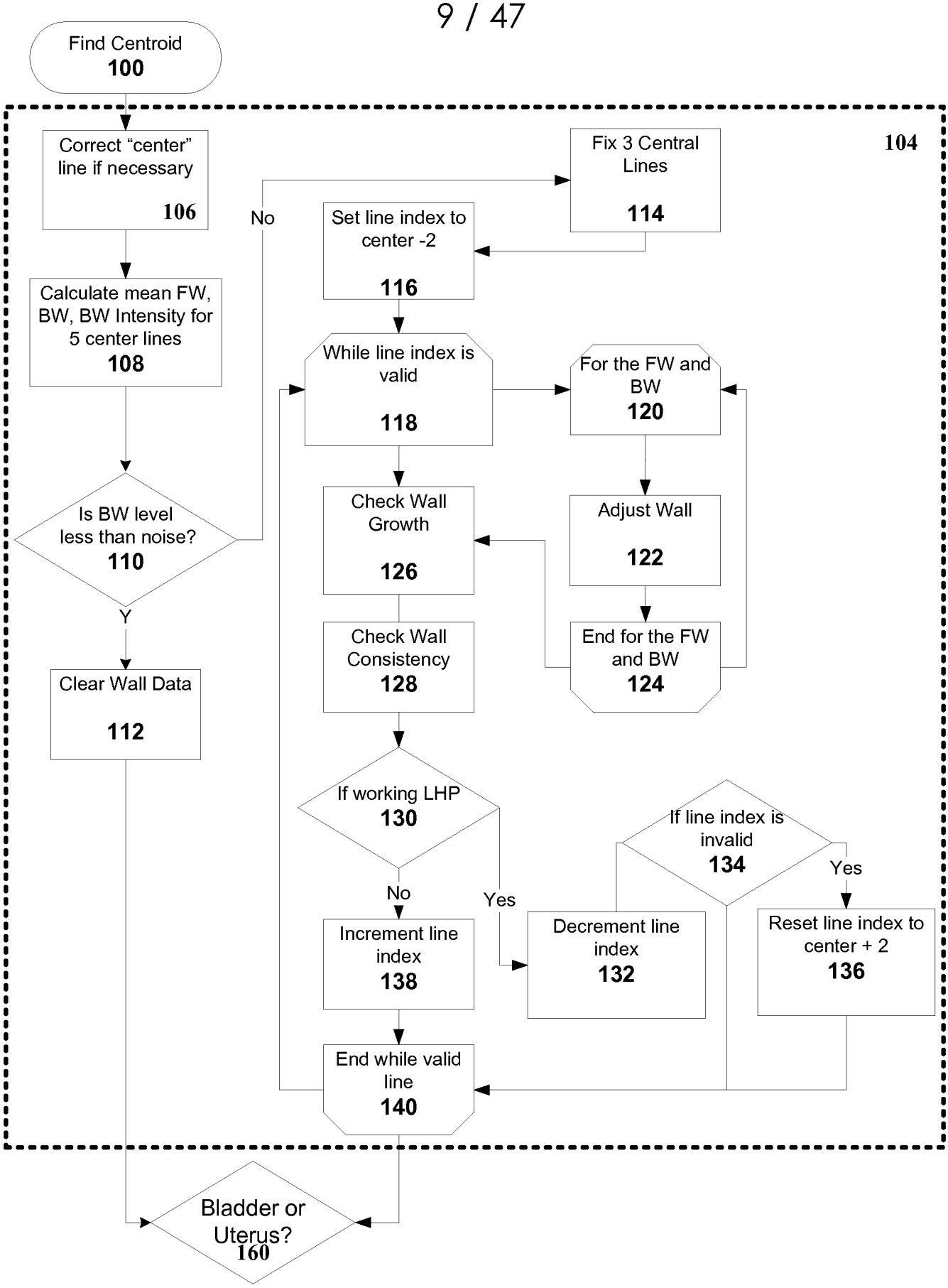
Find Centroid
100
Correct "center" line if necessary
106
Calculate mean FW, BW, BW Intensity for 5 center lines
108
Is BW level less than noise?
110
Y
No
Clear Wall Data
112
Fix 3 Central Lines
114
Set line index to center -2
116
While line index is valid
118
For the FW and BW
120
Adjust Wall
122
End for the FW and BW
124
Check Wall Growth
126
Check Wall Consistency
128
If working LHP
130
No
Yes
Increment line index
138
Decrement line index
132
If line index is invalid
134
Yes
Reset line index to center + 2
136
End while valid line
140
104
Bladder or Uterus?
160

Fig. 7

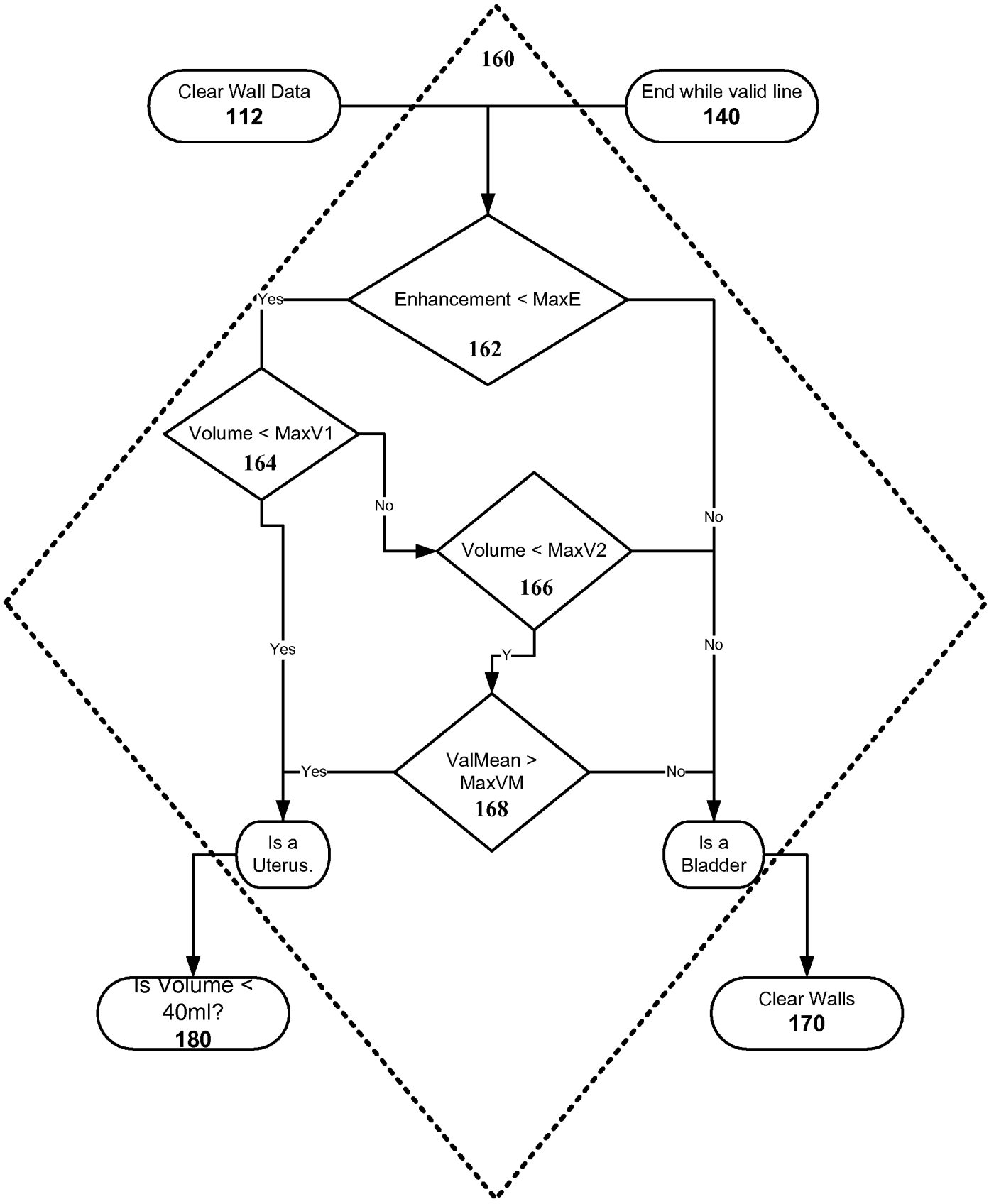
160
Clear Wall Data
112
End while valid line
140
Enhancement < MaxE
162
Yes
Volume < MaxV1
164
No
Volume < MaxV2
166
No
No
Yes
Y
Yes
ValMean > MaxVM
168
No
Is a Uterus.
Is a Bladder
Is Volume < 40ml?
180
Clear Walls
170

Fig. 8

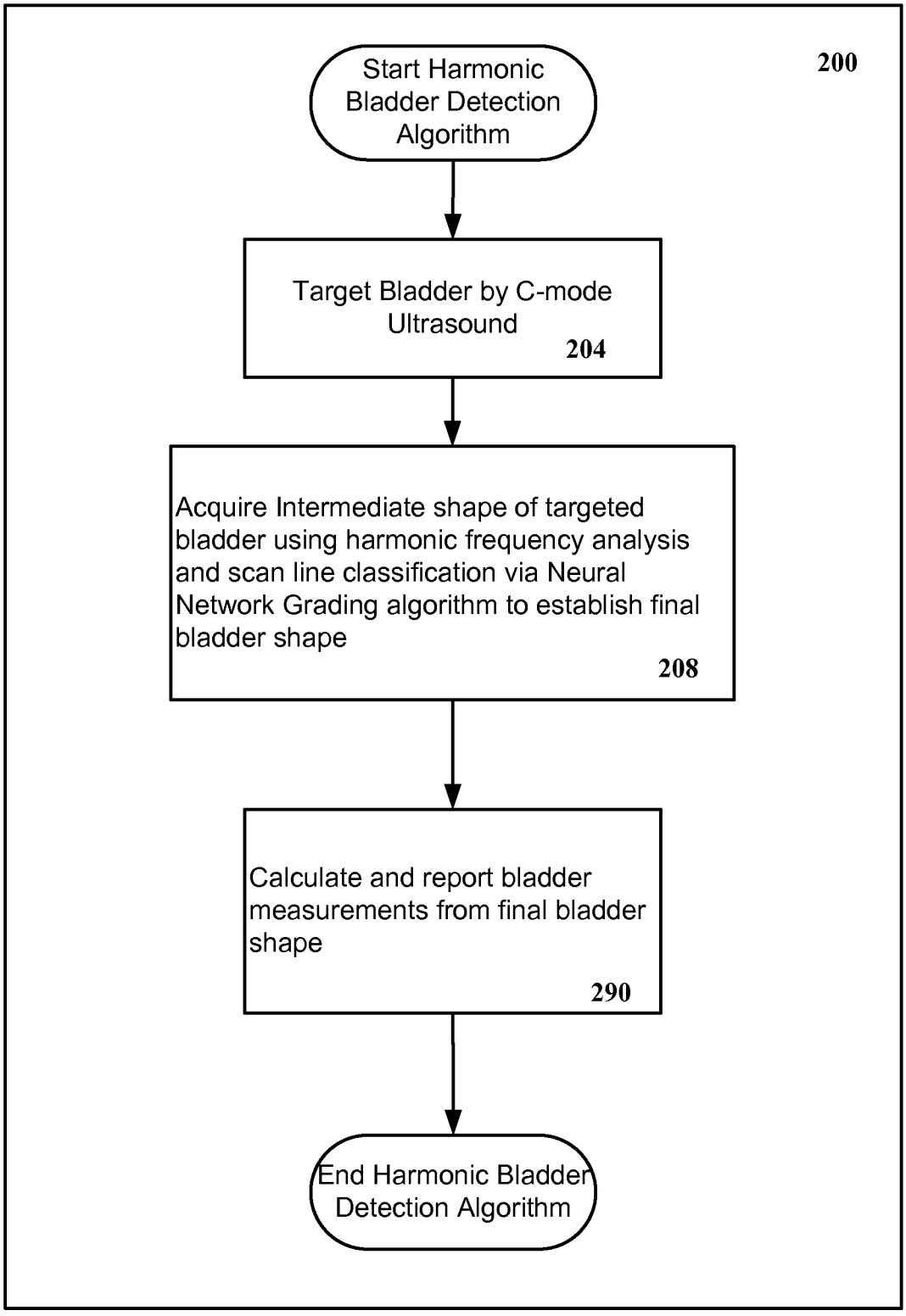
200
Start Harmonic Bladder Detection Algorithm
Target Bladder by C-mode Ultrasound
204
Acquire Intermediate shape of targeted bladder using harmonic frequency analysis and scan line classification via Neural Network Grading algorithm to establish final bladder shape
208
Calculate and report bladder measurements from final bladder shape
290
End Harmonic Bladder Detection Algorithm

Fig. 9A

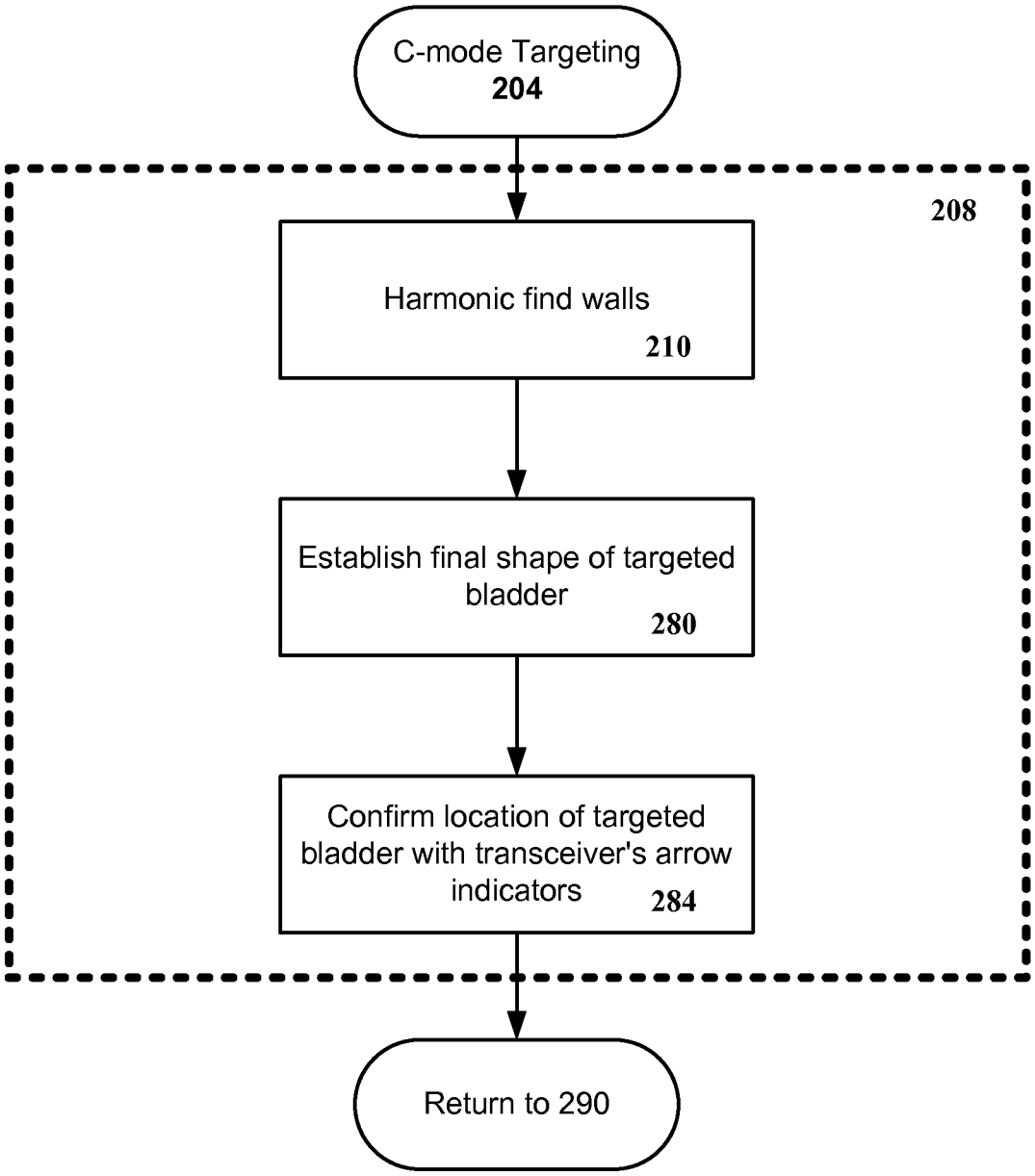
C-mode Targeting
204
208
Harmonic find walls
210
Establish final shape of targeted bladder
280
Confirm location of targeted bladder with transceiver's arrow indicators
284
Return to 290

Fig. 9B

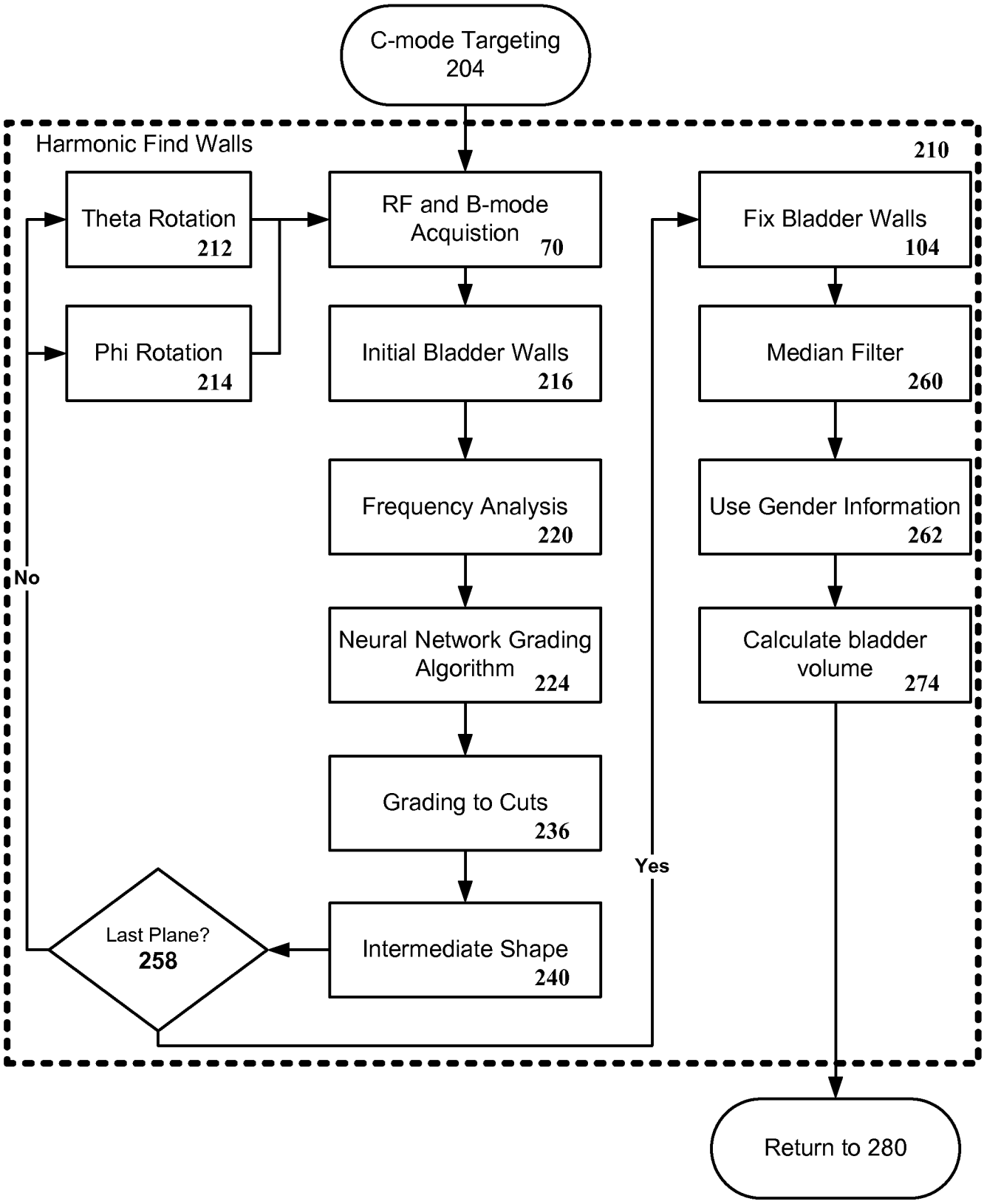
C-mode Targeting
204
Harmonic Find Walls
210
Theta Rotation
212
Phi Rotation
214
RF and B-mode
Acquistion
70
Initial Bladder Walls
216
Frequency Analysis
220
Neural Network Grading
Algorithm
224
Grading to Cuts
236
Intermediate Shape
240
Last Plane?
258
No
Yes
Fix Bladder Walls
104
Median Filter
260
Use Gender Information
262
Calculate bladder
volume
274
Return to 280

Fig. 9C

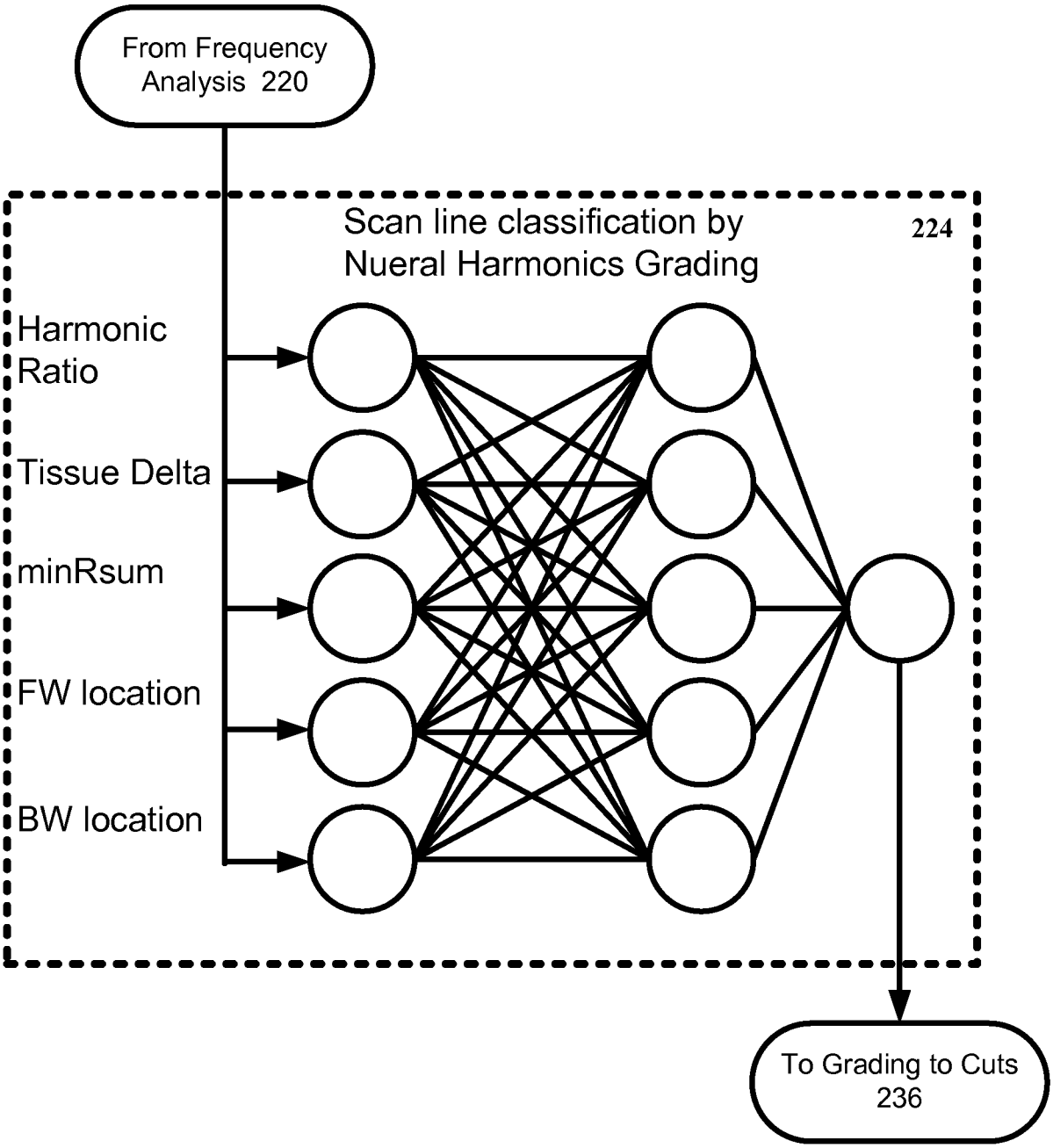
From Frequency Analysis 220
Scan line classification by Nueral Harmonics Grading
224
Harmonic Ratio
Tissue Delta
minRsum
FW location
BW location
To Grading to Cuts 236

Fig. 9D

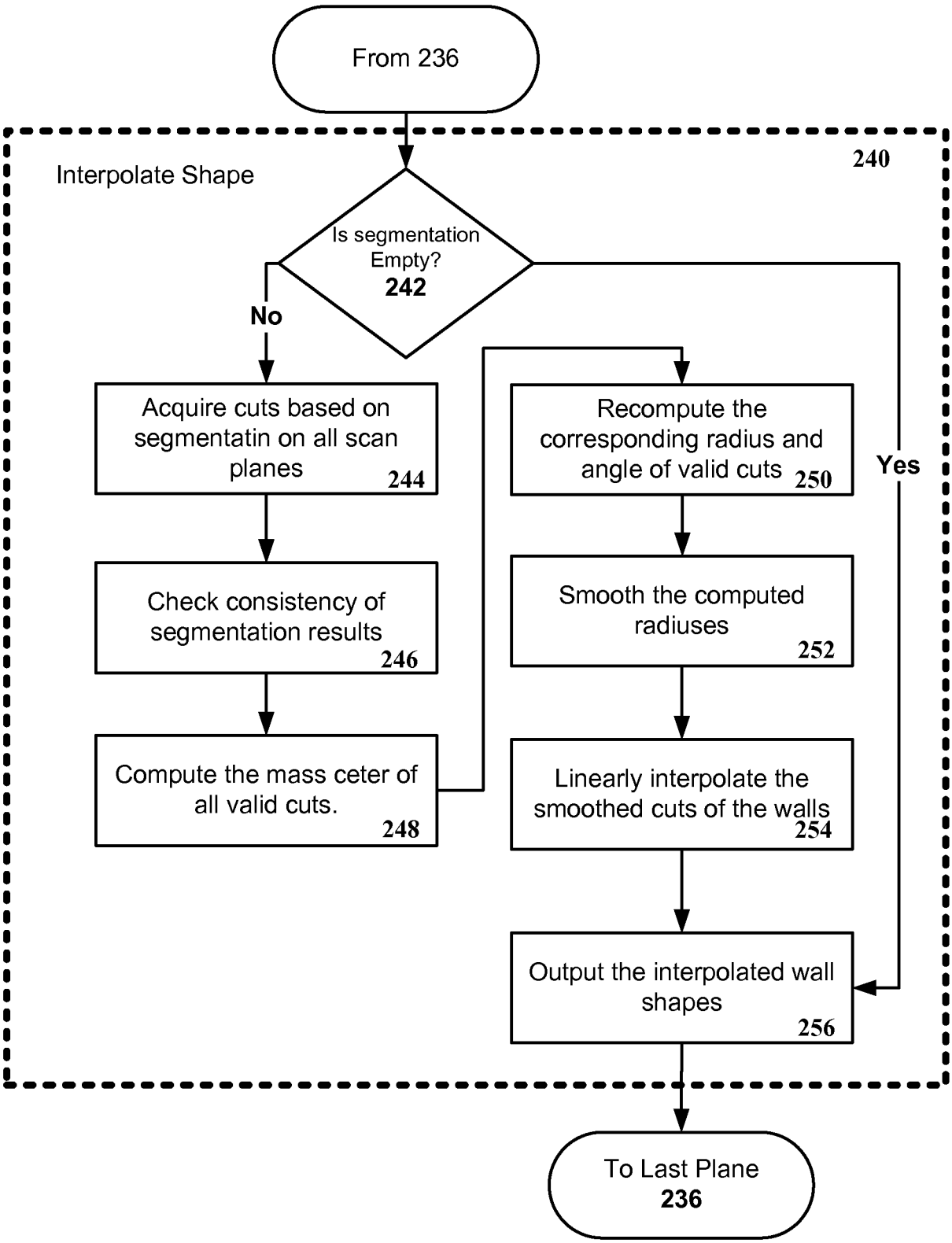
From 236
Interpolate Shape
240
Is segmentation Empty?
242
No
Yes
Acquire cuts based on segmentatin on all scan planes
244
Check consistency of segmentation results
246
Compute the mass ceter of all valid cuts.
248
Recompute the corresponding radius and angle of valid cuts
250
Smooth the computed radiuses
252
Linearly interpolate the smoothed cuts of the walls
254
Output the interpolated wall shapes
256
To Last Plane
236

Fig. 9E

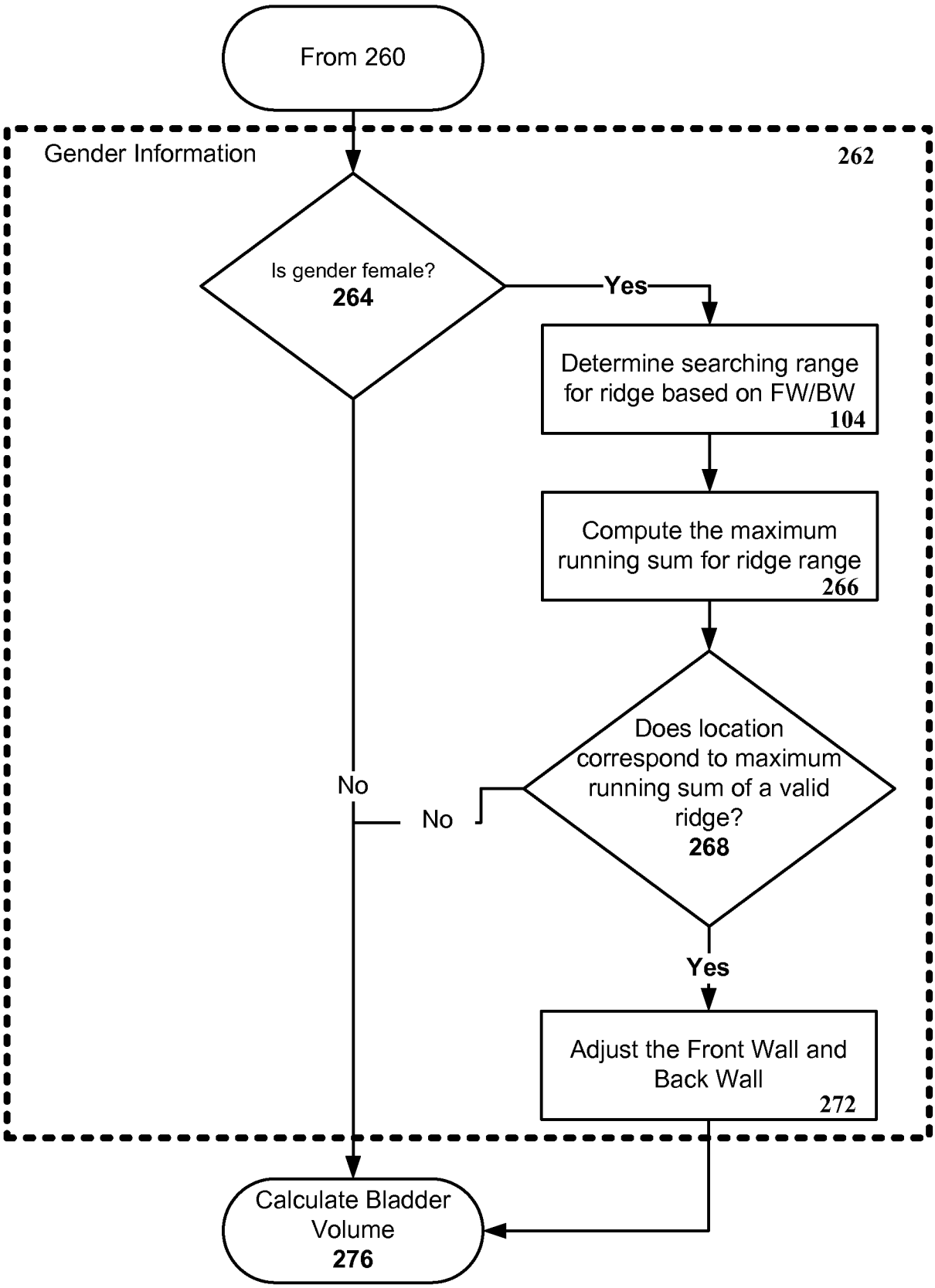
From 260
Gender Information
262
Is gender female?
264
Yes
Determine searching range for ridge based on FW/BW
104
Compute the maximum running sum for ridge range
266
Does location correspond to maximum running sum of a valid ridge?
268
No
No
Yes
Adjust the Front Wall and Back Wall
272
Calculate Bladder Volume
276

Fig. 9F

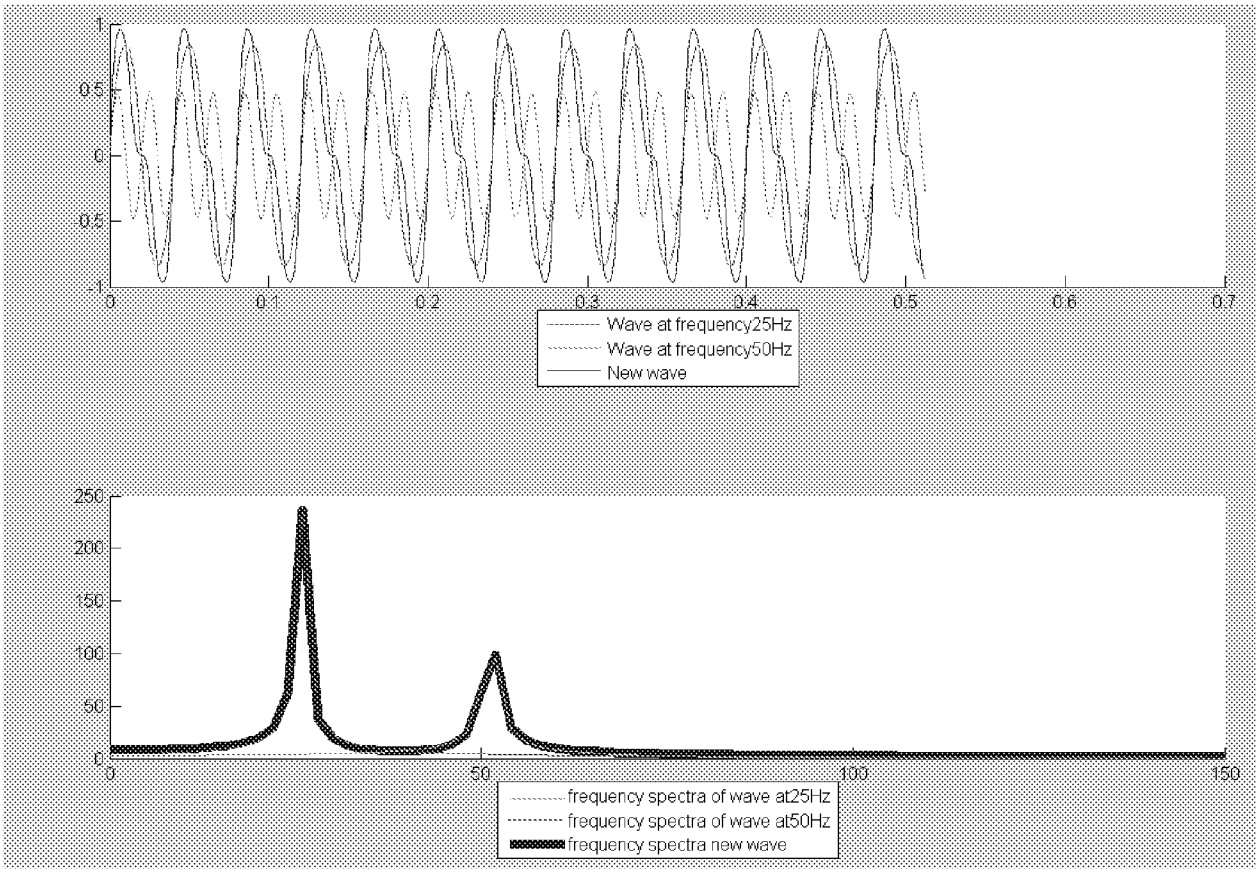

Progressive Sound Wave Distortion with Increasing Harmonics

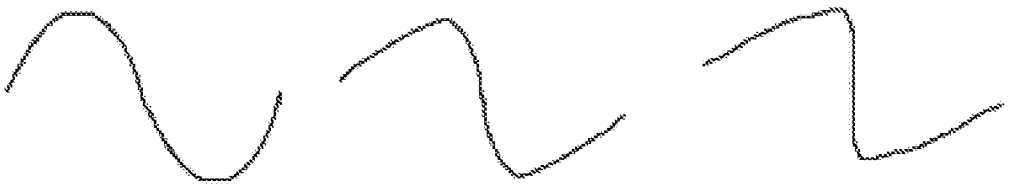

direction of propagation

Fig. 10

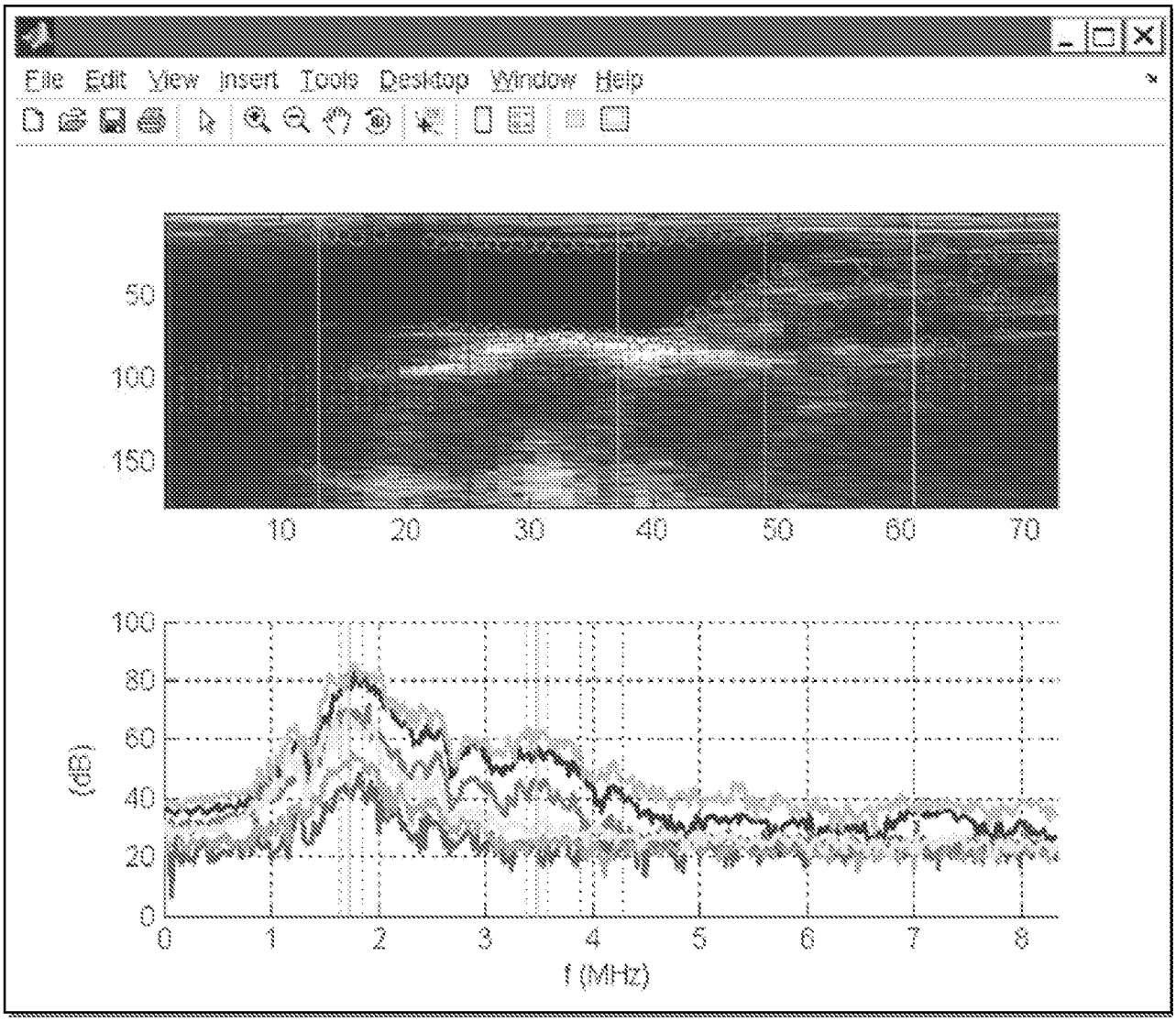
File Edit View Insert Tools Desktop Window Help
50
100
150
10
20
30
40
50
60
70
100
80
60
40
20
0
(dB)
0
1
2
3
4
5
6
7
8
f (MHz)

Fig. 11

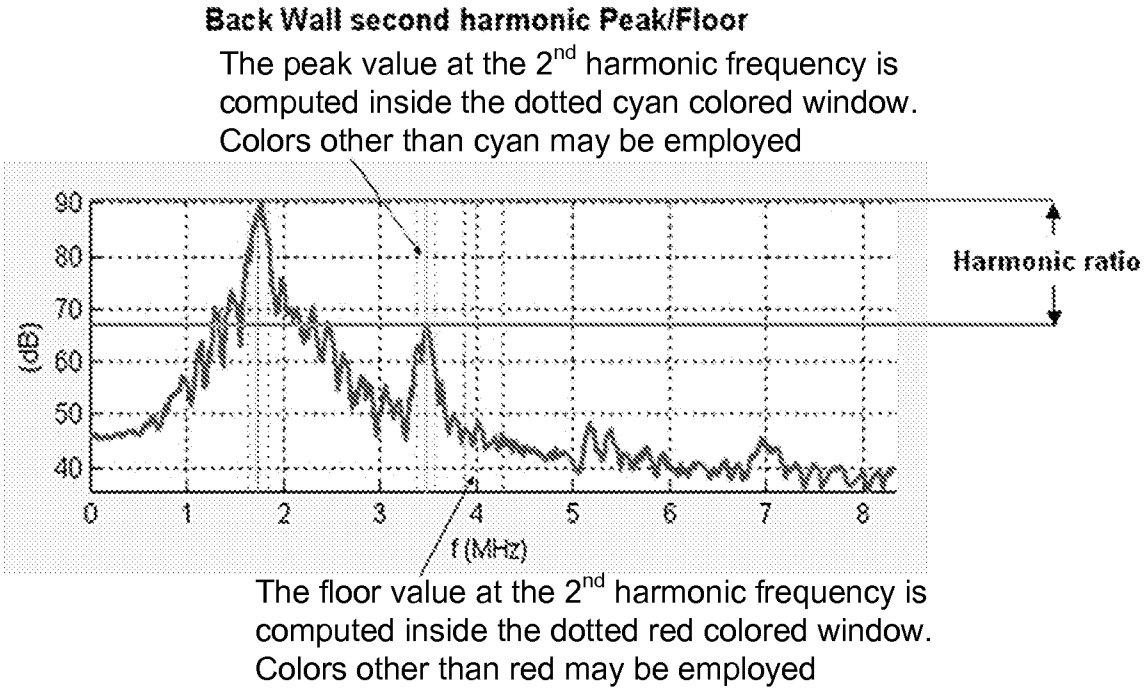
Back Wall second harmonic Peak/Floor
The peak value at the 2nd harmonic frequency is computed inside the dotted cyan colored window. Colors other than cyan may be employed
90
80
70
60
50
40
(dB)
0
1
2
3
4
5
6
7
8
f (MHz)
Harmonic ratio
The floor value at the 2nd harmonic frequency is computed inside the dotted red colored window. Colors other than red may be employed

Fig. 12

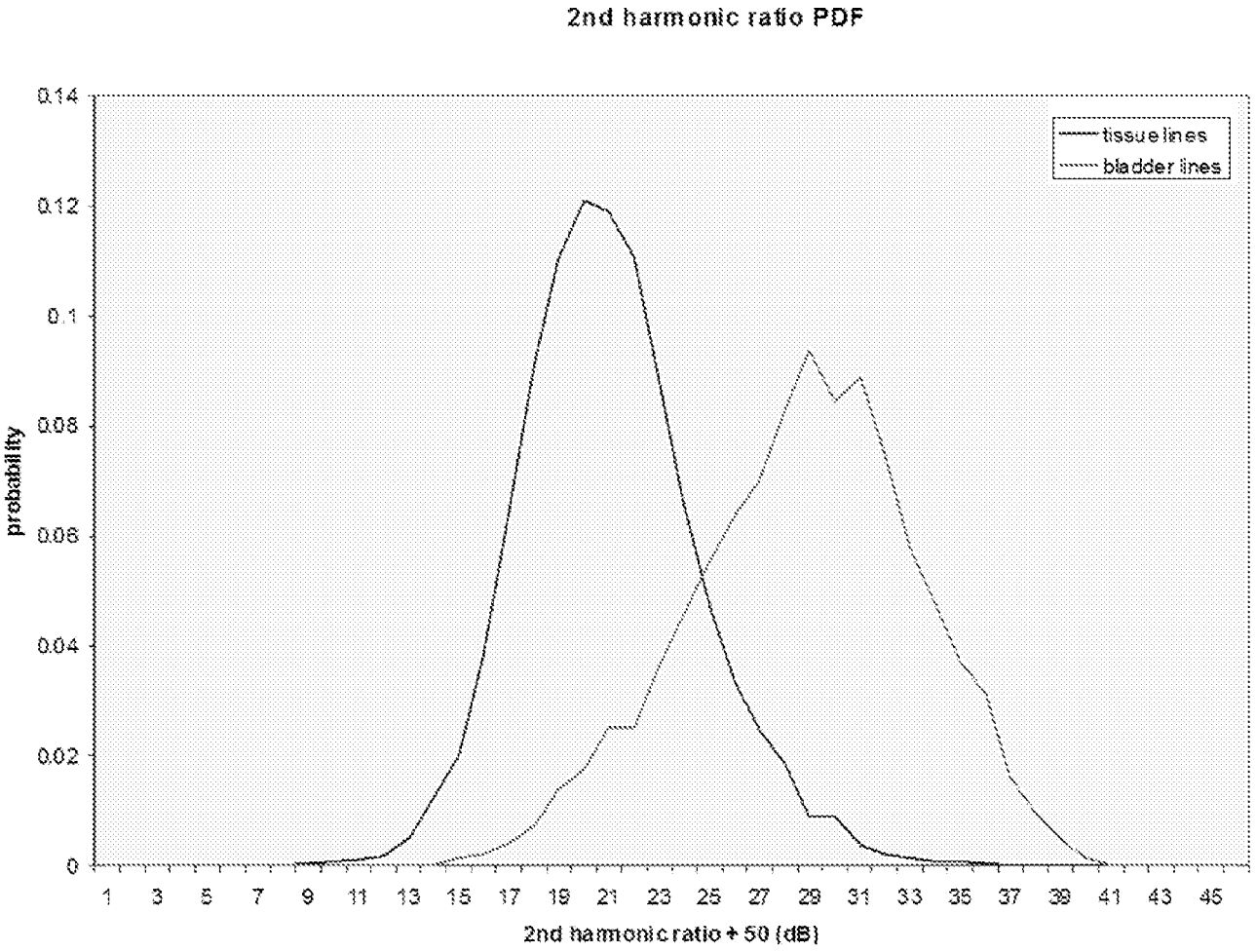
2nd harmonic ratio PDF
tissue lines
bladder lines
probability
0.14
0.12
0.1
0.08
0.06
0.04
0.02
0
1 3 5 7 9 11 13 15 17 19 21 23 25 27 29 31 33 35 37 39 41 43 45
2nd harmonic ratio + 50 (dB)

Fig. 13

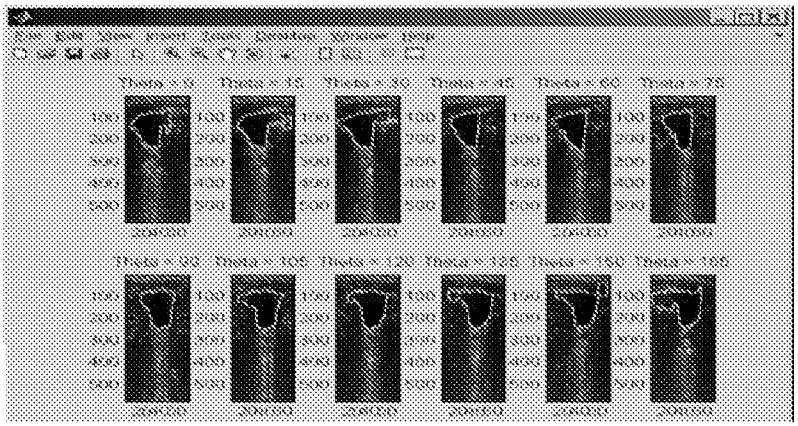

Fig. 14A

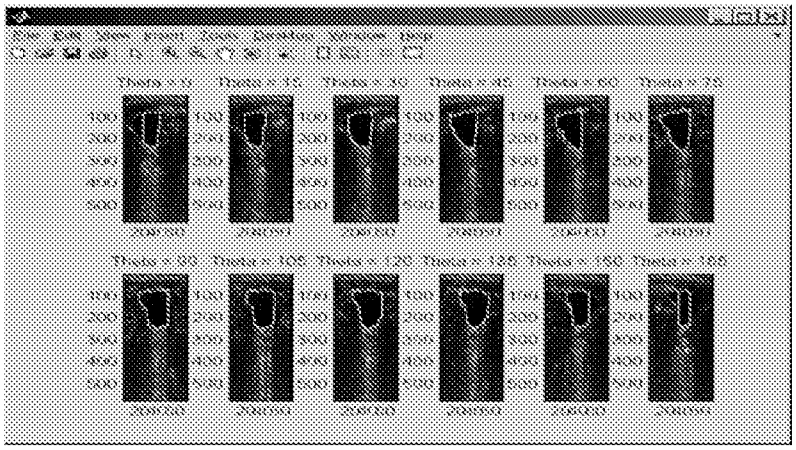

Fig. 14B

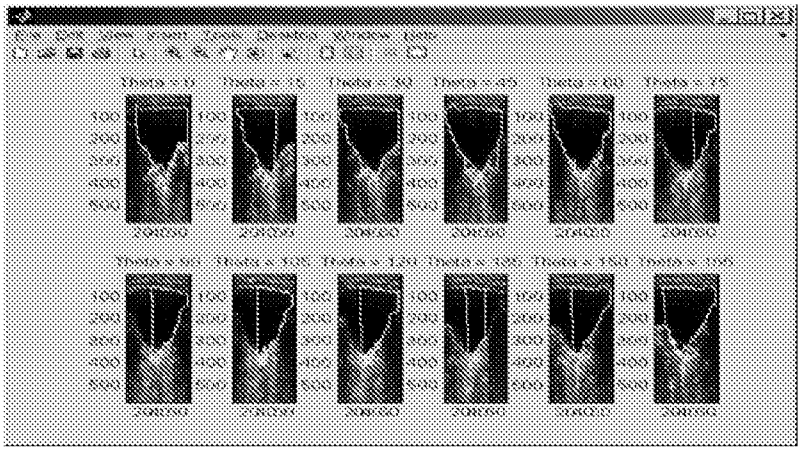

Fig. 15A

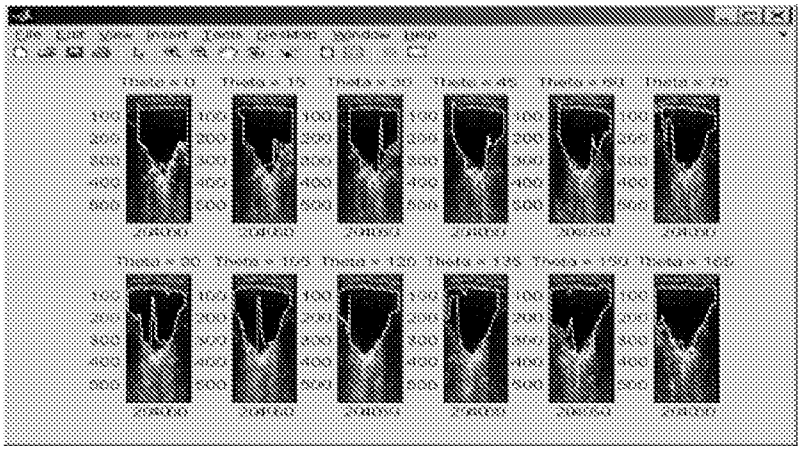

Fig. 15B

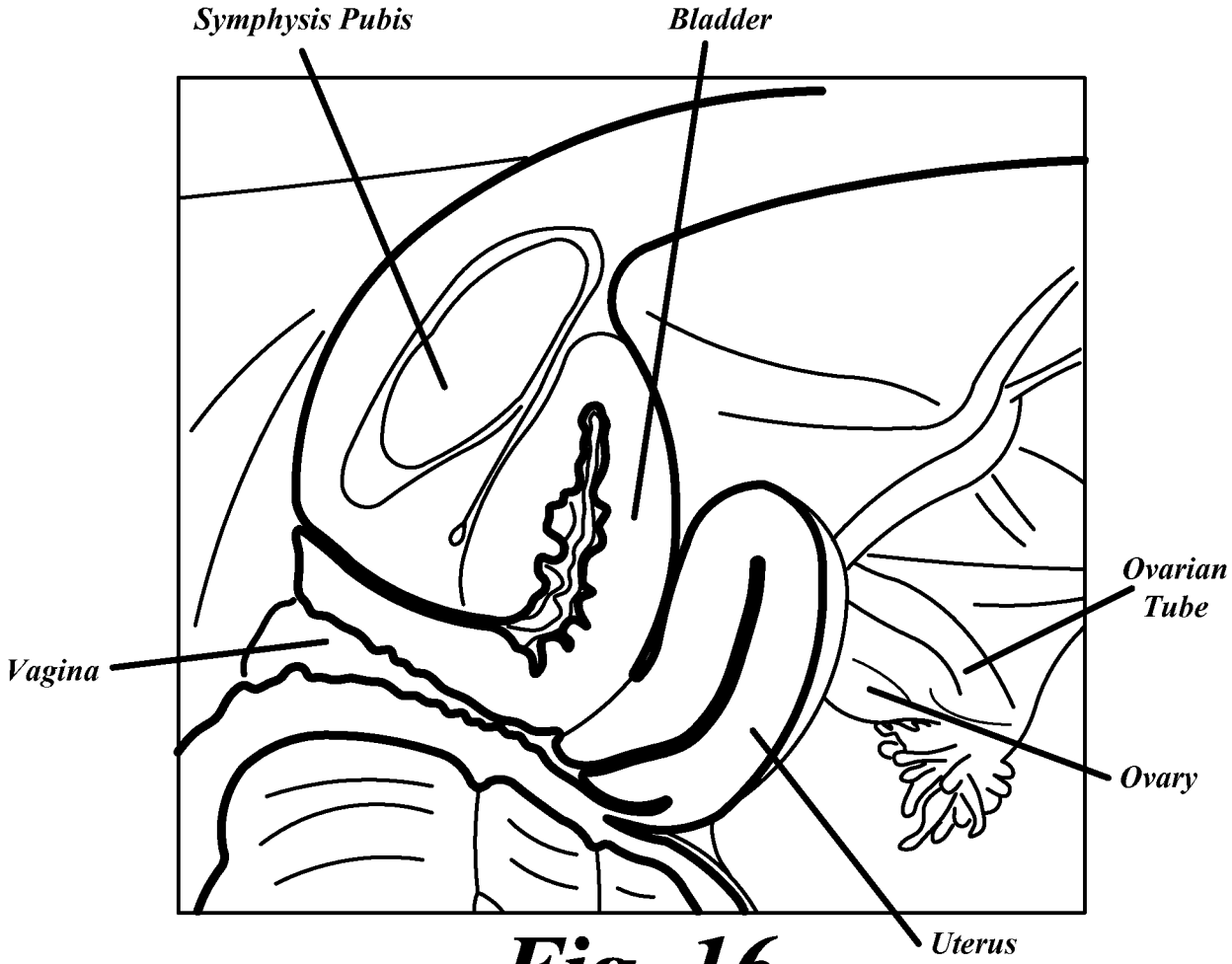

Fig. 16

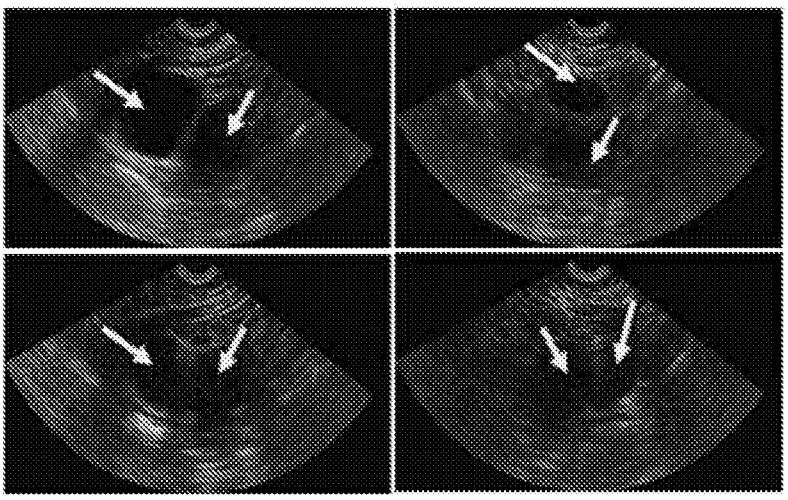

Fig. 17

Ridge between bladder and uterus.
1057 Plane 7, Theta = 90 degrees

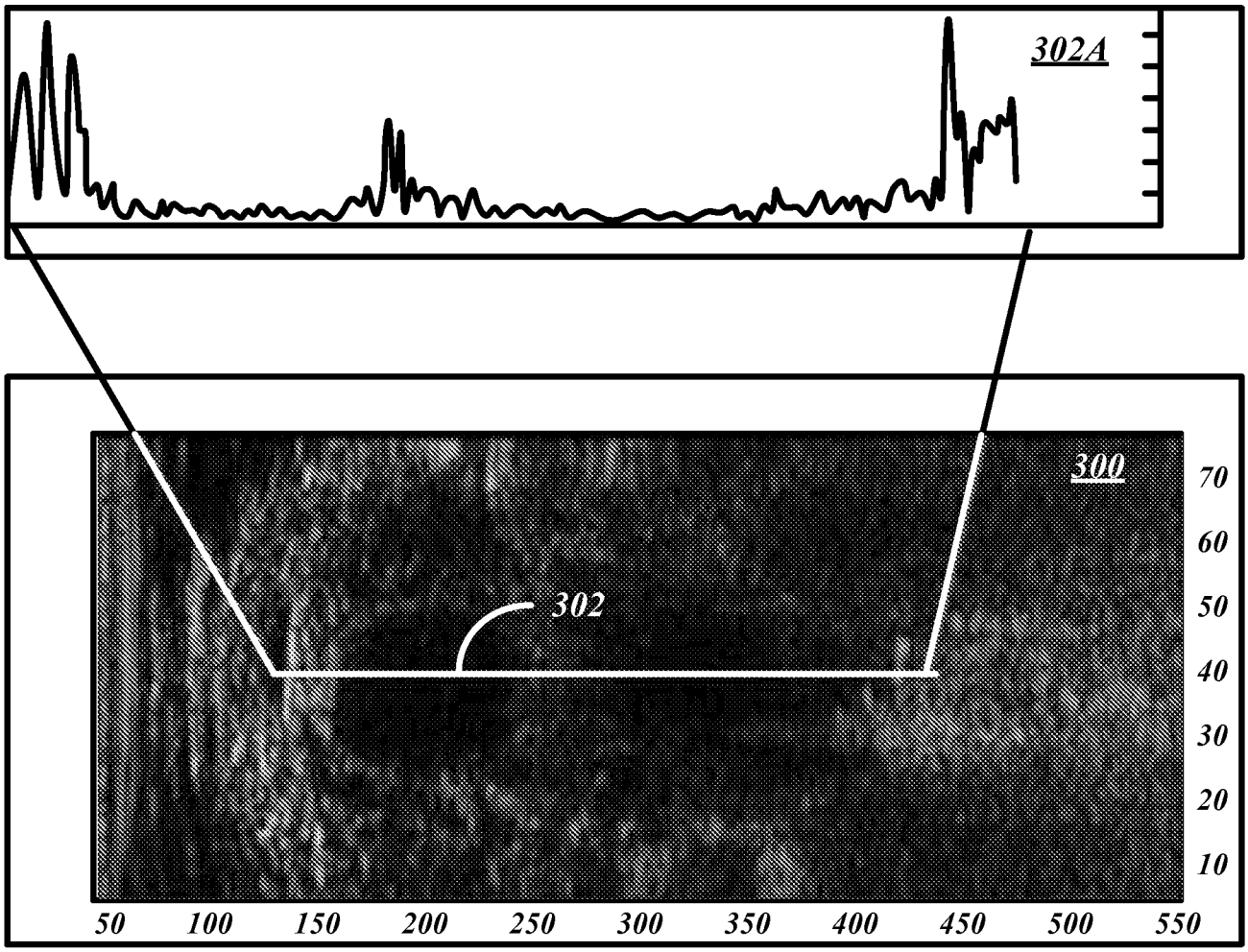

Fig. 18

Ridge between bladder and uterus.
1082 Plane 12, Theta = 165 degrees

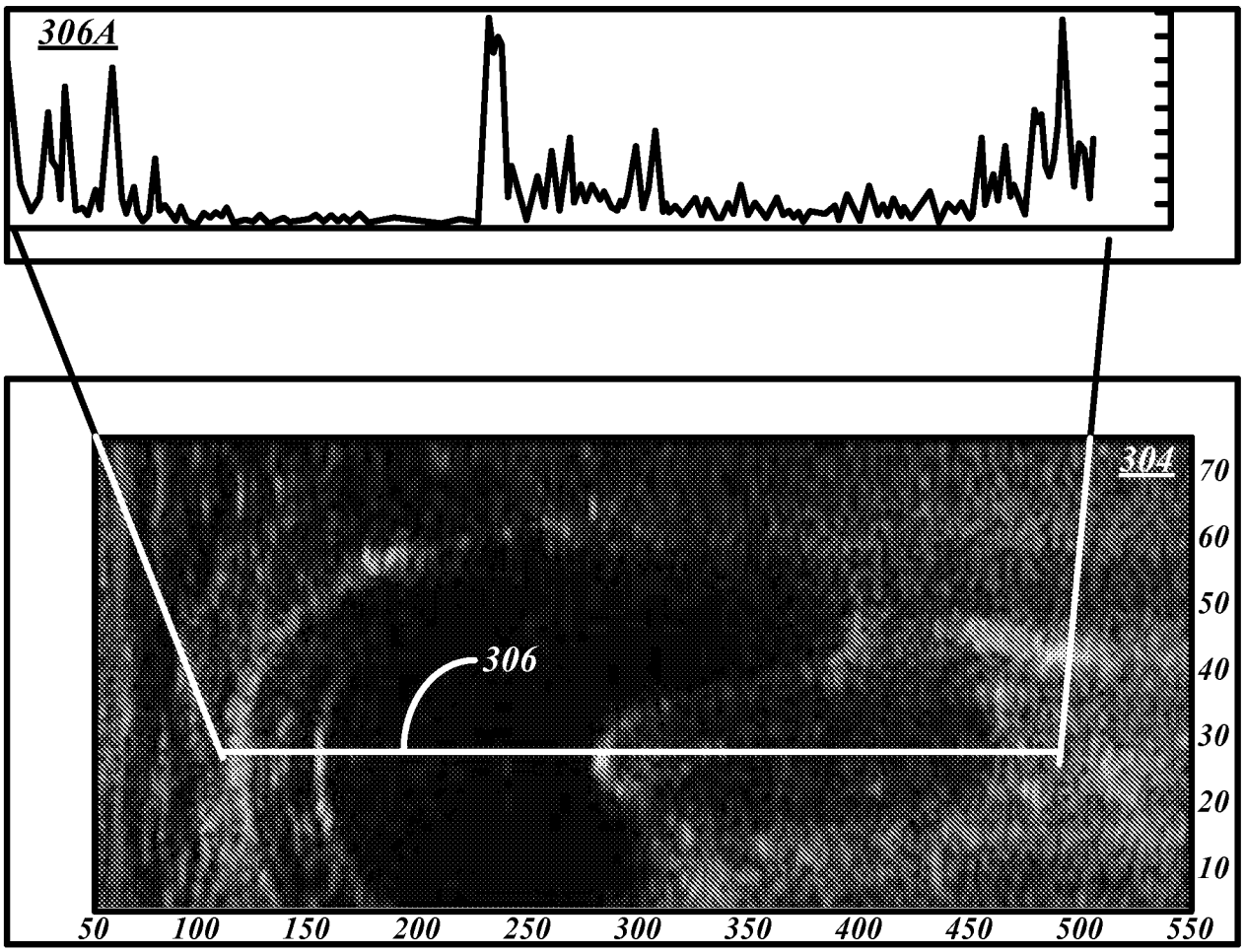

Fig. 19

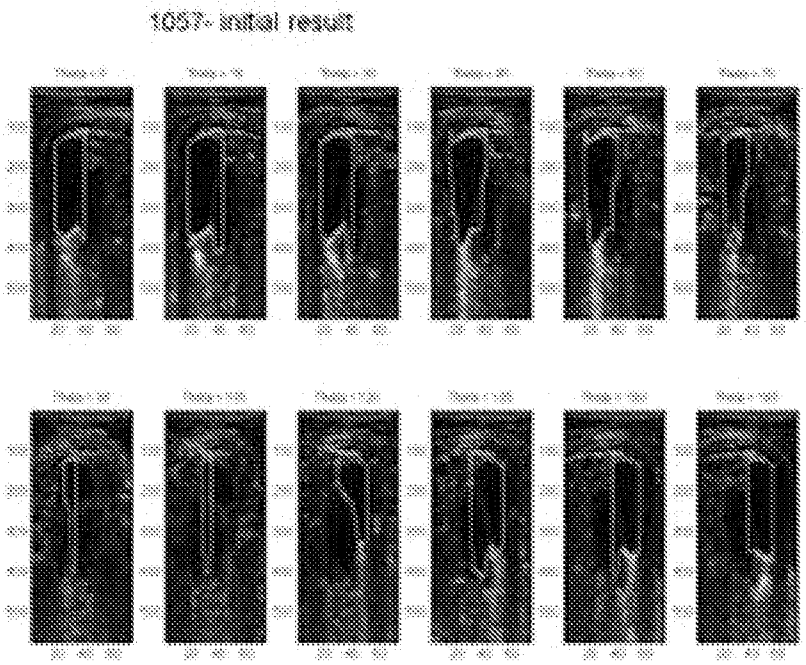

Fig. 20

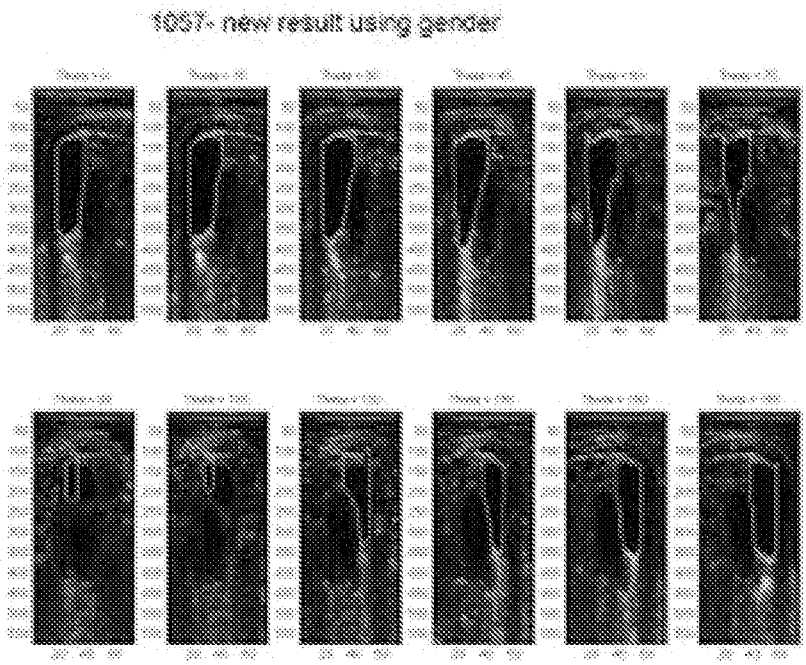

Fig. 21

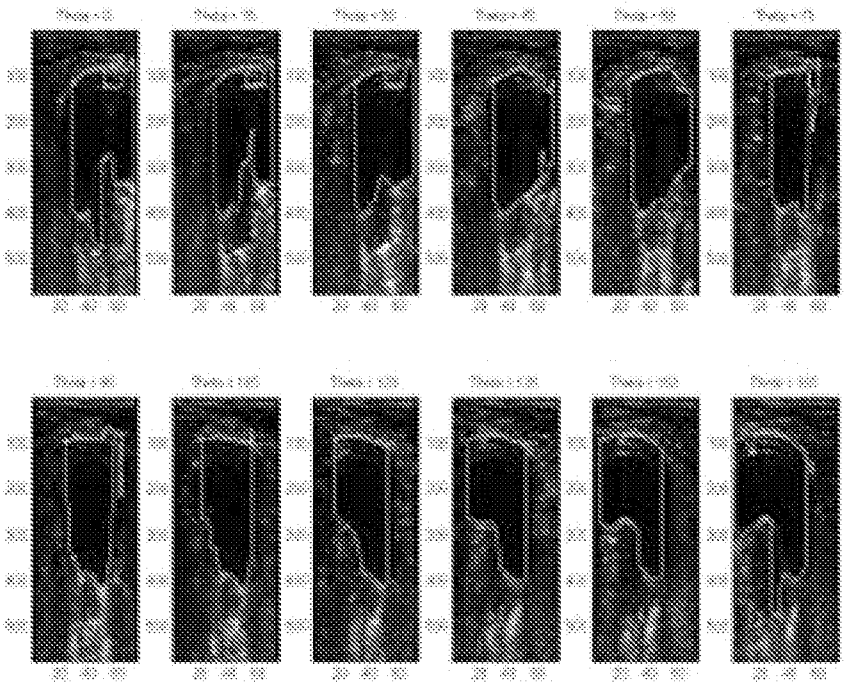

Fig. 22

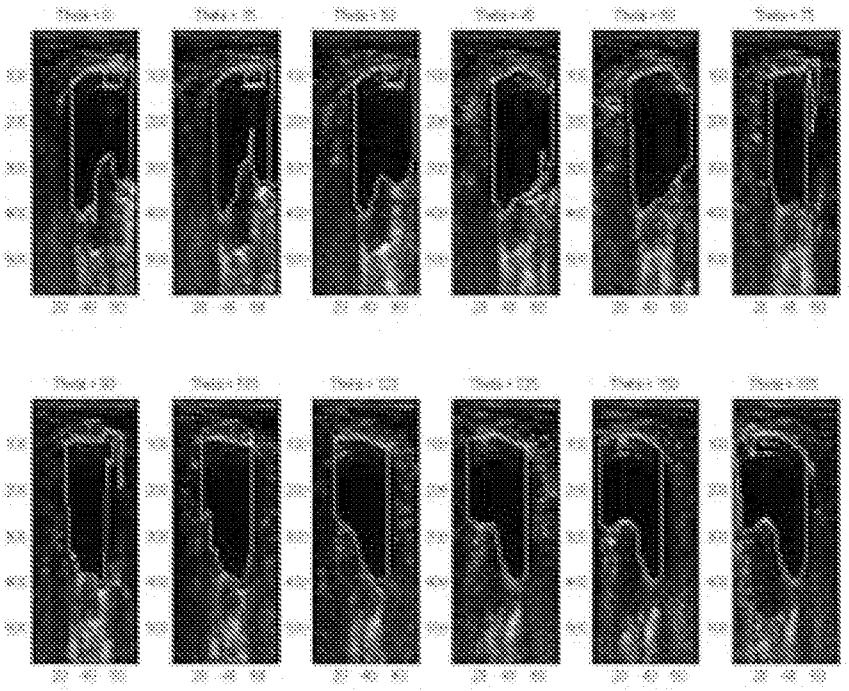

Fig. 23

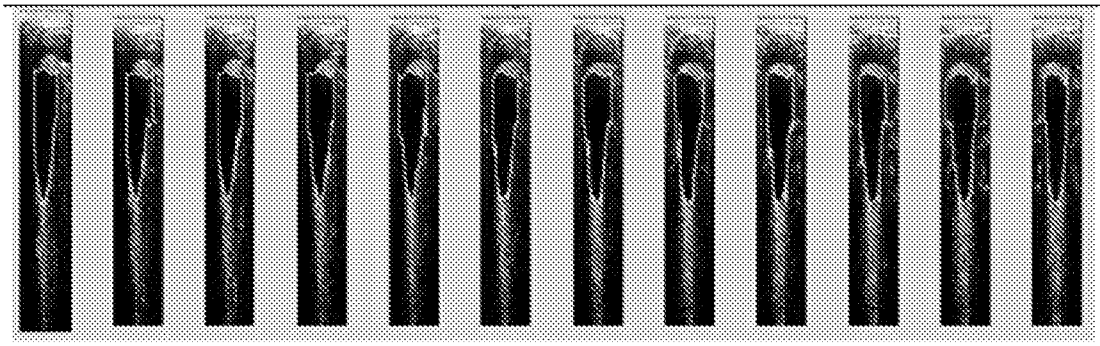

Segmentation from plane 1 - 12

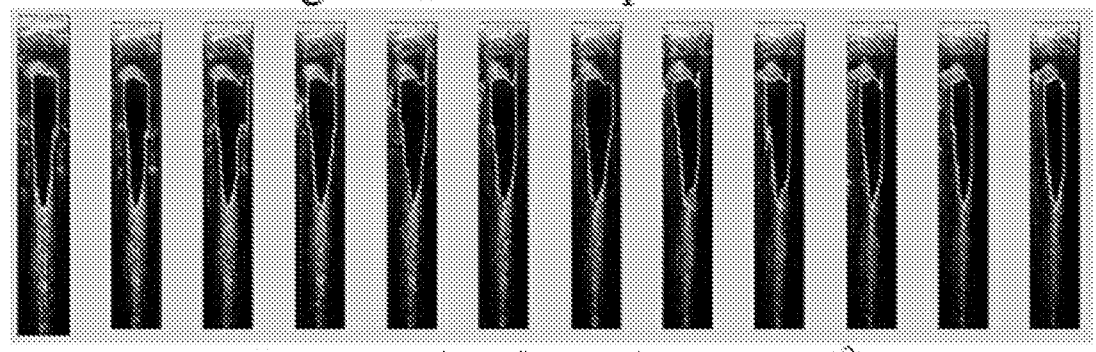

Segmentation from plane 13- 24[2]

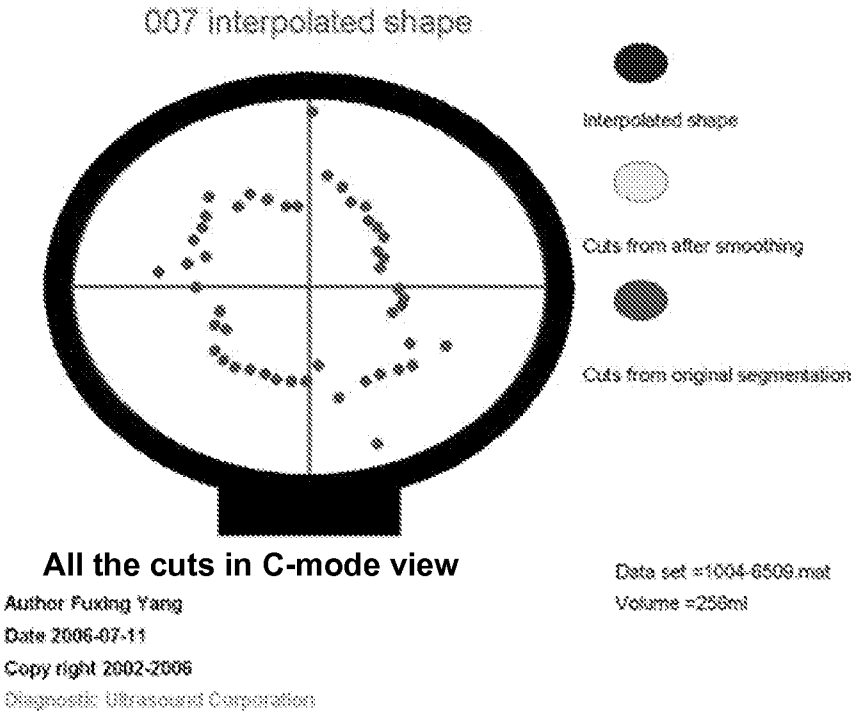

Fig. 24

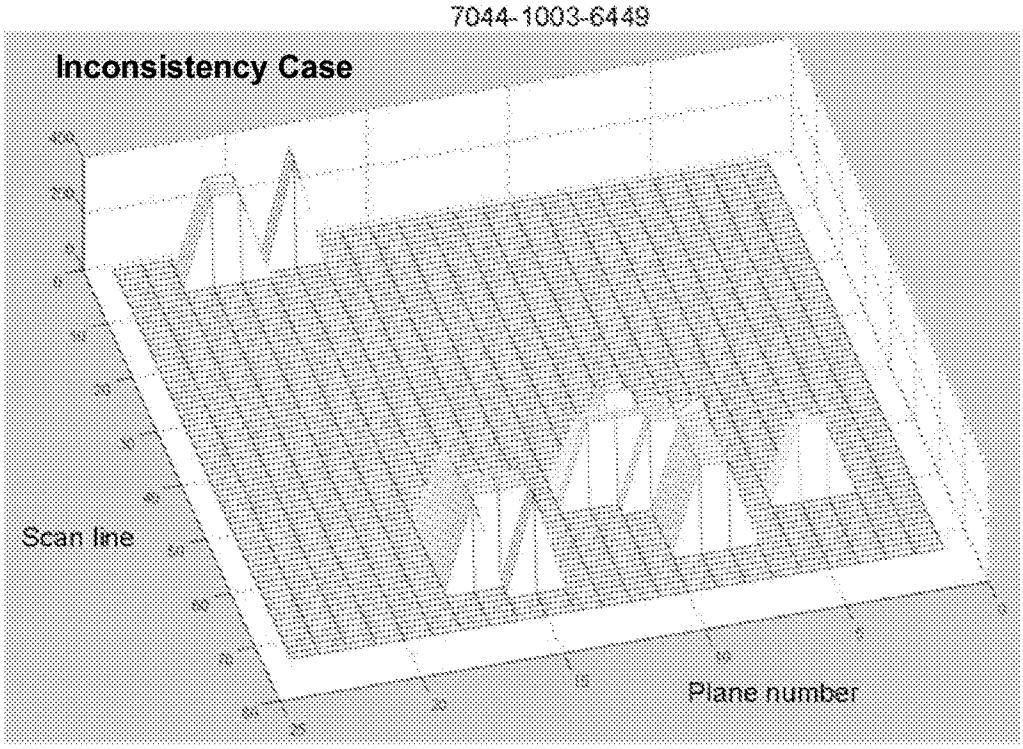

Abnormal case for bladder segmentation, where more than one connected regions based on the segmentation on all planes

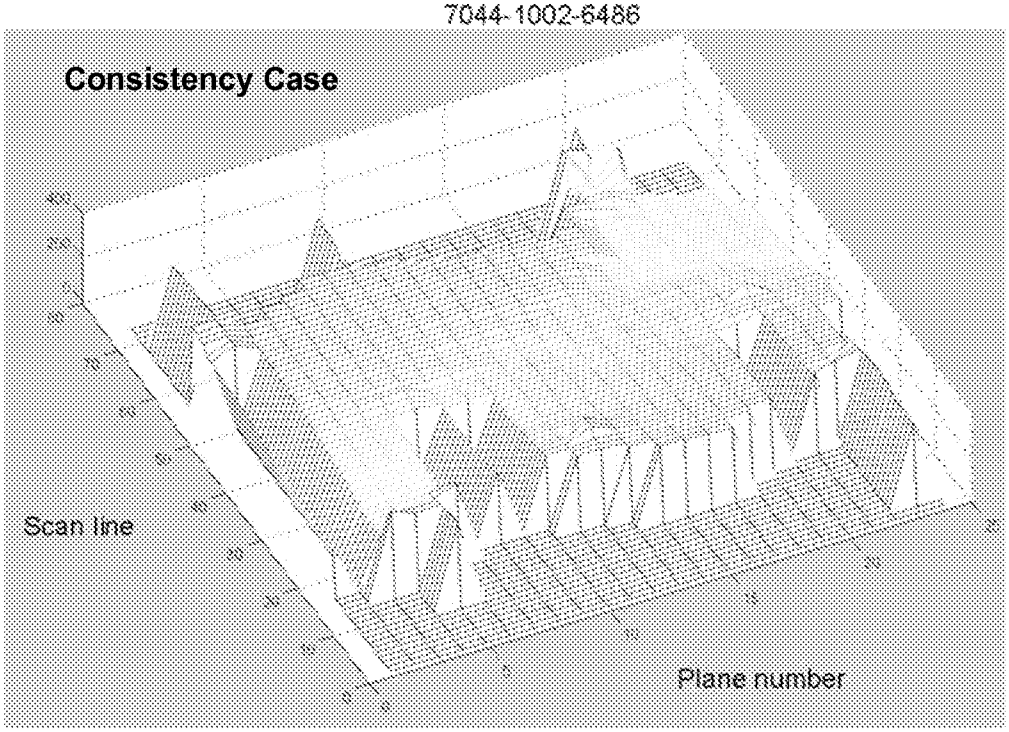

Normal case for bladder segmentation, where only one connected region based on the segmentation on all planes

Fig. 25

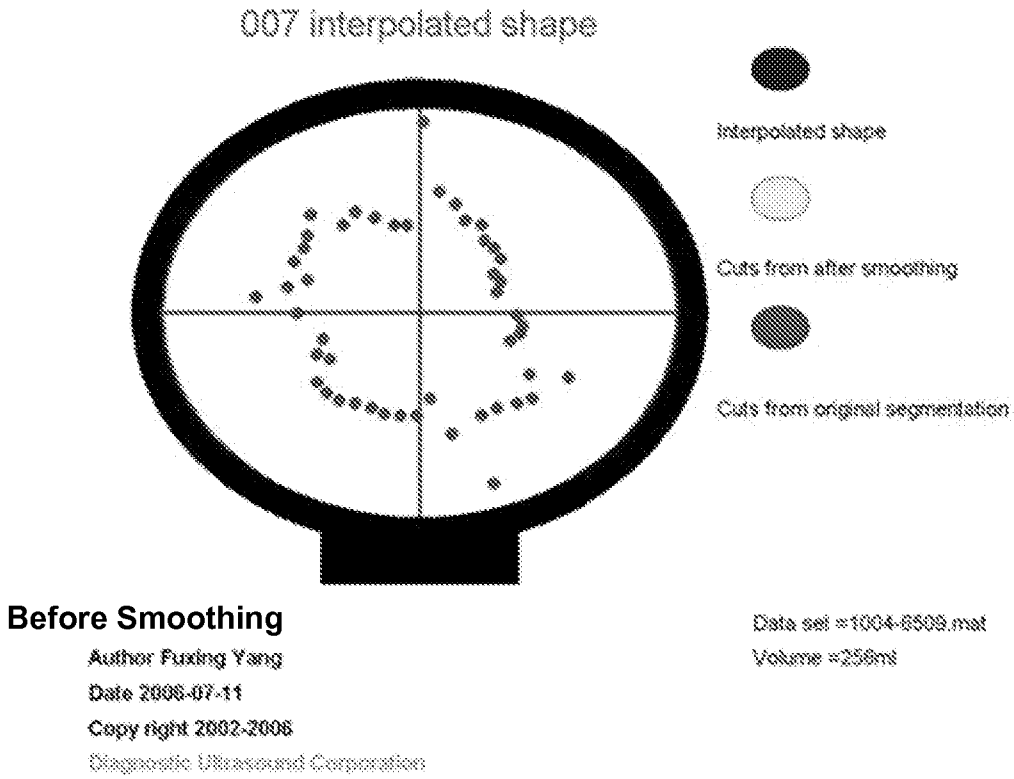
007 interpolated shape
Interpolated shape
Cuts from after smoothing
Cuts from original segmentation
Before Smoothing
Author Fuxing Yang
Date 2006-07-11
Copy right 2002-2006
Diagnostic Ultrasound Corporation
Data set =1004-6509.mat
Volume =256ml

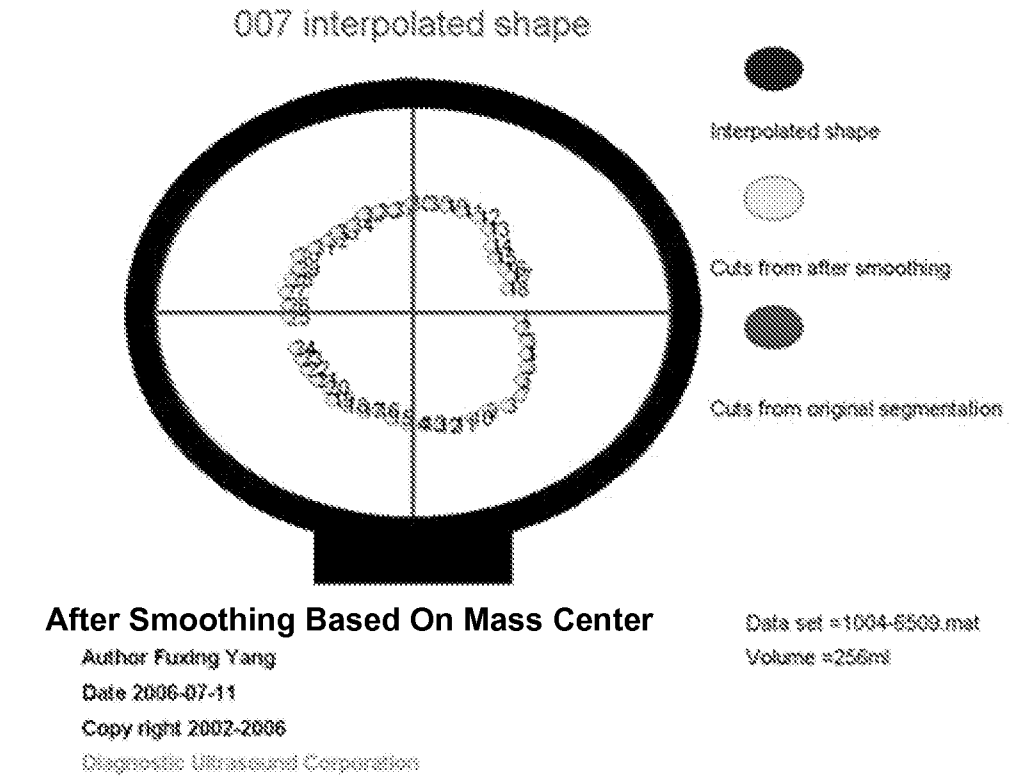
007 interpolated shape
Interpolated shape
Cuts from after smoothing
Cuts from original segmentation
After Smoothing Based On Mass Center
Author Fuxing Yang
Date 2006-07-11
Copy right 2002-2006
Diagnostic Ultrasound Corporation
Data set =1004-6509.mat
Volume =256ml

Fig. 26

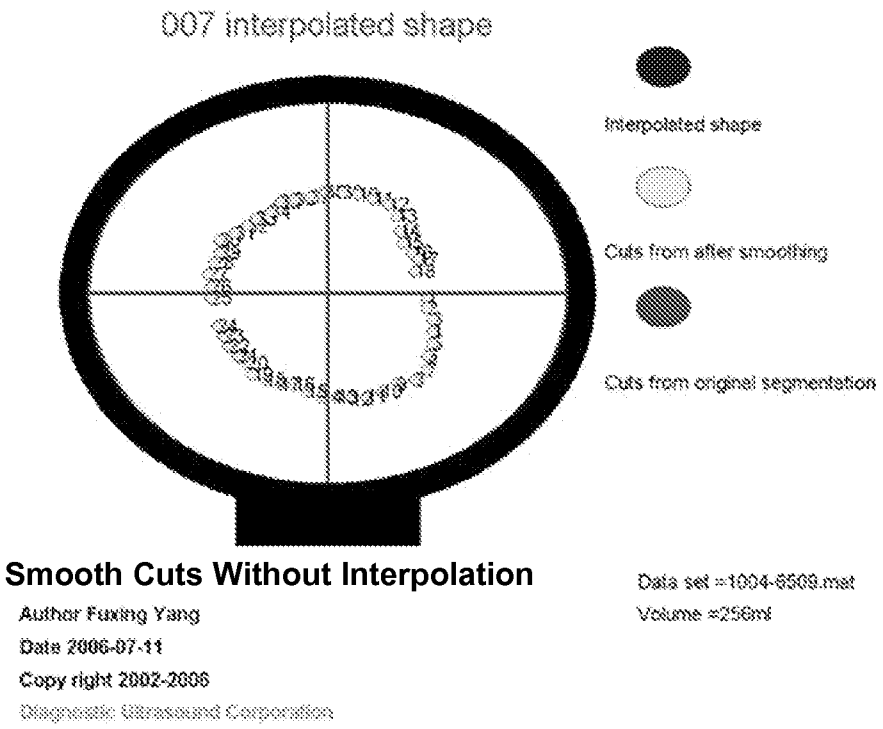
007 interpolated shape
Interpolated shape
Cuts from after smoothing
Cuts from original segmentation
Smooth Cuts Without Interpolation
Author Fuxing Yang
Date 2006-07-11
Copy right 2002-2006
Diagnostic Ultrasound Corporation
Data set =1004-6509.mat
Volume =256ml

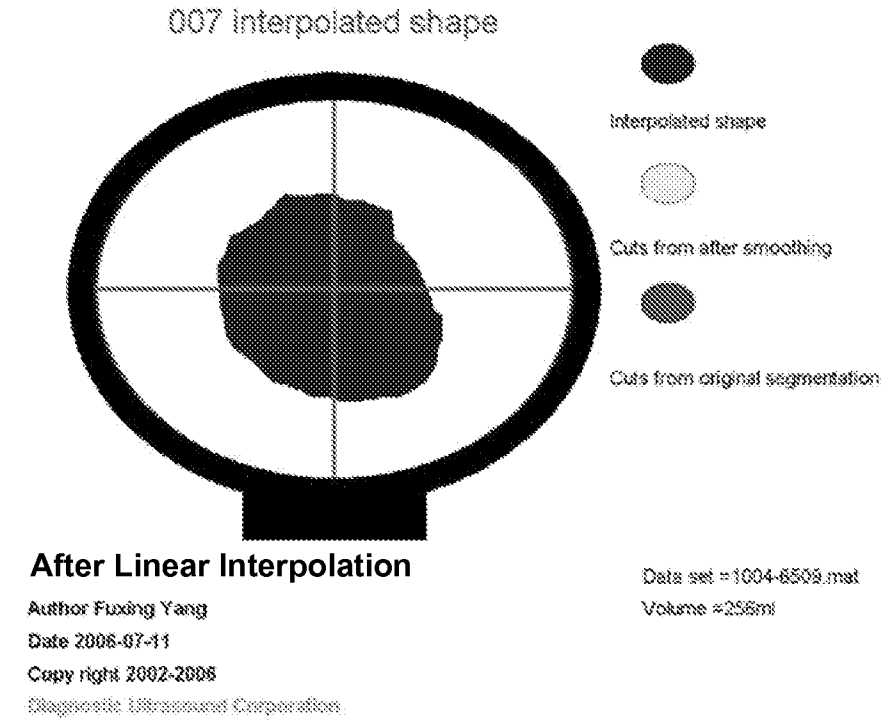
007 interpolated shape
Interpolated shape
Cuts from after smoothing
Cuts from original segmentation
After Linear Interpolation
Author Fuxing Yang
Date 2006-07-11
Copy right 2002-2006
Diagnostic Ultrasound Corporation
Data set =1004-6509.mat
Volume =256ml

Fig. 27

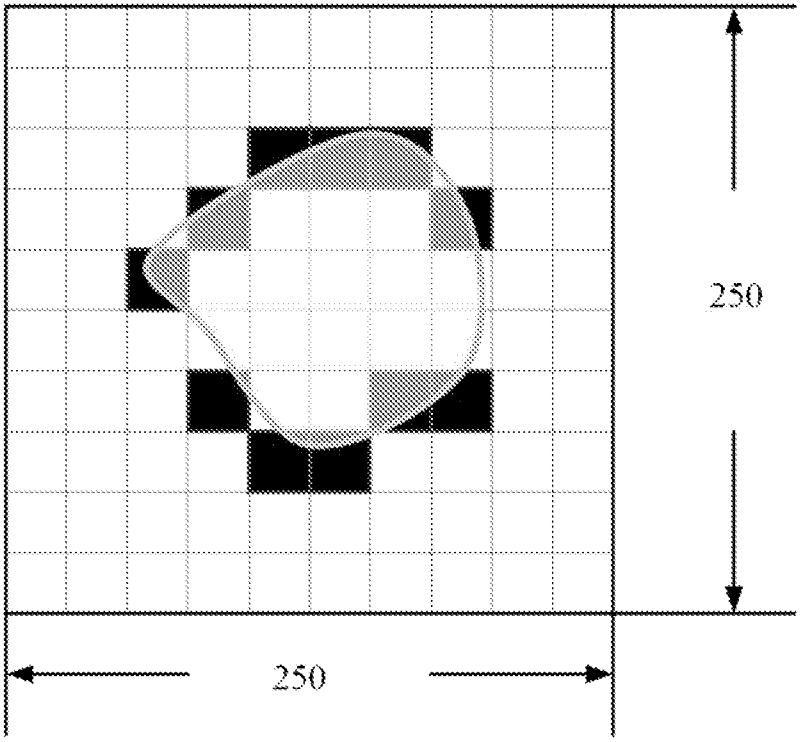

Fig. 28

empty (default starting mode, no arrow)	good aiming (all arrows blink)	(single blinking arrow)	(single solid arrow)
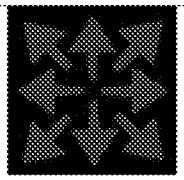	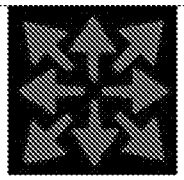	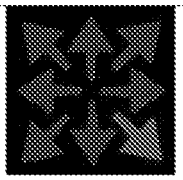	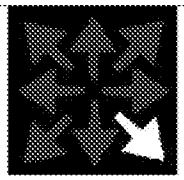

Different arrow feedback modes

Fig. 29

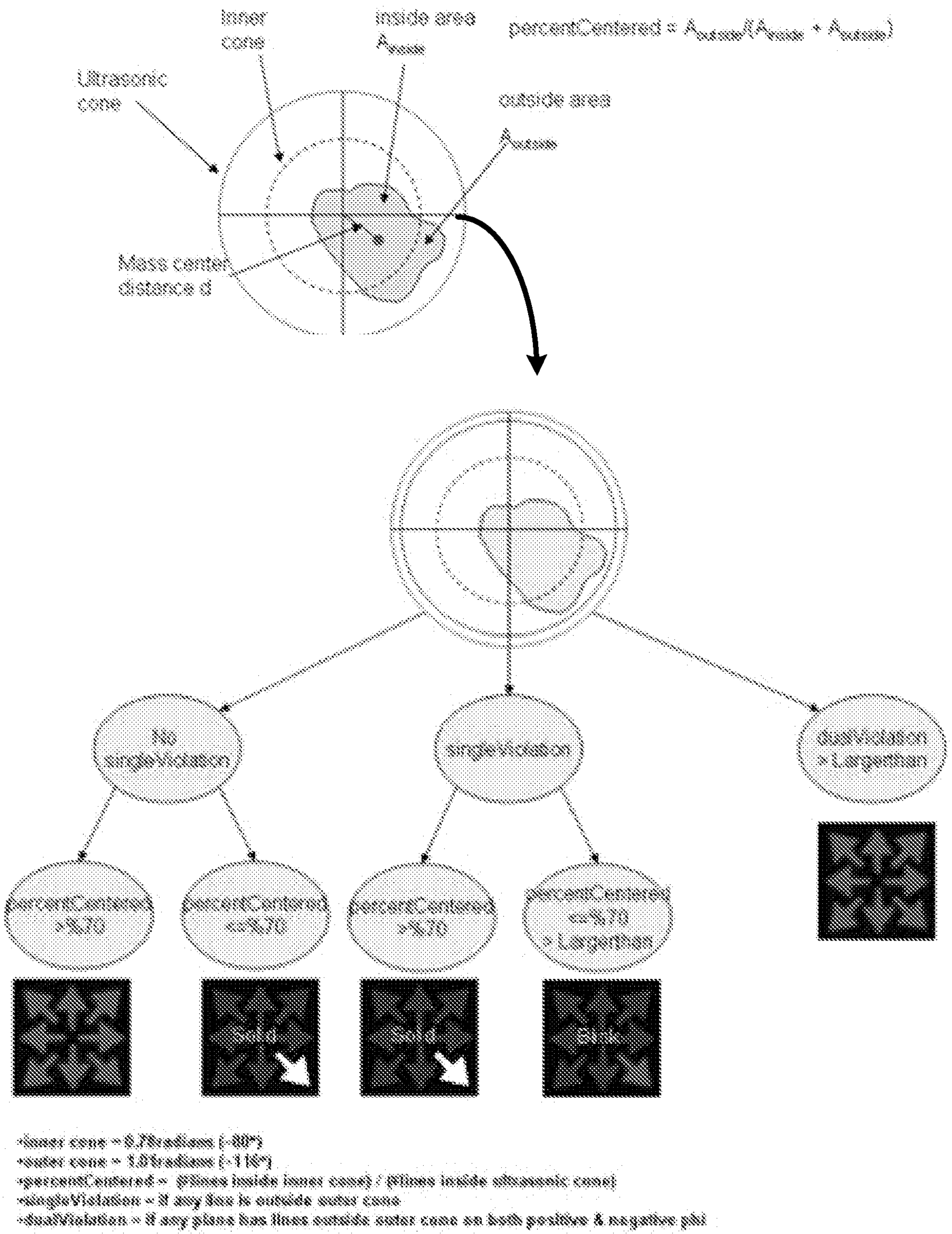
Inner cone
inside area A_{inside}
percentCentered = $A_{outside}/(A_{inside} + A_{outside})$
Ultrasonic cone
outside area $A_{outside}$
Mass center distance d
No singleViolation
singleViolation
dualViolation > Largerthan
percentCentered >%70
percentCentered <=%70
percentCentered >%70
percentCentered <=%70 > Largerthan
•inner cone = 0.78radians (~80°)
•outer cone = 1.01radians (~116°)
•percentCentered = (#lines inside inner cone) / (#lines inside ultrasonic cone)
•singleViolation = if any line is outside outer cone
•dualViolation = if any plane has lines outside outer cone on both positive & negative phi

Fig. 30

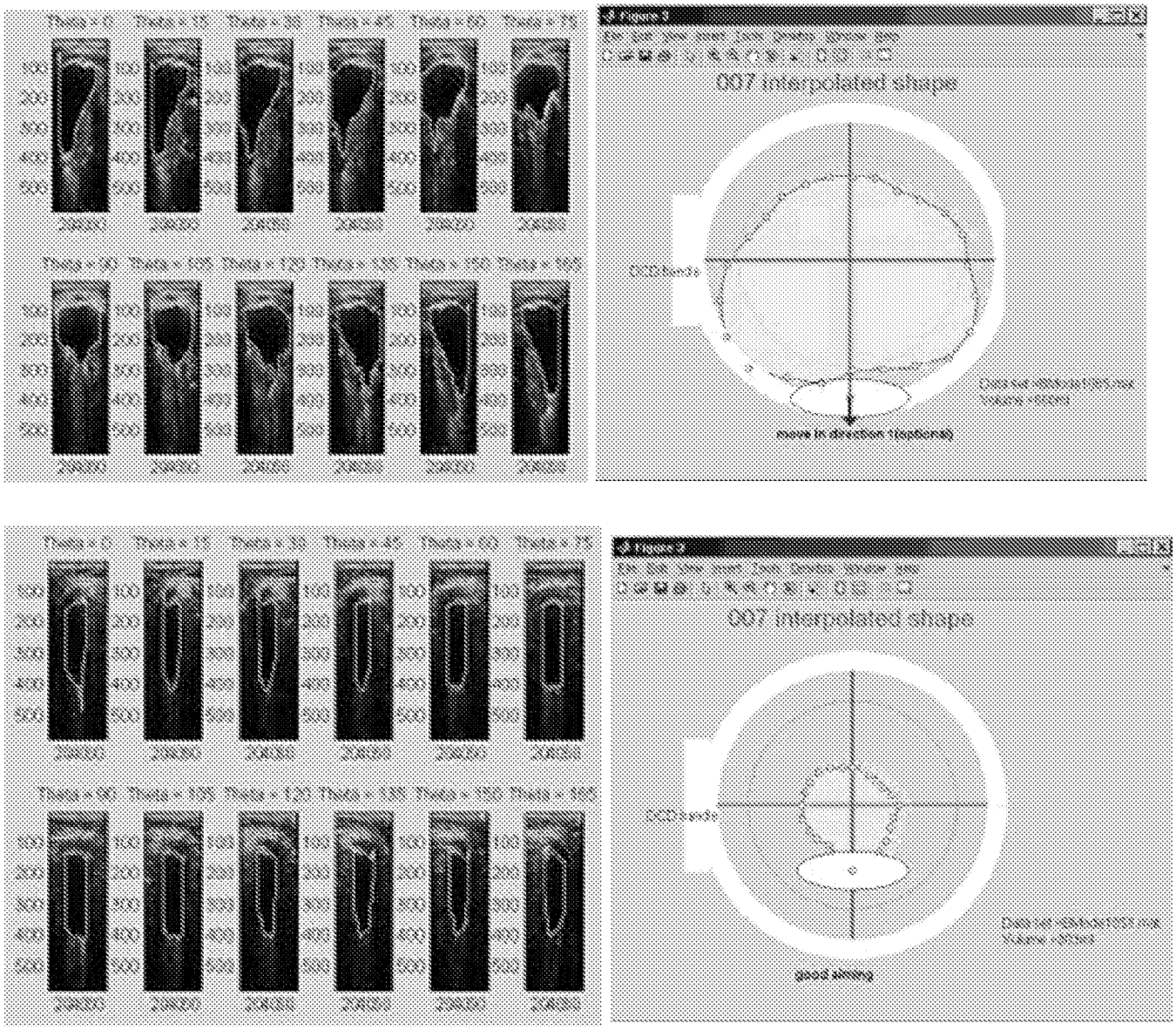

Shadow, segmentation and pubic bone

Fig. 31

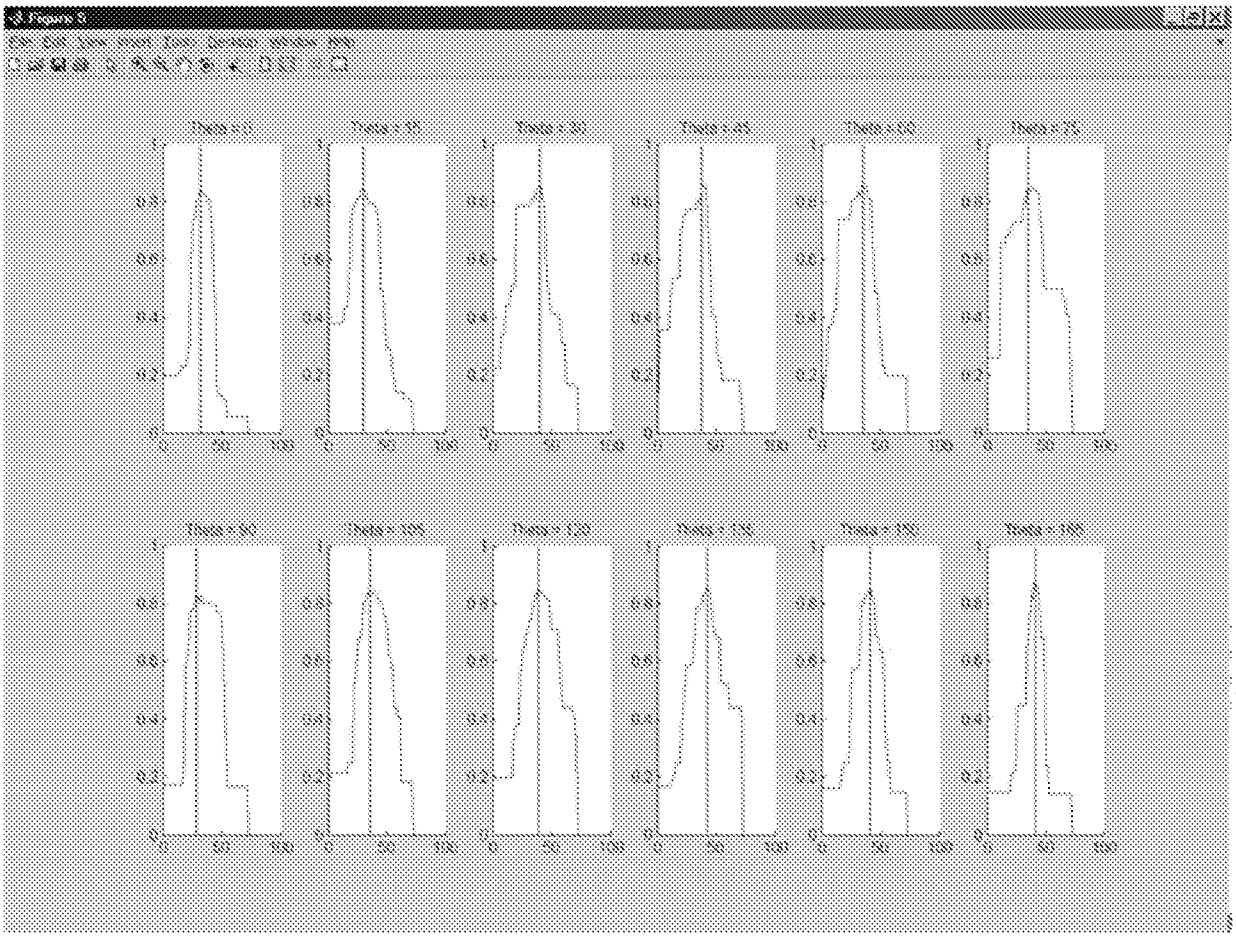

Example of grading results

Fig. 32

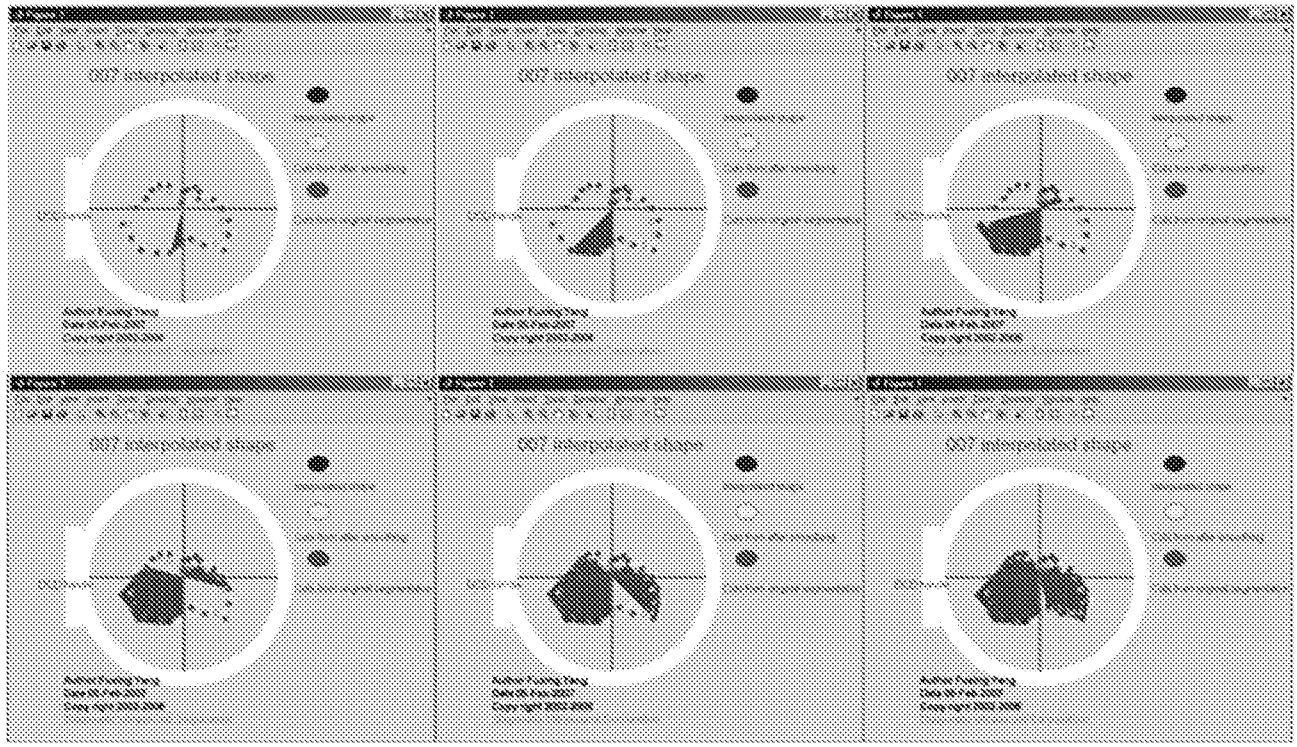

A series of intermediate C-mode shapes

Fig. 33

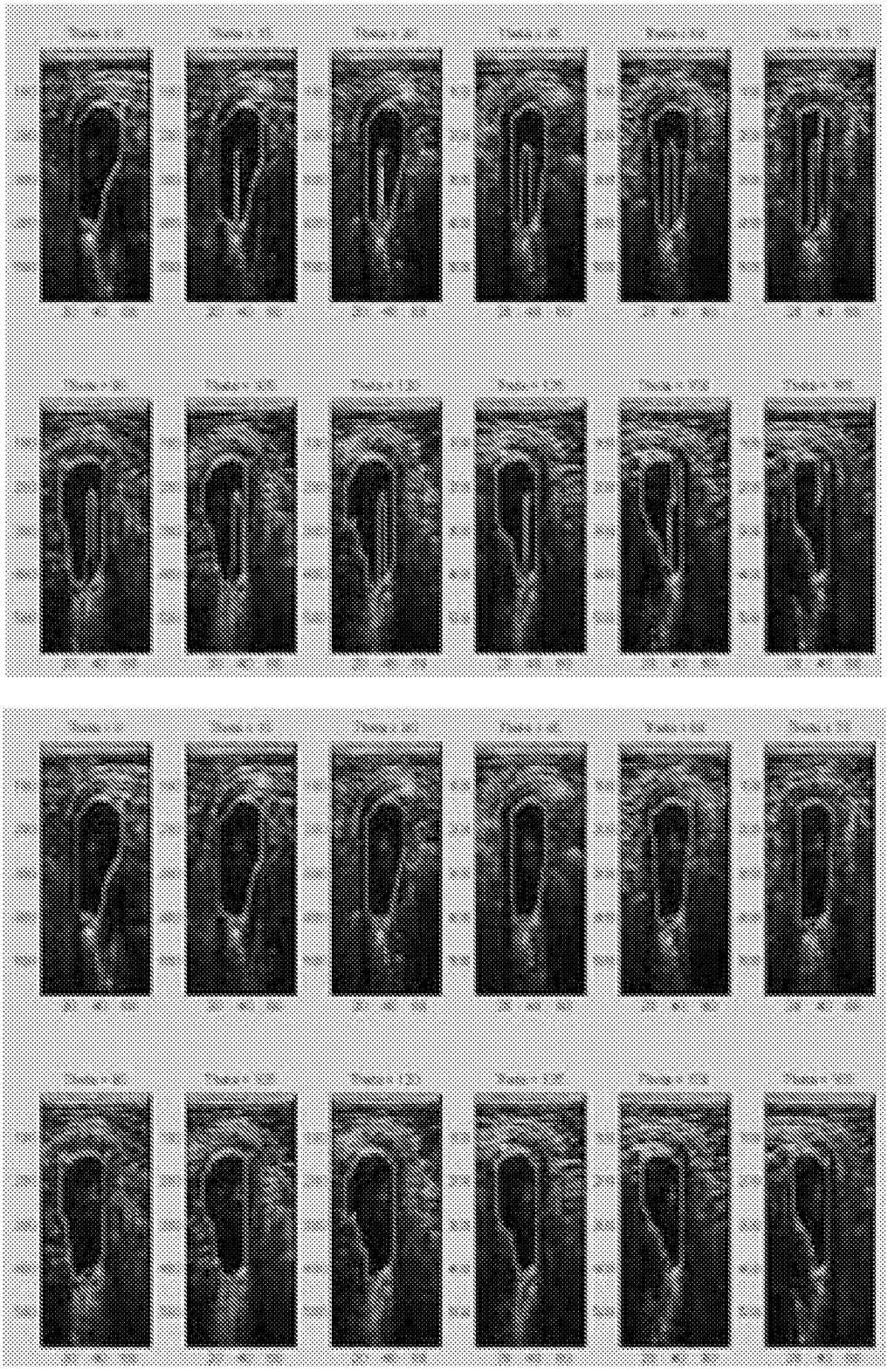

Fig. 34

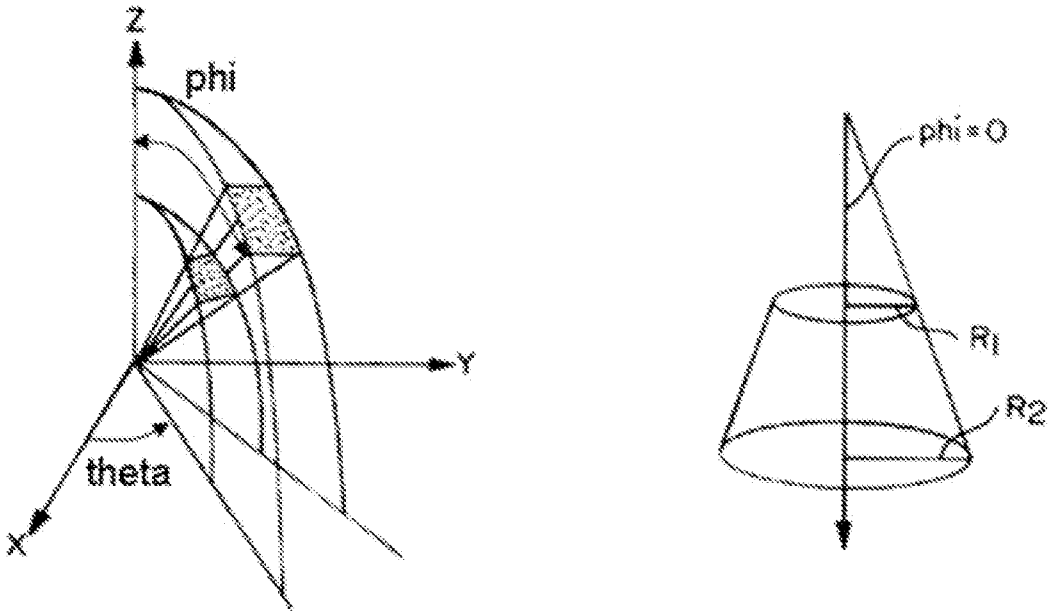

Fig. 35

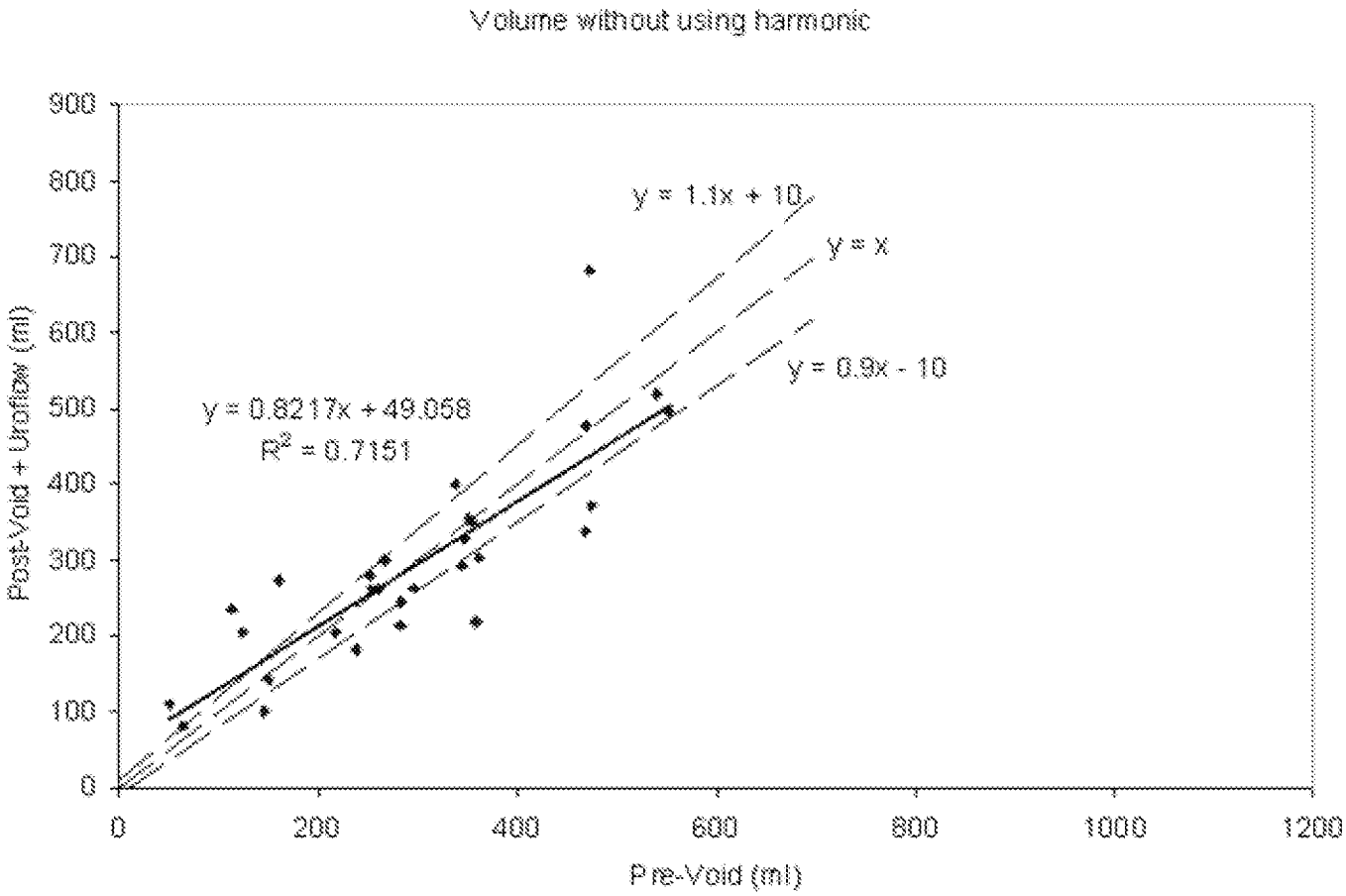
Volume without using harmonic
y = 1.1x + 10
y = x
y = 0.9x - 10
y = 0.8217x + 49.058
R² = 0.7151
Post-Void + Unoflow (ml)
Pre-Void (ml)
0
100
200
300
400
500
600
700
800
900
0
200
400
600
800
1000
1200

Fig. 36

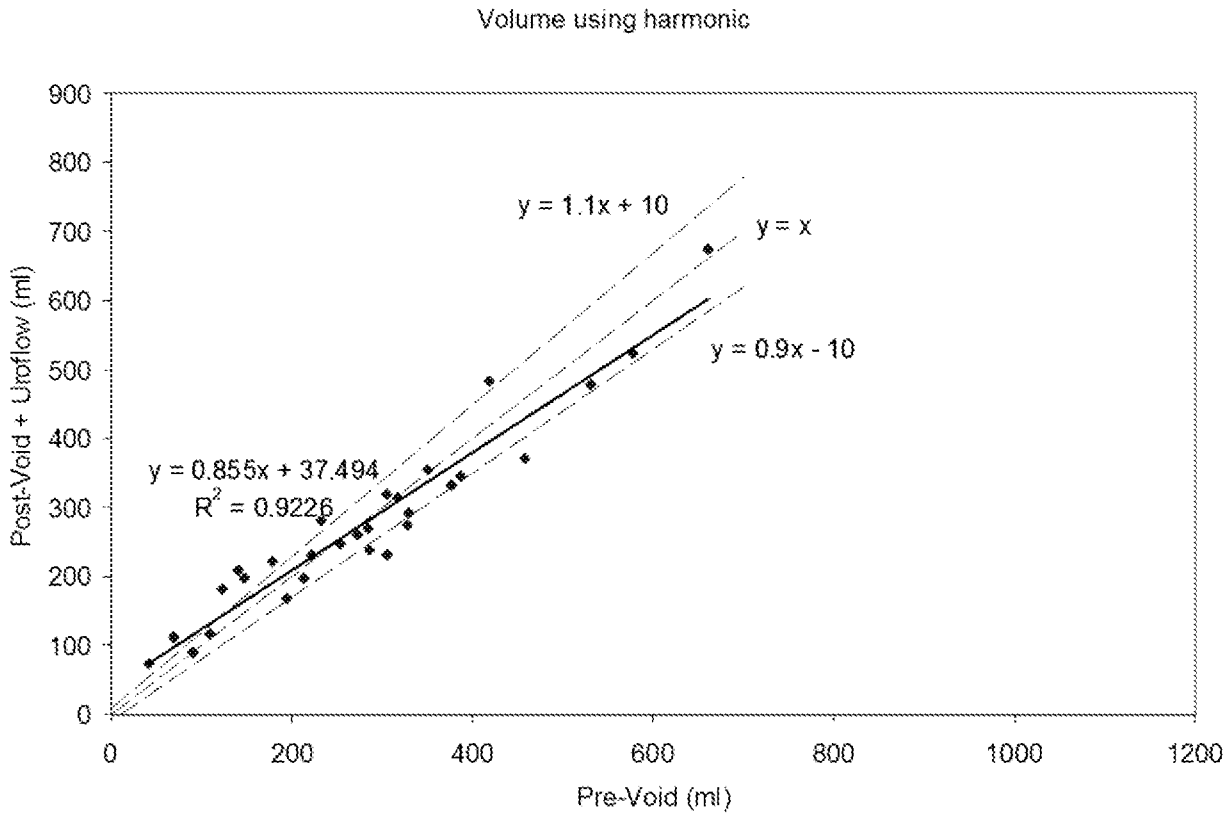
Volume using harmonic
Post-Void + Uroflow (ml)
Pre-Void (ml)
y = 1.1x + 10
y = x
y = 0.9x - 10
y = 0.855x + 37.494
R2 = 0.9226
0
100
200
300
400
500
600
700
800
900
0
200
400
600
800
1000
1200

Fig. 37

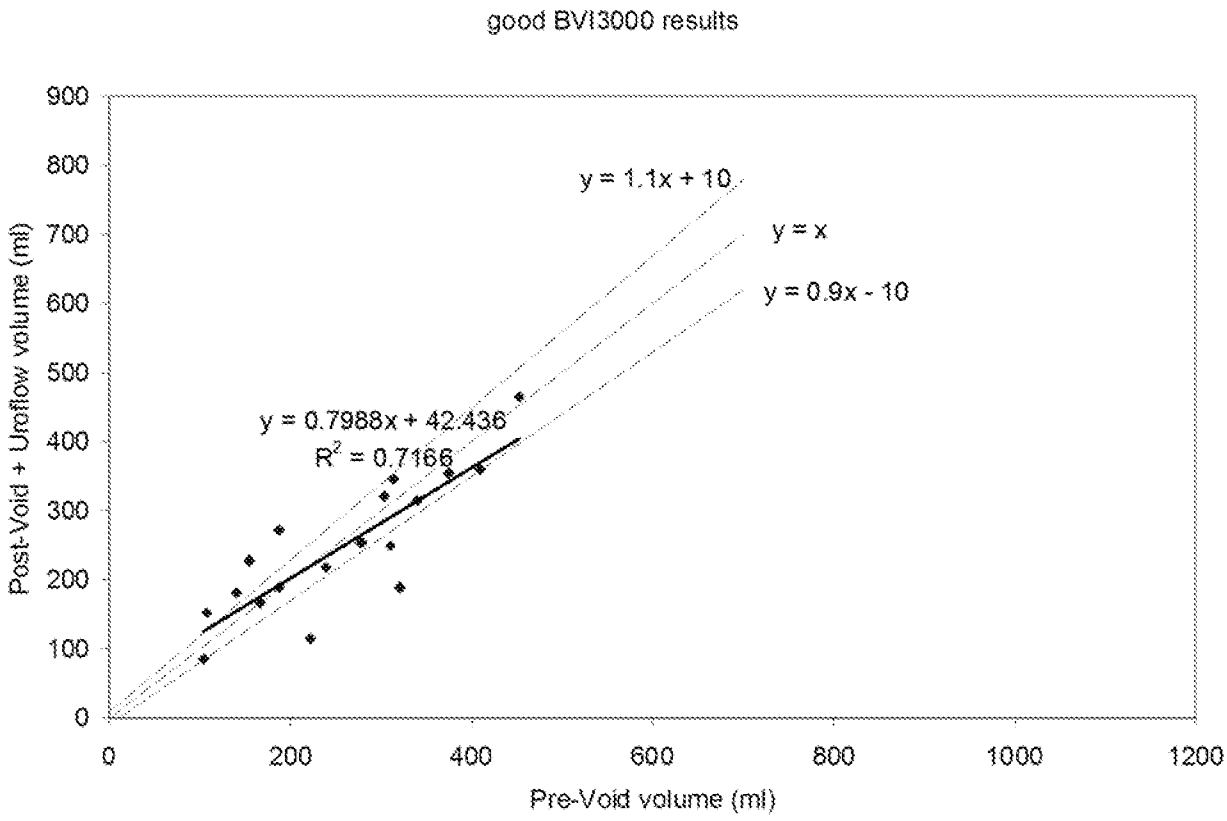
good BVI3000 results
Post-Void + Uroflow volume (ml)
Pre-Void volume (ml)
y = 1.1x + 10
y = x
y = 0.9x - 10
y = 0.7988x + 42.436
R2 = 0.7166
0
100
200
300
400
500
600
700
800
900
0
200
400
600
800
1000
1200

Fig. 38

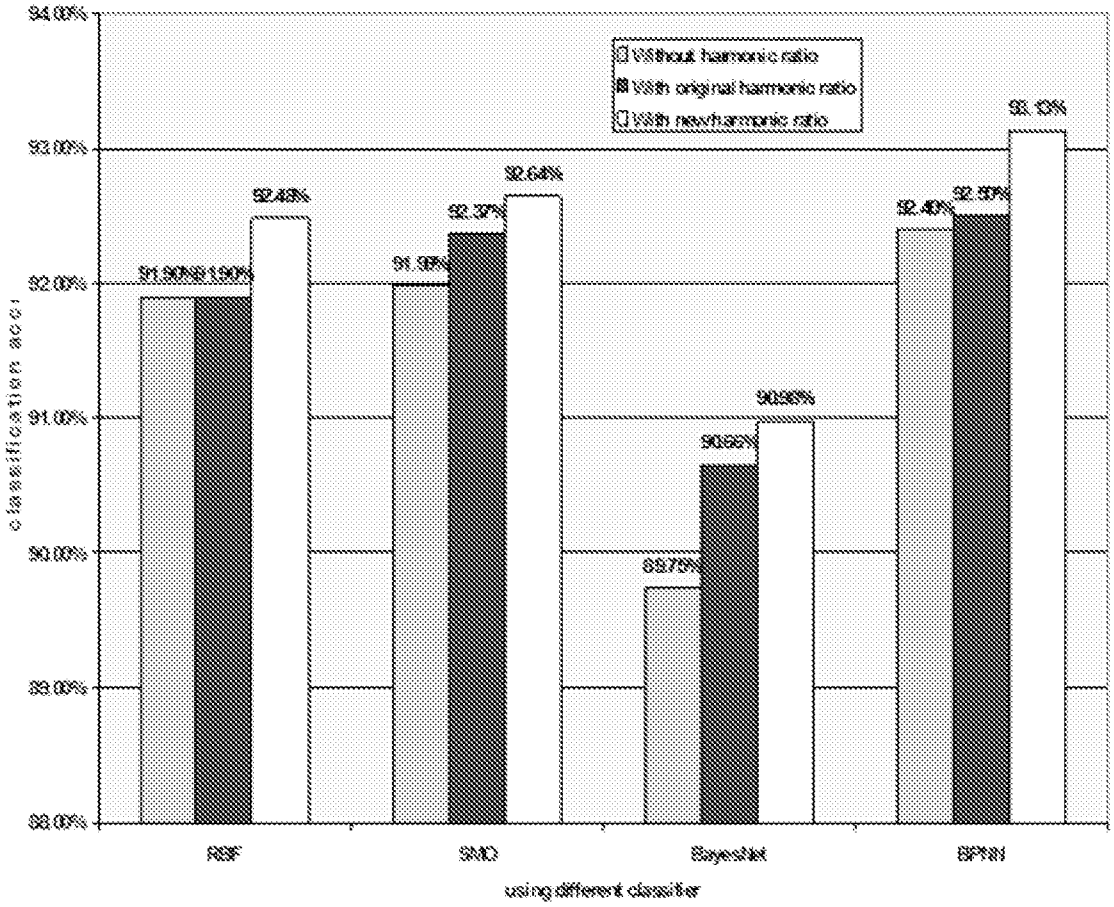
94.0%
93.0%
92.0%
91.0%
90.0%
89.0%
88.0%
Without harmonic ratio
With original harmonic ratio
With newharmonic ratio
92.64%
92.40%
92.5%
RBF
SMO
Bayesnet
BPNN
using different classifier

Fig. 39

Algorithm – KI threshold

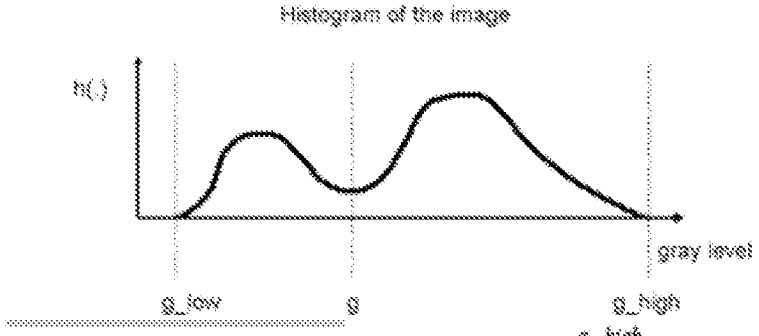

$$s_1 = \sum_{i=g\_low}^{g} h(i) \qquad s_2 = \sum_{i=g}^{g\_high} h(i)$$

$$sg_1 = \sum_{i=g\_low}^{g} (h(i)*i) \qquad sg_2 = \sum_{i=g}^{g\_high} (h(i)*i)$$

$$sgg_1 = \sum_{i=g\_low}^{g} (h(i)*i*i) \qquad sgg_2 = \sum_{i=g}^{g\_high} (h(i)*i*i)$$

$$\mu_1 = sg_1 / s_1 \qquad \mu_2 = sg_2 / s_2$$

$$\sigma_1 = sgg_1 / s_1 - \mu_1 * \mu_1 \qquad \sigma_2 = sgg_2 / s_2 - \mu_2 * \mu_2$$

Find the g which minimize the following energy and the threshold = g

$$E_{kj} = 1 + 2*(s_1 * \log(\sigma_1) + s_2 * \log(\sigma_2)) - 2*(s_1 * \log(s_1) + s_2 * \log(s_2))$$

Fig. 40

B Mode 1058 plane 1 after thresholding at 29

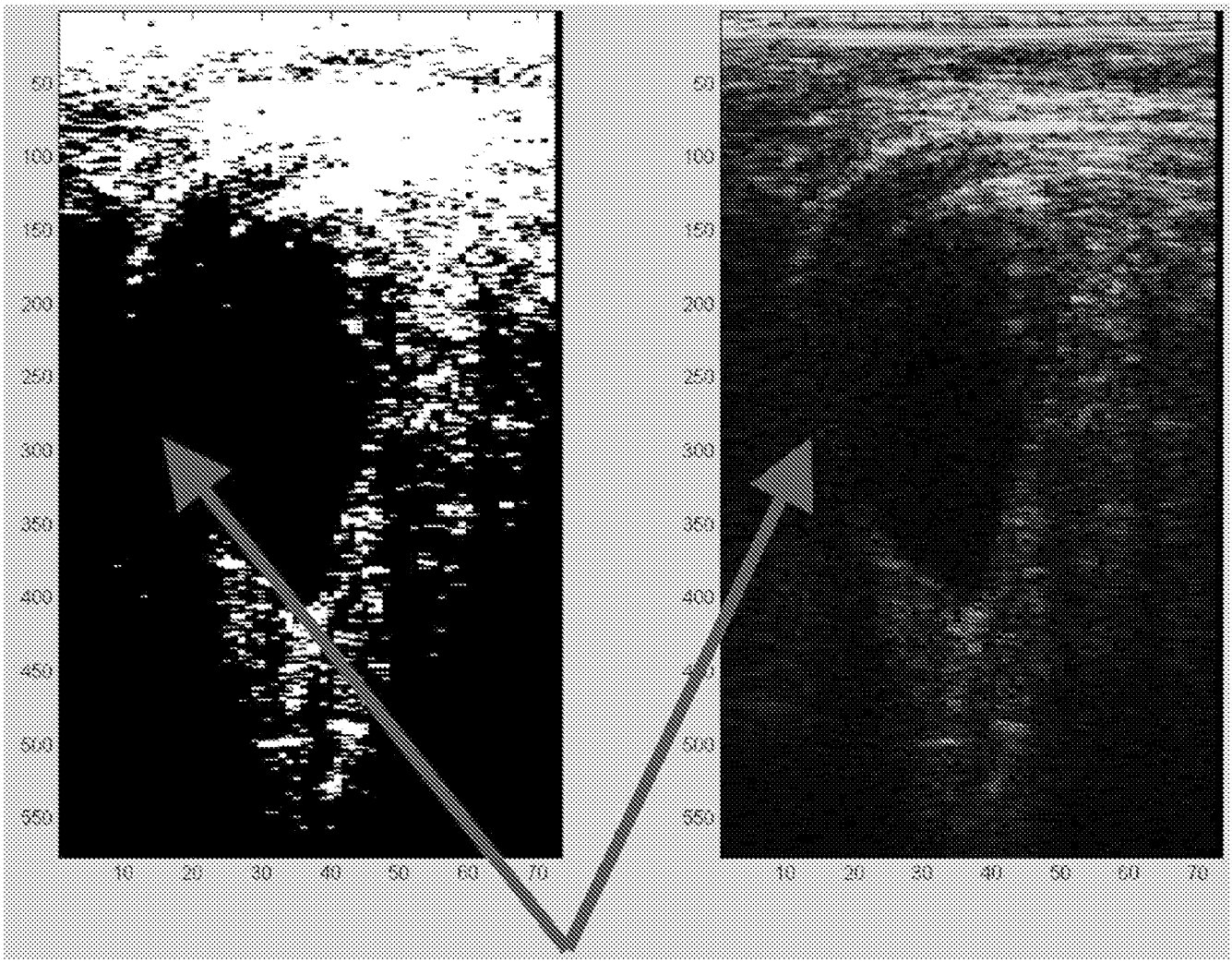

Fig. 41A

B Mode 1065 plane 1 after thresholding at 28

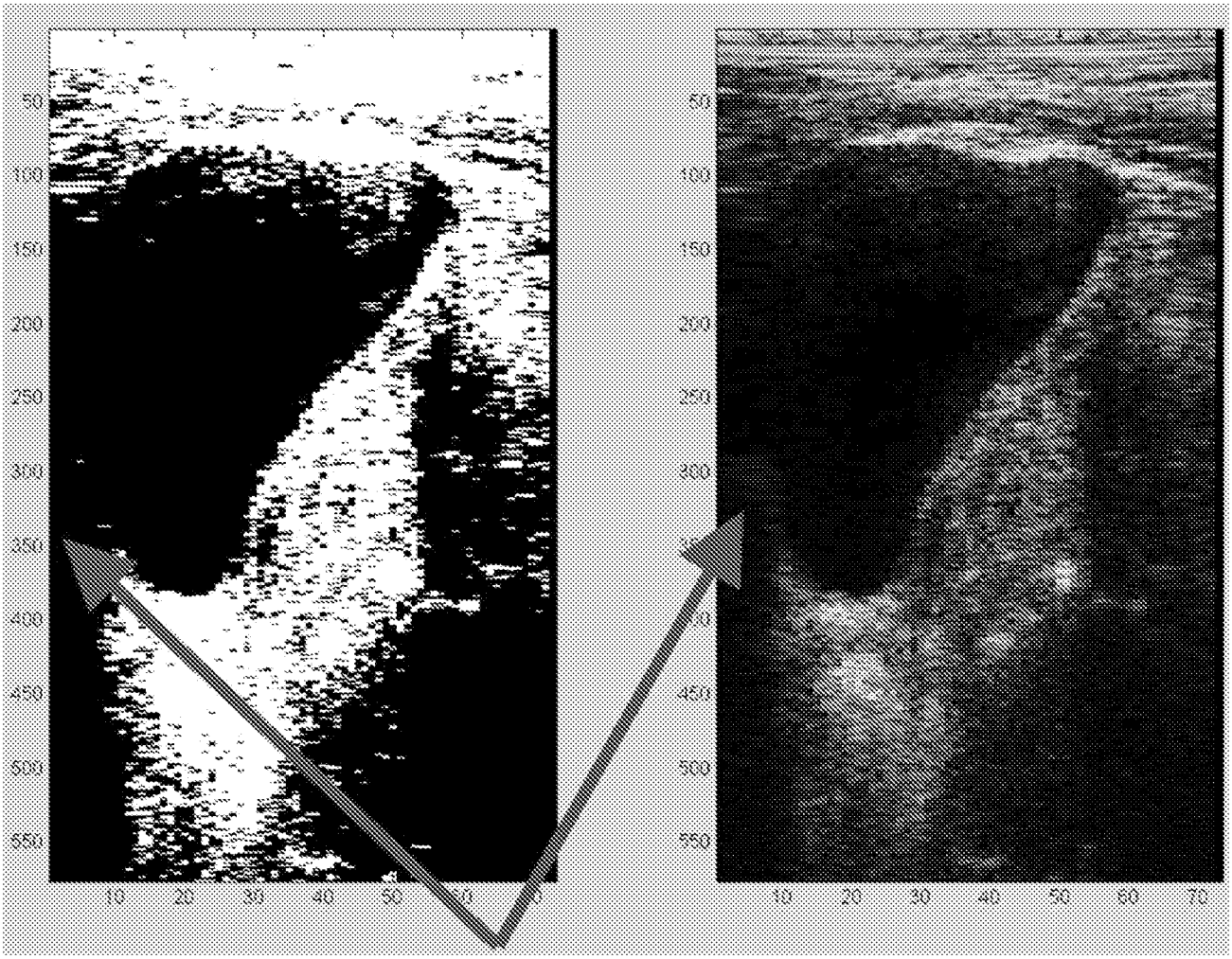

Fig. 41B

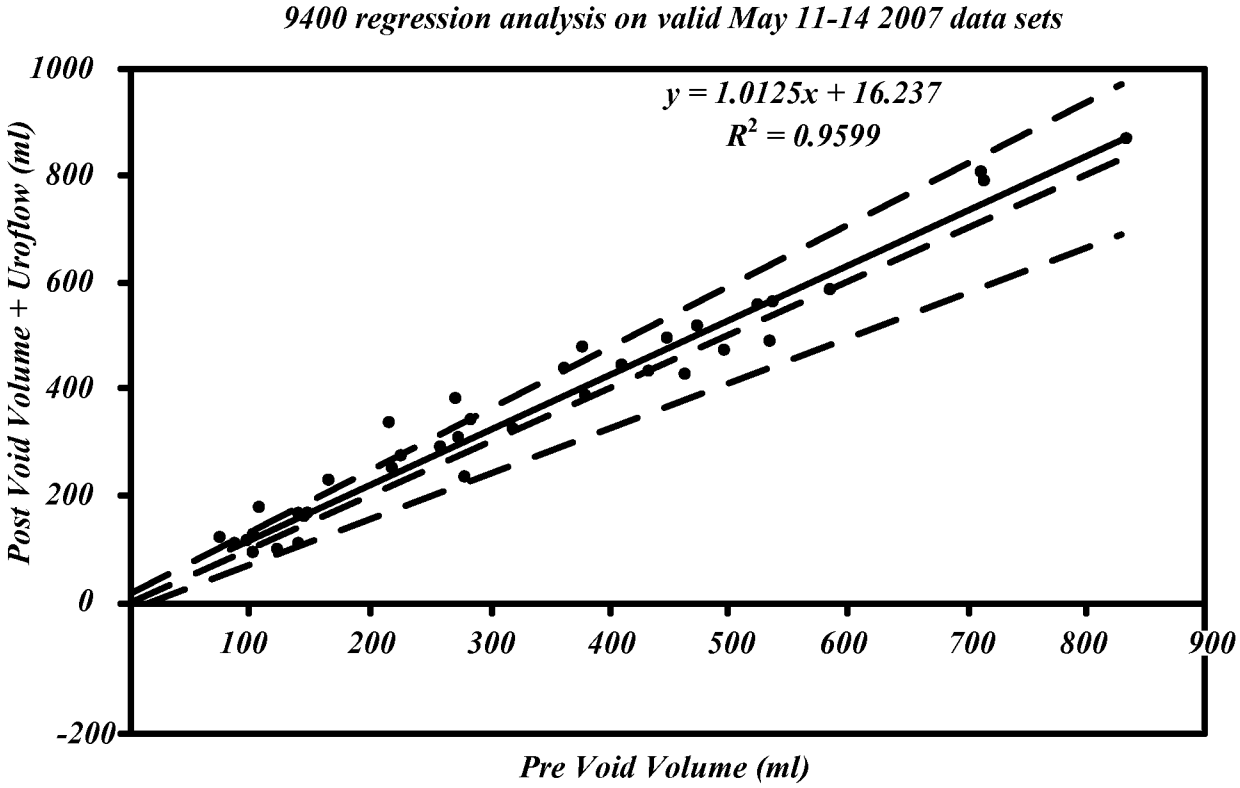
9400 regression analysis on valid May 11-14 2007 data sets
y = 1.0125x + 16.237
R2 = 0.9599
Post Void Volume + Uroflow (ml)
1000
800
600
400
200
0
-200
100
200
300
400
500
600
700
800
900
Pre Void Volume (ml)

Fig. 42

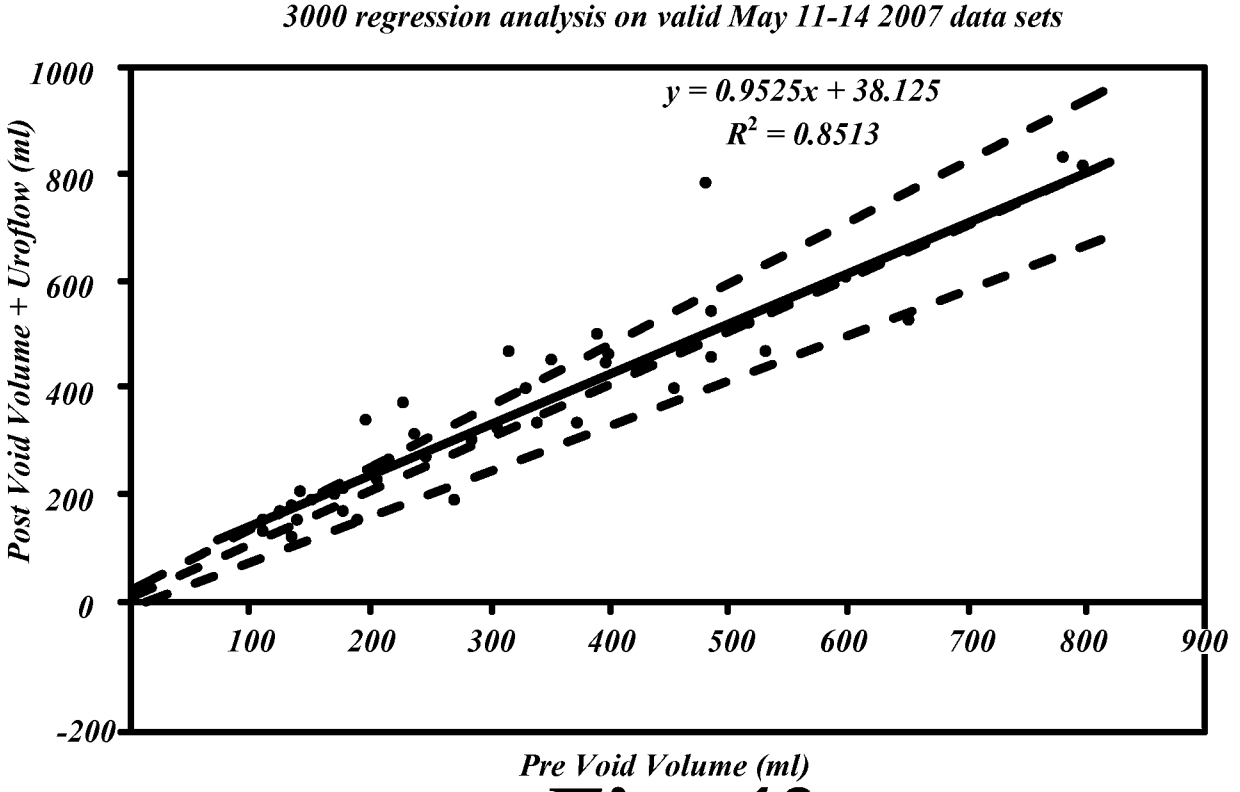
3000 regression analysis on valid May 11-14 2007 data sets
y = 0.9525x + 38.125
R2 = 0.8513
Post Void Volume + Uroflow (ml)
1000
800
600
400
200
0
-200
100
200
300
400
500
600
700
800
900
Pre Void Volume (ml)

Fig. 43

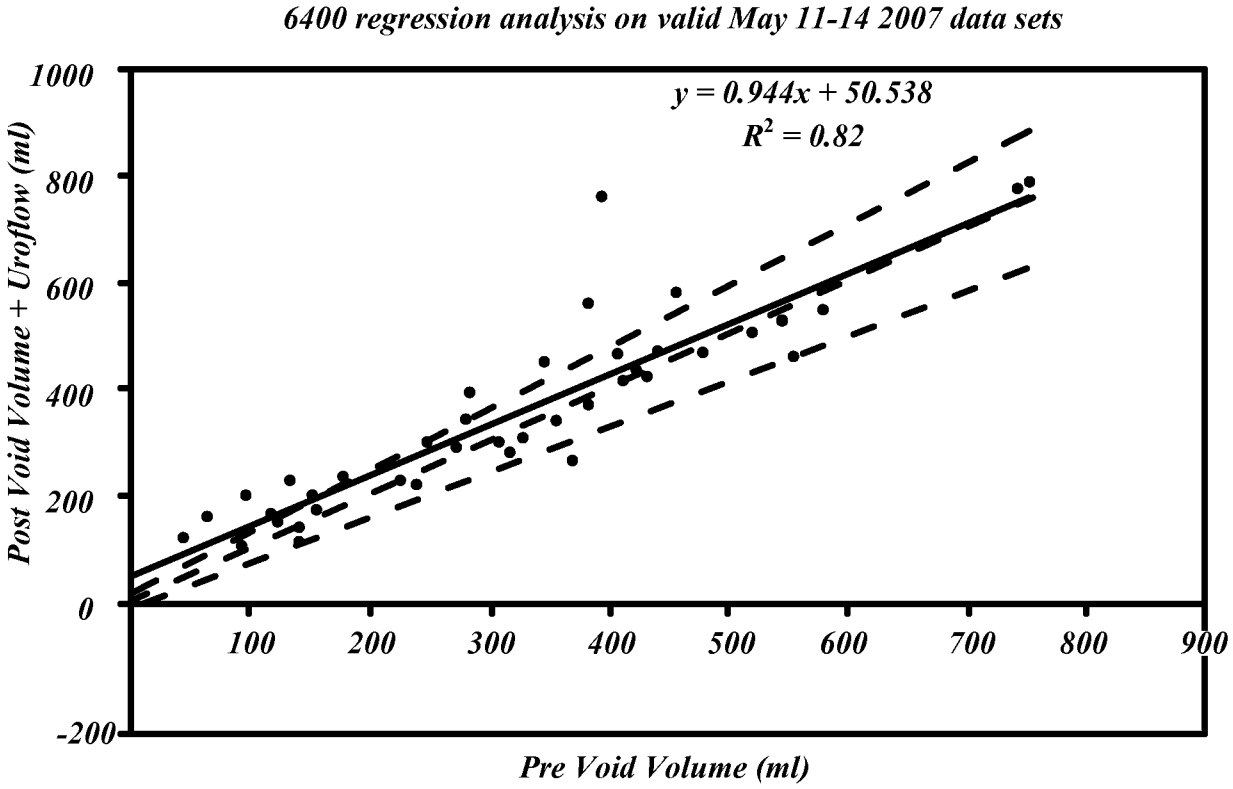
6400 regression analysis on valid May 11-14 2007 data sets
y = 0.944x + 50.538
R2 = 0.82
Post Void Volume + Uroflow (ml)
1000
800
600
400
200
0
-200
100
200
300
400
500
600
700
800
900
Pre Void Volume (ml)

Fig. 44

专利名称(译)	使用超声谐波成像进行膀胱检测的系统和方法		
公开(公告)号	EP2155067A2	公开(公告)日	2010-02-24
申请号	EP2008755614	申请日	2008-05-15
申请(专利权)人(译)	VERATHON INC.		
当前申请(专利权)人(译)	VERATHON INC.		
[标]发明人	YANG FUXING MCMORROW GERALD		
发明人	YANG, FUXING MCMORROW, GERALD		
IPC分类号	A61B8/00 A61B5/20 A61B8/08 G01S7/52 G01S15/89 G06T5/00 G06T5/10		
CPC分类号	A61B8/08 A61B8/0858 A61B8/4254 A61B8/4455 A61B8/462 A61B8/463 A61B8/467 A61B8/469 A61B8/483 A61B8/565 A61B2560/0456 G01S7/52038 G01S15/8977 G06T5/001 G06T5/10 G06T2207/10132 G06T2207/20056		
代理机构(译)	CARTER，STEPHEN JOHN		
优先权	60/938446 2007-05-16 US 60/938359 2007-05-16 US 60/938371 2007-05-16 US		
其他公开文献	EP2155067B1 EP2155067A4		
外部链接	Espacenet		

摘要(译)

描述了配备和配置为执行谐波分析并提取与受试者的目标器官相关的谐波信息的系统，方法和超声波收发器。该方法利用神经网络算法来建立感兴趣区域内的目标器官或结构的改进的分割准确度。精确用于检测膀胱并确定子宫存在与否的神经网络算法被最佳地应用于更好的分段，从而赋予优化膀胱几何形状，面积和体积的测量的能力。